Investigation of Non Linear and Photocatalytic Properties of Pristine and Cr doped ZnO Nanorods

Project report submitted to the

University of Kerala

In partial fulfillment of the requirements for the award of the degree of

MASTER OF SCIENCE IN PHYSICS

2020-2022

ABSTRACT

Metal oxide nanoparticles are the potential candidates in research area. According to the synthesis method, precursors, conditions we can tune the properties of the nanomaterials. Here in the present work we prepared the Cr-doped zinc oxide nanoparticles using hydrothermal method. Structural analysis of prepared sample are characterised by using X-ray diffraction studies and FE-SEM analysis is used to analyse the rod like morphology of the sample. Elemental compositions are investigated using Energy Dispersive X-ray analysis. The optical properties of pristine and doped materials are studied using UV visible spectroscopy and energy band gap is also calculated. Vibrational bands are analysed by Raman spectra and Functional group identified using FTIR. Oxidations state and presence of elements are identified using XPS spectrum. Third order non linear properties of the prepared samples are studied using Z-scan method. According to increasing of concentration materials shows both saturable absorption and reverse saturable absorption. Photocatalysis properties of prepared samples are investigated using methyleneblue as model dye under sunlight and the result shows that the materials is a good photocatalytic material.

Contents

1. General Introduction to Nanotechnology

2. Synthesis and Characterization Techniques ……..... (49)

CHAPTER-1

1.1 GENERAL INTRODUCTION TO NANOSCIENCE AND NANOTECHNOLOGY.

"Nanoscience" is the emerging science of objects that are intermediate in size between the largest molecules and the smallest structures that can be fabricated by current photolithography; that is, the science of objects with smallest dimensions ranging from a few nanometers to less than 100 nanometers [1]. Nanoscience is concerned with materials and systems whose structures and components exhibit novel and significantly improved physical, chemical and biological properties, phenomena and processes, because of their small nanoscale size. Structural features in the range of about 10 Å to 1000 Å, determine important changes as compared to the behaviour of isolated molecules (10Å) or of bulk materials (>0.1 μm). Nanoscience aims to understand the novel properties and phenomena of nano-based entities [1]. The linguistic form nano originates from the classical Latin nanus or its ancient Greek etonym nanos meaning "dwarf". In 1958, nano, together with giga, tera, and pico, was adopted in the newly formed International System of units. In 1974, Norio Taniguchi introduced the term nanotechnology at an engineering conference in Tokyo. Feynman's lectures or Norio Taniguchi's original use of the term "nanotechnology" are often cited as the starting points for the concept, scientists have long investigated nanoscale materials and wondered about the nature of materials on small length scales[1].

Nanotechnology can be understood as a technology of design, fabrication and applications of nanostructures and nanomaterials, as well as fundamental understanding of physical properties and phenomena of nanomaterials and nanostructures [2]. According to National Science Foundation and NNI, nanotechnology is the ability to understand, control, and manipulate matter at the level of individual atoms and molecules, as well as at the "supramolecular" level involving clusters of molecules (in the range of about 0.1 to 100 nm), in order to create materials, devices, and systems with fundamentally new properties and functions because of their small structure. Nanotechnology aims to gain control of structures and devices at the atomic, molecular and supramolecular levels, and to learn how to efficiently manufacture and use these devices [3-5].

The idea of nanotechnology started in the 1950s, though the name wasn't invented until 1974. In a way, though, nanotechnology has been around for centuries. After all, a lot of chemistry

is about controlling nanoscale objects – atoms and molecules – and since ancient times, artists have used the special properties of gold and other metal nanoparticles to color glass, but without knowing about 'nanoparticles'. In recent years nanotechnology has become one of the most important and exciting forefront fields in Physics, Chemistry, Engineering and Biology. It shows great promise for providing us in the near future with many breakthroughs that will change the direction of technological advances in a wide range of applications

Fig 1.1: A schematic representation of nanomaterials and their applications.

1.2 History of Nanotechnology

Michael Faraday synthesized colloidal gold particles as early as 1857, which was one of the first scientific reports. James Clerk Maxwell was the person who introduced the concept of nanotechnology in 1867 based on the experiment, a tiny entity known as Maxwell's Demon able to handle individual molecules. The first observations and size measurements of nano-particles were made during the first decade of the 20th century. Zsigmondy was the person who made a detailed study of gold sols and other nanomaterials with sizes down to 10

nm and less. Zsigmondy was also the first who used a nanometer explicitly for characterizing particle size. He determined it as 1/1,000,000 millimeter [4].

In 1856 the researcher, Michel Faraday discovered and prepare the first metallic colloids. Colloidal are fine particles that are suspended in a solution. Faradays gold colloidal had special electronic and optical properties and are known as one of the many interesting metallic nanoparticles [5].

The concept of Nano-technology was again touched up by Physics Nobel Laureate Richard Feynman in 1959 through his talk at Caltech on the occasion of the American Physical Society meeting. This talk was entitled "There's Plenty of Room at the Bottom". In this lecture, Feynman made the hypothesis "Why can't we write the entire 24 volumes of the Encyclopaedia Britannica on the head of a pin?", and described a vision of using machines to construct smaller machines and down to the molecular level. This new idea demonstrated that Feynman's hypotheses have been proven correct, and for these reasons, he is considered the father of modern nanotechnology [4].

Fig1.2.1: Michel faraday and display of his colloidal solutions of gold

Later, Norio Taniguchi, a Japanese scientist was the first to use and define the term "nanotechnology" in 1974 as: "nanotechnology mainly consists of the processing of separation, consolidation, and deformation of materials by one atom or one molecule". After Feynman had discovered this new field of research catching the interest of many scientists, two approaches have been developed describing the different possibilities for the synthesis of nanostructures. These manufacturing approaches fall under two categories: top-down and bottom-up, which differ in degrees of quality, speed, and cost. In the 1986s Drexler

independently coined the term nanotechnology in his book “Engines of creation: The coming era of Nanotechnology” based on Feynman's concepts [4].

Another milestone in nanoscience is the discovery of carbon nanotubes in 1991 by Sumio Lijima. It's a tubular structure of carbon atom sheets, with a thickness scaled in less than a few nanometres. Carbon nanotubes consist of a single honeycomb-like sheet of carbon atoms. These carbon atoms are called Graphene and it is rolled up in a tube form. Nanotubes have diameters almost comparable to molecules, so a carbon nanotube could be considered a single molecule. Because of their size, carbon nanotubes behave both as molecules and as solids, or as their hybrid, and have unique physical and chemical properties [5].

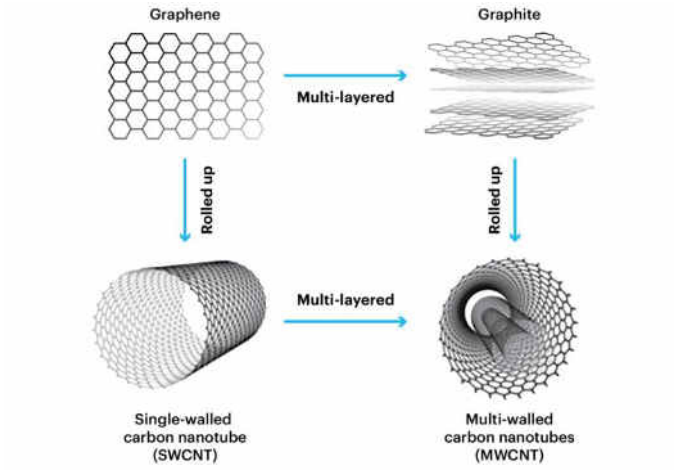

Fig 1.2.2- Single and multi-walled carbon nanotube

Carbon nanotubes have been widely used commercially in the fields of polymers, displays, engineering plastics, thin films, coatings, anti-corrosion paints, transparent and non-transparent conductive electrodes, anti-static packaging and hydrophobic coatings. The idea of using carbon nanotubes in the last decade has gained a lot of attention [6]. The ligand was bound to the external surface of the carbon nanotube to produce “gear teeth”. It is essential that the gear teeth be positioned exactly at atomic levels to work it efficiently. In the work of Han Jie et al, it is clear that the gear teeth can be made and operated. The gear operation depends on certain conditions. The gear will work if the rotation rate is below 100GHz, the temperature is lower than 600–1000 K and rotational energy is less than the teeth tilting energy at 20. If the slipped gear will be slow down the functioning of the gear will be resumed [7].

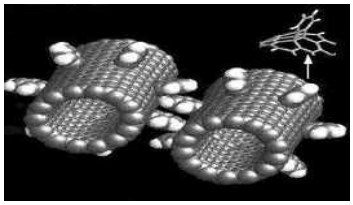

Fig 1.3.1 Carbon nanotube-based gears with benzyne teeth

1.3 Nanoparticles

Nanoscale materials, or nanomaterials, are materials where at least one relevant length scale is within the range of nanometres. Nanomaterials were widely used at this scale because of the unique optical, magnetic, and electrical properties that will emerge. These emerging properties could have a great impact in fields such as electronics, medicine, and other filed.

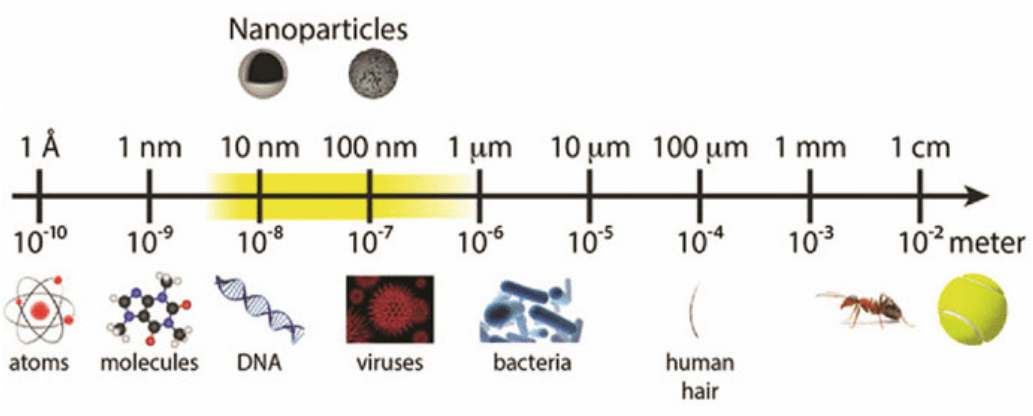

Fig 1.3.1 Comparison of different sizes of material with nanoscale dimensions

There are a lot of naturally occurring nanoparticles in our nature. Many important functions of the living organism take place at the nanoscale crystal. The researchers already found that the nanostructure of Lotus leaves creates water-repellent surfaces used today to make stain-proof clothing, other fabric, and materials. Human bodies and animals use natural nanoscale materials such as protein and other molecules. Nanomaterials can also be found in volcanic ashes, sea spray, and also products obtained from burning or combustion. In the 10th-century nanoscale, gold was used in stained glass and ceramics [8].

Artificially prepared nanoparticles or engineered nanoparticles is also now available and is designed for many commercial product and process. It can be found in sunscreen, cosmetics, sports goods, tires, etc. Engineered nanomaterials are designed at the nanometre level because of their small size and novel properties which are not present in their conventional, bulk counterpart.

Nanomaterials are also founded in ancient times. One visible property of the nanoparticles is that can change their color. At the nanoscale, gold particles can be orange, purple, green, or red depending on the size of the particle. This property is used in stained glass and the ruby-red color of many stained-glass windows of the churches of the Byzantine Empire from the medieval era is one example of this. It is a technique of staining glass for windows using metal oxide and it's in the 7th century of CE. The five main colours used to 'stain' glass were bright ruby red, which came from copper oxide, sapphire blue from cobalt oxide, green from iron oxide, yellow from sulphur or soot, and purple from manganese oxide. These materials were added to the glass while it was being heated [9].

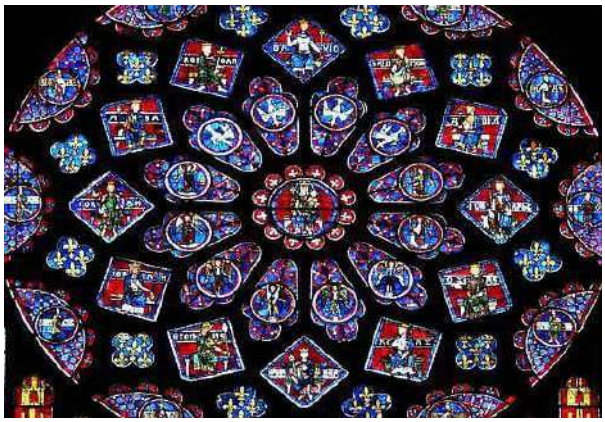

Fig 1.3.2: A detail of the North Rose window of Chartres Cathedral, France. Dating to c. 1231 CE it has the theme of the Old Testament prophecies being fulfilled with Mary as their instrument.

Another most important specimen is the Roman-era Lycurgus cup in the 4th century. It is a roman glass cage cup made up of a dichroic glass, which show different colour depending on whether or not light is passing through it. The dichroic effect is achieved by making the glass with tiny proportions of nanoparticle of gold and silver dispersed in colloidal form throughout the glass materials which have diameter comparable to the wavelength of visible light. As a consequence, a form of plasmonic excitation (an oscillation of the free electrons at the surface of a metal particle at a certain frequency) can occur. The red colour observed is a result of absorption of light (~520 nm) by the gold particles. The purple colour results due to the absorption by the larger particles while the green colour is attributed to the light scattering by colloidal dispersions of silver particles with size >40 nm. Light reflections are enhanced as the waves are highly absorbed and scattered, reducing transmission. This absorption has orientation dependence. In the cup, colour properties depend primarily on reflection when the

light is external to the cup and on absorption and transmission when the light source is internal [10].

Fig1.3.3- Lycurgus cup

Lustreware or Lusterware is also a remarkable iridescent (It is the phenomenon of certain surfaces that appear to gradually change colour as the angle of view or the angle of illumination changes) metallic shine in the 9th century. It is developed by metallic oxides in an over glaze finish, which give n a second firing at s lower temperature in a “muffle kiln”. The lusterware effect is a final coating applied over the ceramic glaze and fixed by a light second firing, applying small amount of metallic compounds mixed with something to make it paintable [11].

Fig.1.3.4- Lustreware

1.4 Classifications of Nanoparticles

The nanoparticles can be classified into different type basis on the morphology, size and dimension. Some of the important classes of nanoparticles are mentioned below.

Classification based on dimensions

Based on dimension nanoparticles are classified into four categories.

- Zero dimensional nanostructure material (0D)

- ❖ One dimensional nanostructure material (1D)
- ❖ Two dimensional nanostructure material (2D)
- ❖ Three dimensional nanostructure material (3D)

1. **Zero dimensional nanostructure material (0D)**

   The particle that has nano-dimension in 3 directions is called zero dimensional nanostructure material. It contains single crystal, polycrystalline and amorphous particle with all possible morphologies such as sphere, cube and platelets. Colloids, nanodots and nanocluster are example for 0D material.

2. **One dimensional nanostructure material (1D)**

   For 1D nanoparticle one dimension will outside the nanoscale. This class includes nanotubes, nanorods, nanowire, filament, wires, and whiskers etc. They are also known as quantum wires. These materials are used in sensors, energy device and conductors in small portable and wearable device.

3. **Two dimensional nanostructure material (2D)**

   For 2D nanoparticle are the thinnest nanomaterials due to their thickness and dimensions on macroscale. These materials have a layered structure with string in plane bonds and weak van der Waals between layers. 2D nanomaterials are highly diverse in terms of their mechanical, chemical and optical properties, as well as in size, shape, biocompatibility and degradability. These diverse properties make 2D nanomaterials suitable for a wide range of applications, including drug delivery, imaging, tissue engineering and biosensors etc.

4. **Three dimensional nanostructure material (3D)**

   These are the materials that are not confined to the nanoscale in any dimensional. In three dimensional materials the free electrons can move in the X, Y and Z direction. This class can contain bulk powders, dispersion of nanoparticles [12].

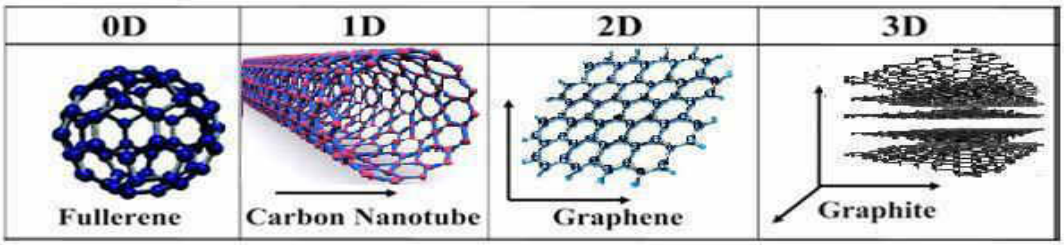

Fig 1.4.1- Examples for 0D, 1D, 2D, and 3D carbon nanostructures

1.5 Properties of Nanoparticles

Now days the application of nanoparticles is commonly used in different field due to the different properties of the nanoparticles. The large surface area, mechanically strong, optically active and chemically reactive makes nanoparticles unique and suitable applicant for different applications. Based on degrees of freedom there are change in the properties of a nanomaterials.

1. Physical properties

- Large fraction of surface atoms.
- Large surface energy.
- Spatial confinement.
- Reduced imperfections.
- Lower melting point.
- Lower phase transition temperature.

2. Mechanical Properties

The different kind of mechanical parameters like elastic modules, stress and strain, hardness and friction can be surveyed to know the exact mechanical nature of nanoparticles. Likewise the surface coating, coagulation and lubrication is also the mechanical properties. A nanoparticle shows dissimilar mechanical properties when compared to the micro particles. Decent controls over mechanical features of NPs and their interactions with any kind of surface are vital for enlightening the surface quality and elevating material removal [14].

3. Optical and Electrical Properties

Optical properties and electrical properties of nanoparticles are inter depend. The optical absorption peak of a semiconductor nanoparticles will shifts to a short wavelength due to an increased band gap. The optical absorption peak of metal was shifted by hundreds of nm. The colour of metallic nanoparticle may change with their sizes due to surface Plasmon resonance. Noble metals have size dependent optical properties and exhibit a strong UV–visible extinction band that is not present in the spectrum of the bulk metal. This band results when the incident photon frequency is constant with the collective excitation of the conduction electrons and is known as the localized surface plasma resonance (LSPR) . The peak wavelength of the LSPR spectrum is depend on the size, shape and inter particle spacing

between the nanoparticles as well as its own dielectrical properties and those of its local environment including the substrate, solvent and adsorbents [15].

When spherical metallic nanoparticles are irradiated by light, the oscillating electric field causes the conduction electrons to oscillate coherently. This relative displacement from the nuclei causes a restoring force due to coulomb attraction to arise and cause the electron cloud to oscillate. This collective oscillation of the electron cloud is known as Plasmon resonance. As this phenomenon is usually seen at the surface of the metal, it is also known as surface Plasmon resonance. Plasmon physic is developing in the field such as optical trapping, chiroptical effects, magneto-plasmonics, and plasmon-enhanced catalysis [16].

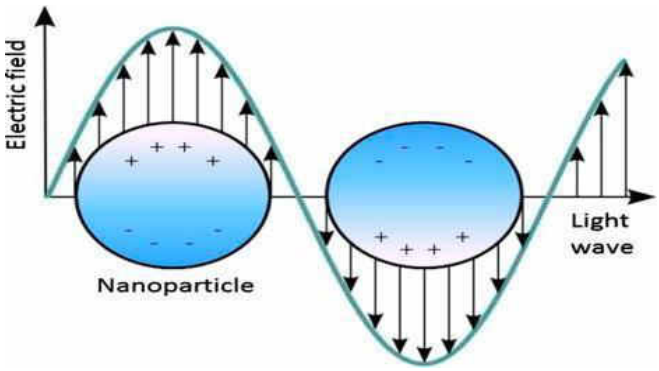

Fig 1.5.1-Graphical illustration exemplifying the localized surface plasmon(LSPR) on nanoparticle outer surface

4. Magnetic Properties

Magnetic properties of nanomaterials were different from that of bulk materials. Ferromagnetism of bulk materials disappears and transfers to super paramagnetic in nanometre scale due to the huge surface energy. Iron oxide nanoparticles were used to improve MRI images of cancer tumours. The nanoparticles were coated with a peptide that binds to a cancer tumour. Once the nanoparticles were attached to the tumour, the magnetic property of the iron oxide enhances the images from the magnetic resonance imaginary scan.

The magnetic properties are also used for the storage of information due to the ease of preservation of their magnetisation without the application of power. This behaviour is shown by nanoparticles that have magnetic properties and even defects in the nanoparticle structure and it is depend on the temperature [17].

5. Antibacterial Properties

Antibacterial agents are very important in the textile industry, water disinfection, medicine, and food packaging. Organic compounds used for disinfection have some disadvantages, including toxicity to the human body; therefore, the interest in inorganic disinfectants such as metal oxide nanoparticles is increasing. In recent years, various techniques have been proposed on the pathway of nanoparticle – biomolecule interaction. Doping is a widely used method for improving the antimicrobial properties of nanoparticles [18]. It is speculated that future research would be focused upon developing new dopant materials and methods to incorporate them into suitable nanoparticles. Also, the process of development of these antibacterial surfaces and their activities should have no negative impact on the environment. N A Smirnov *et al* [19] demonstrated the antibacterial properties of silicon nanoparticles, prepared by laser ablation, in several liquids on Gram-positive and Gram-negative bacteria. The presence of singlet and other oxygen species on the sample surface led to the damage of bacterial membranes, thereby destroying them effectively. Mohamed *et al* conducted research where gold nanoparticles along with laser exposure were used as a local antibacterial approach to inhibit the growth of C. pseudo tuberculosis [20].

6. Thermal Properties

Nanoparticle metals have thermal conductivities higher than fluids in the solid form. The oxides like alumina (Al_2O_3) have thermal conductivity higher than water. Fluid that contains suspended solid particles is expected to display significant enhanced thermal conductivities relative to conventional heat transfer fluid. Nanofluids were produced by dispersing nanoscale solid particles into liquids. Nanofluids exhibit superior properties relative to those of conventional heat transfer fluids and fluids containing microscopic-sized particles. The heat transfer takes place at the surface of the particles because of this it is desirable to use particles with a large total surface area [21].

1.6 Applications of Nanoparticles

Nanobioremediation

Nanomaterials exhibited unique physical and chemical properties which drag much attention in the field of environmental science especially in bioremediation. It provides a good clean up strategy for some type of wastes but not for all type. That is it is not a feasible method for high concentrations of chemicals that are toxic to microorganism. These include heavy metals and salt. The remediation of contaminants by use of existing technology is not effective and efficient in cleaning up the environment. Hence, nanomaterials may be applied for

bioremediation, which will not only have less toxic effect on microorganisms, but will also improve the microbial activity of the specific waste and toxic material which will reduce the overall time consumption as well as reduce the overall cost [22].

1. **Application of Nanomaterials in treatment, anti-infection and detection of corona virus.**

Several studies have been conducted on the application of nanomaterials in the treatment, anti-infection and detection of some types of corona virus. Thus, an overview of studies regarding the effectiveness of nanoparticles for diagnostic and therapeutic purposes was presented envisioning the possibility of applying nanomaterials in development of a highly effective vaccine against corona viruses [23].

2. **Water treatment**

The nanoparticles most important used in water treatment to purify the water by means of several mechanism inclusive of the adsorption of dye, heavy metals and other pollutants inactivation and removal of pathogens and conversion of harmful material into less harmful compound By using the method of molecular nanotechnology manufacturing we can solve the water shortage problem. Most of the water is used in industry and agriculture, both of these requirements would be greatly reduced by producing molecular manufacturing. Almost half of the world population lacks access to basic sanitation. Much water is wasted today because it is almost but not entirely pure. Modern technologies require only initial manufacturing and a modest power supply. Physical filter with nanometre-scale pores can remove 100% of bacteria, viruses and even prions. As with anything build by molecular nanotechnology initial manufacturing costs for water treatment system would be extremely low [24].

1.7 Synthesis Methods of Nanomaterials

The synthesis of nanomaterials leads to the future success of this new technology and in principle; the synthesis of nanoparticle can be mainly done by two processes: Top-down approaches and bottom-up approaches.

- **Top-down approach**

Top-down method is the process of breaking down of bulk material into small nanosized particles. Top-down approaches are inherently simpler and depend either on removal or division of bulk material or on miniaturization of bulk fabrication processes to produce the desired structure with appropriate properties. The imperfection in structure is one of the difficulties in thus method. For example, nanowires made by lithography are not smooth and may contain a lot of impurities and structural defects on its surface. high-energy wet ball

milling, electron beam lithography, atomic force manipulation, gas-phase condensation, aerosol spray, etc are example for such technique [25].

We attempt to concentrate on thermal technologies that supply heat to a fabrication process because they make up a broad category. Of them, electrospinning is a technique for creating nano thread materials. Whether it is heat, electricity, or solar energy, high energy methods need an excessive amount of energy input. The initial regulated method for producing carbon nanotubes was arc discharge. Both solar flux and laser ablation are effective. Quality regulation and potential upscale are the issue. Although energy-intensive and requiring expensive facilities and equipment, lithographic procedures are top-down processes capable of creating, for the most part, micronized features.

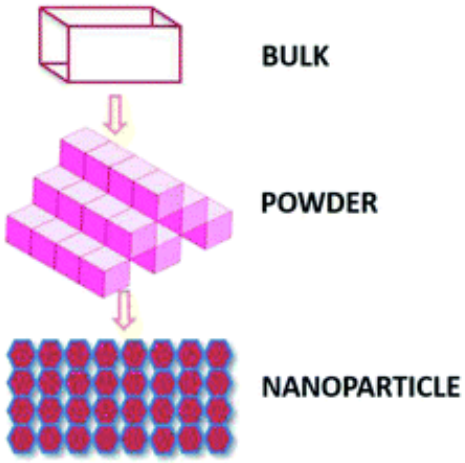

Fig 1.7.1 Top-down method

- Ball milling

Ball milling is the process of grind powders into fine particles. Normally the addition of solvent molecule will breaks the reactant in traditional method, but in ball milling the reactants are broken by using mechanical force. Mechano chemistry is a term that is relatively new. Numerous review articles have been written about the use of ball milling in the synthesis and reactions of organic molecules. Solvent-free ball milling is rarely used in the synthesis of organic compounds. But during the past ten years, this method has been increasingly popular because to its ease of use, low cost, environmental friendliness, and ability to produce extremely high yields. These factors will undoubtedly lead to a growth in basic and applied science research in the future [26].

Fig 1.7.2- Ball milling process

- Electron Beam Lithography

Electron beam lithography is also known as e-beam lithography (EBL) which is a process of scanning a focused beam of electrons to draw custom shapes on a surface covered with an electron-sensitive film called a resist (exposing).The resist's solubility is altered by the electron beam, allowing for the selective removal of either the exposed or non-exposed portions of the resist by soaking it in a solvent (developing).Similar to photolithography, the goal is to produce incredibly minute structures in the resist that can then be transferred to the substrate material, frequently through etching. The main benefit of electron-beam lithography is its ability to directly write patterns with sub-10 nm resolution. This type of maskless lithography is only suitable for the production of photomasks, low-volume semiconductor devices, and research and development due to its high resolution and poor throughput [27].

Fig 1.7.3- Electron beam lithography

- Gas phase condensation

The term "gas-phase synthesis" refers to a group of bottom-up techniques for creating multifunctional nanoparticles (NPs) from single atoms or molecules. The goal of this review is to highlight recent successes made utilising this strategy and assess its potential in comparison to alternative physical or chemical NP production methods. More particular, magnetron-sputter gas-phase condensation is highlighted because, due to its fast kinetics and non-equilibrium processes, it enables flexible development of complex, sophisticated NPs. The four phases of nanoparticle synthesis are aggregation, shell-coating, mass-filtration, and deposition. We present the production of NPs with various functionality for various applications, including magnetic, plasmonic, catalytic, and gas sensing, with an emphasis on how each kind is primarily dependent on a particular stage of the manufacturing process and the resulting physical and chemical properties [28].

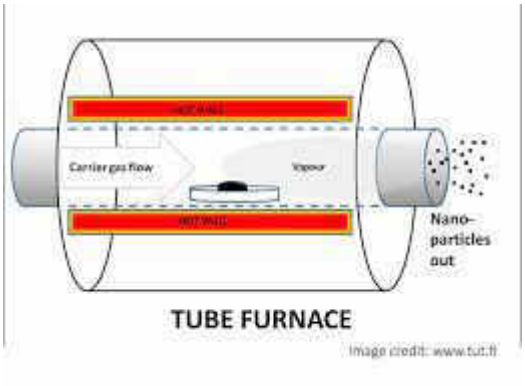

Fig 1.7.4 Gas phase synthesis

➢ Bottom-up Approach

The alternate strategy of top down is called "bottom-up," which has the potential to produce less waste and is therefore more cost-effective. A substance is constructed from the bottom up, atom by atom, molecule by molecule, or cluster by cluster. This is referred to as a bottom-up technique. Many of these methods are still in research or are only now starting to be applied in the manufacture of nanopowders for commercial purposes. Some of the well-known bottom-up methods used to create luminous nanoparticles include the oraganometallic chemical route, revere-micelle approach, sol-gel synthesis, colloidal precipitation, hydrothermal synthesis, template assisted sol-gel, electrodeposition, etc.[25]

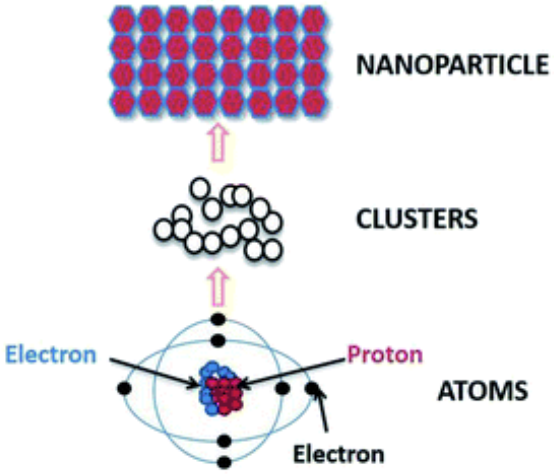

Fig 1.7.5-Bottom up method

- Hydrothermal method

Hydrothermal method is a standard preparation route, especially for powdery nanostructure. Hydrothermal synthesis refers to the heterogeneous reactions for synthesizing inorganic materials in aqueous media above ambient temperature and pressure. In this case, an aqueous mixture of precursors is heated in a sealed stainless-steel autoclave above the boiling point of water, and consequently the pressure within the reaction autoclave is dynamically increased above atmospheric pressure. This effect of high temperature and pressure provides a one step process to produce highly crystalline materials without the need of post annealing treatment. The hydrothermal synthesis could obtain magnetic nanomaterials with very high crystallinity due to their high temperature and high-pressure reaction conditions. Hydrothermal method has several advantages such as low cost, easy experimental setup, and high yield.

As a result of the main thermodynamic and kinetic features of the hydrothermal process, the main advantages of the hydrothermal synthesis are:

- One step process for powder synthesis or oriented ceramic films.
- Minimized consumption of energy, particularly for complex and doped oxides.
- Products with much high homogeneity than solid state processing.
- Products with higher density than gas or vacuum processing.
- One of the few methods enabling for obtaining of controlled doped or complex material system

Fig 1.7.6- The hydrothermal reaction set up

- Sol-gel Synthesis

The sol-gel process is a more chemical method (wet chemical method) for the synthesis of various nanostructures, especially metal oxide nanoparticles. In this method, the molecular precursor (usually metal alkoxide) is dissolved in water or alcohol and converted to gel by heating and stirring by hydrolysis/alcoholysis. Since the gel obtained from the hydrolysis/alcoholysis process is wet or damp, it should be dried using appropriate methods depending on the desired properties and application of the gel. For example, if it is an alcoholic solution, the drying process is done by burning alcohol. After the drying stage, the produced gels are powdered and then calcined. The sol-gel method is a cost-effective method and due to the low reaction temperature there is good control over the chemical composition of the products. The sol-gel method can be used in the process of making ceramics as a moulding material and can be used as an intermediate between thin films of metal oxides in various applications. The materials obtained from the sol-gel method are used in various optical, electronic, energy, surface engineering, biosensors, and pharmaceutical and separation technologies (such as chromatography). The sol-gel method is a conventional and industrial method for the synthesis of nanoparticles with different chemical composition. The basis of the sol-gel method is the production of a homogeneous sol from the precursors and its conversion into a gel. The solvent in the gel is then removed from the gel structure and the remaining gel is dried. The properties of the dried gel depend significantly on the drying method. In other words, the “removing solvent method” is selected according to the application in which the gel will be used. Dried gels in various ways are used in industries such as surface coating, building insulation, and the production of special clothing. It is worth mentioning that, by grinding the gel by special mills, it is possible to achieve nanoparticles [29].

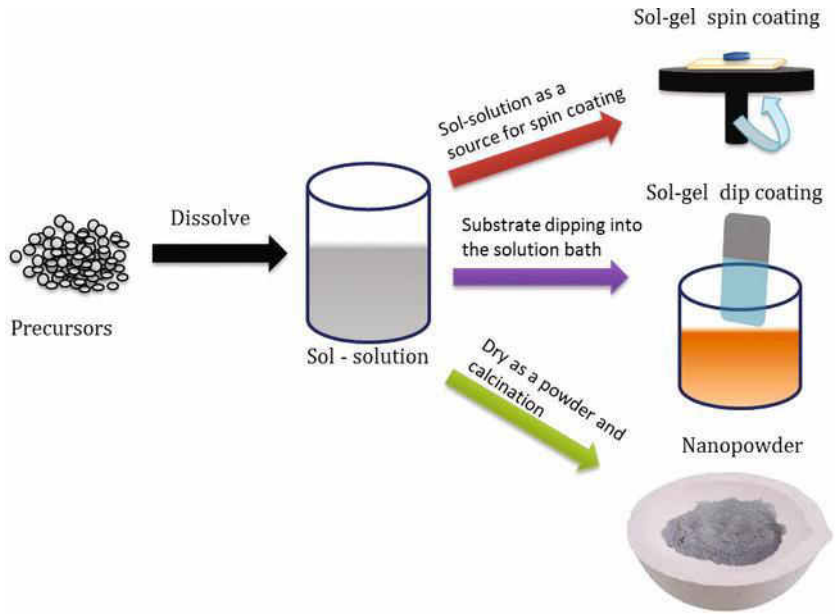

Fig1.7.7-Sol gel synthesis

- Electrodeposition

Electrodeposition is a flexible low-cost method of fabrication of a wide variety of two- and three-dimensional materials such as coatings and films. The principles of the electrodeposition process are based on principles of electrochemical phenomena associated with the reduction or deposition of electroactive and accompanying species on the cathode surface. This would make the electrodeposition process more controllable if one considers the electrochemical principles into account for target purposes and applications. However, many empirical factors in designing and controlling of electrodeposition process exist. Anticorrosion coatings have been a major part of corrosion protection tools employed for years. Electrodeposition is one successful method to fabricate coatings. Thanks to remarkable advances in nanoscience and nanotechnology and exotic effects of the nanoscale size on properties and functionalities of materials, electrodeposition of nanocoatings has become an interesting subject of research recently. In this chapter, the electrodeposition of anticorrosion nanocoatings is described. After a brief overview of the electrodeposition, two types of nanocoatings including nanocomposites and nanocrystalline, their electrodeposition principles, and corrosion behaviour based on conventional electrochemical studies are explained [30]

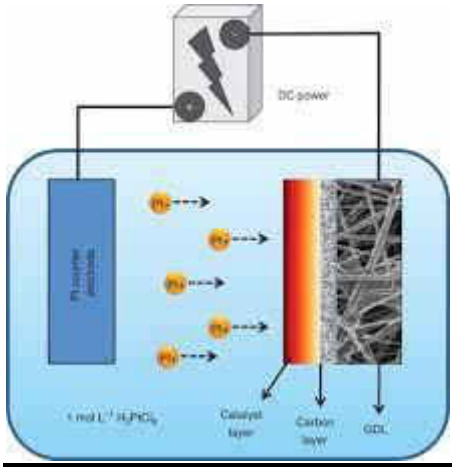

Fig 1.7.8-Electro deposition

1.8 Zinc Oxide

Zinc oxide is an inorganic white powdered compound with formula ZnO which is insoluble in water. ZnO is present in earth crust as in the mineral Zincites which contain manganese and other impurity. It is widely used in cosmetics, food supplements, rubbers, plastics, ceramics, glass, cement, lubricants, paints, ointments, adhesives, sealants, pigments, foods, batteries, ferrites, fire retardants, and first-aid tapes etc. It is a n-type semiconductor with wide band gap. The electrical resistivity becomes 0.01Ω m at 25^0C. The resistivity can be reduced by quenching from high temperature or by heat treatment in an appropriate environment to increase the concentration of interstitial zinc [31]. Zinc oxide nanoparticles are also called as oxydatum, permanent white, oxozinc, zinci oxicum, and ketozinc. These nanoparticles exhibit anticorrosive, UV-filtering, antibacterial and antifungal activities [32].

The application of zinc oxide nanoparticles has studied for years, it has an eminent role in areas ranging from biomedical imaging to drug delivery, and zinc oxide nanoparticles have proven to be a promising candidate for photodynamic therapy. Zinc oxide nanoparticles have been newly applied as varistors that protect circuits from voltage spikes. Exposing zinc oxide nanoparticles to different bacterial and fungal species caused different morphological changes such as transformation from spiral to coccoid, with membrane disruption, cellular damage, and cell lysis[33]

Zinc Oxide has three main crystal structures hexagonal wurtzite, cubic zinc blend and rarely observed cubic rock salt. The wurtzite is most stable at ambient condition and it is most common which shows in fig (b). The zinc blend has a cubic lattices form. In the both cases zinc and oxides centres are tetrahedral. At high pressure ZnO is converted into rocksalt.

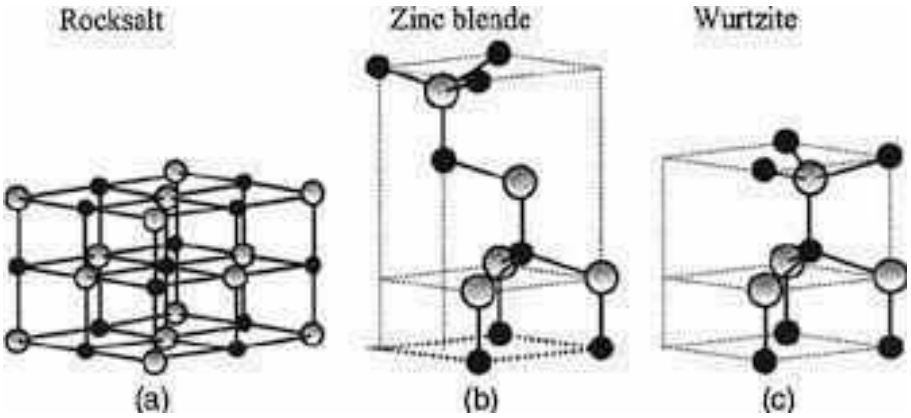

Fig 1.8.1 ZnO crystal structures: cubic rocksalt (a), cubic zinc blende (b) and hexagonal Wurtzite (c):

The ZnO is also known as II - VI semiconductor because Zinc and oxygen is belonging to 2^{nd} and 6^{th} groups. As a semiconductor it has good transparency, high electron mobility, wide band gap, strong room temperature luminescence, etc. These properties of semiconductor are applicable in transparent electrodes in liquid crystal displays and in energy-saving or heat-protecting windows and electronic applications of ZnO as thin-film transistor and light - emitting diodes. ZnO has direct band gap of 3.37eV and have a binding energy of 60meV [34-35]. In biological system also zinc takes a major role so ZnO is suitable for in –vivo bio imaging and cancer detection. One of the challenges to be met in the field of display and light-emitting technology is to develop solid-state white light-emitting sources based on existing silicon-based technology. Due to their unique properties such as low power consumption, high efficiency, long lifetime, reduced operating costs, and free of mercury, solid-state white-light emitting sources have immense potential applications. In order to produce white light, phosphors emitting blue, green, and red wavelengths are needed. A semiconducting nano crystalline luminescent material, which has higher molar absorption and exhibits broadband emission without self-absorption, might overcome this problem [36].

The zinc oxide nanoparticle is also used in varistors. These particles having a size range from 5-40 nm. Doped zinc oxide nanoparticle with the highest density and electrical conductivity resulted in a higher critical electric field and a higher coefficient of nonlinearity (α) when seen in the logE versus log J curve [37]. The paper confirmed that the critical voltage of the varistor is dependent on two factors: the grain size and the zinc oxide nanoparticle size [38]. ZnO has some disadvantages such fast recombination of photogenerated electron-hole pairs,

it is only active with UV light, and it suffers from photocorrosion. To overcome these limitations ZnO has to be combined with the materials such as metal, semiconductor and nanotubes [39].

ZnO produce luminescence in visible spectral range due to the different intrinsic defects. Defects are generally incorporated under controlled conditions through annealing [40], substitution [41], mechanical milling [42], etc. Most ZnO crystal is synthesized by traditional high temperature solid state reaction. ZnO can be prepared in large scale with low cost by simple solution based methods like chemical precipitation [42-43], sol-gel synthesis [44] and hydrothermal reaction [45-46].The hydrothermal method has many advantage on other growth process like it is a low process temperature and we can control the particle size very easily. The low reaction temperatures make this method an attractive one for microelectronics and plastic electronics [47]. The particle properties such as morphology and size can be controlled via the hydrothermal process by adjusting the reaction temperature, time and concentration of precursors.

- **Wurzite Structure**

The wurtzite structure is the member of hexagonal crystal system and it consists of tetrahedrally coordinated zinc and sulfur atoms that are stacked in an ABABABABAB pattern. The structure is made up of two interpenetrating hexagonal close packed (hcp) sublattices, each of which consist of one type of atom displaced with respect to each other along the three fold c-axis by the amount of U=3/8(U=length of the bond parallel to the c axis, in units of c).Each of these sublattics has 4 atom per unit cell every atom of one kind is surrounded by four atoms of the other kind which are coordinated at the edges of a tetrahedron. The wurtzite structure is shown in fig below

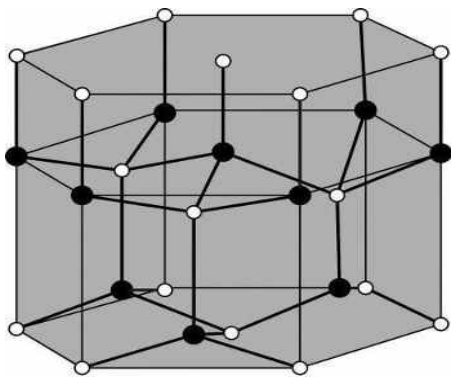

Fig 1.8.2: Crystal structure of ZnO

The atoms are also grouped in a tetrahedral symmetry in the wurtzite structure, with each atom having four 1 close neighbours of a different sort and twelve 2 near neighbours of the same kind. It is interesting to observe that the atomic configuration in the wurtzite structure along the a3 axis resembles the atomic configuration in the ZnS structure along the [111] direction. Each unit cell in the wurtzite structure has four atoms. As a result, $(\sqrt{3}/8)\ a^2c$ gives the wurtzite structure's average volume per atom. Numerous piezoelectric and pyroelectric crystals have the uniaxial symmetry of the wurtzite structure [48].

For ZnS or wurtzite the lattics parameter is given by a = 3.81 Å, c = 6.23 Å, c/a = 1.64 [28].Like other II-VI semiconductors, wurtzite ZnO can be transformed to the rock salt structure at relatively external hydrostatic pressure. The reason for the transformation is that the reduction of the lattice dimensions causes the interionic coulomb interaction to favor the ionicity more over the covalent nature. However the rock salt structure cannot be stabilized by the epitaxial growth. Also the crystal structure exhibits polarity [49].

1.9 Properties of Zinc Oxide

- ✓ Optical Property

The optical properties of semiconductor depend on intrinsic and extrinsic effects. The Intrinsic optical transitions occur between electrons in the conduction band and holes in the valence band, including exitonic effects due to the Coulomb interaction. The condition for exitonic formation is the group velocity of the electron and hole should be same. The excitation can be classified into free and bounded. Extrinsic properties are determined by dopants or defects, which create discrete electronic states in the band gap, and therefore influence the optical absorption and emission process. From the work of B. K. Meyer et al [50] the optical properties of excitonic recombination in bulk, n-type ZnO is referred. This work offers a complete treatment and analysis of the excitonic spectra received from ZnO and assigns many defect-associated spectral features, as well as donor-acceptor pair (DAP) emission. A broad peak is extending from ~1.9 to ~2.8 eV is common optical feature of ZnO [51].

- ✓ Thermal Properties

Thermal expansion coefficient (TEC) The change in temperature affects the lattice parameters of semiconductors. Thermal expansion coefficients are defined as α_a and α_c for in and out of plane cases, respectively. The stoichiometry, presence of extended defects and free

carrier concentration also affect the thermal expansion coefficient. Thermal conductivity Thermal conductivity (k), having a kinetic nature, is determined by vibration, rotation and electronic degree of freedom. It is really important property of semiconductors when these materials are used in high-power, high-temperature optoelectronic devices. The electronic thermal conductivity is very small, having light carrier concentration, which is negligible. For high pure crystals, phonon-phonon scattering is ideally proportional toT-1 at the temperatures higher than the Debye temperature. Point defects, such as vacancies, impurities and isotope fluctuations in ZnO affect the thermal conductivity of ZnO material [52-54]

- ✓ Electrical Property

A semi conductor device with wide band gap can have a high breakdown voltage, lower noise generation and can operate at higher temperatures with high power operation. The electron transport in semiconductor is depends on electric fields. That is the performance will be different at low and high electric field. In ZnO energy distribution of electron is unaffected at low electric field due to the much low energy from the electric field when compared to the thermal energy. At high electric field the energy distribution become equivalent to thermal energy. The electron distribution function changes significantly from its equilibrium value. When the temperature become higher than lattice temperature electrons become hot. At short and critical time there is no energy loss to lattice. To make higher frequency device the electron drift velocity must be higher than steady state value [55-56].

1.10 Defects in ZnO

Crystal defect is the imperfection in the regular geometrical arrangement of the atoms in a crystalline solid. These defects often have a profound effect on the properties of material. There are 3 types of imperfections. Point defects, line defects (dislocation) and surface defects. These imperfections were useful in many applications. The dislocation defects are useful in increasing the strength of metals and alloys. The defects can be intentionally created to apply some of the applications such as electronic, magnetic, optical and mechanical properties. The grain boundaries, region between different grains of polycrystalline material, represent one type of defects.

In nanostructured ZnO (as well as in other materials), the small length scales and large surface-to-volume ratio mean that surface defects play a stronger role in controlling properties. It is important to understand defects in ZnO doped with aliovalent ions, either purposefully for achieving certain functionality or through accidental doping during the

growth process [57].Vacancies, interstitials, and anti-sites of Zn and of O are considered to be the native defects in ZnO. The O vacancy, Zn interstitial and Zn anti-site, which are associated with O deficiency or Zn excess, are donor-type defects. The Zn vacancy, O interstitial, and O anti-site are acceptor-type defects associated with Zn deficiency or O excess. The interstitials can be located at the octahedral and tetrahedral sites, as shown in figure figure. Phonon calculations predict the Zn interstitial at the tetrahedral site to be dynamically unstable. The O interstitial can form in an O_2-molecule-like configuration as a result of large atomic relaxation. Such a defect cannot be simply characterized as a point defect at the lattice and at interstitial sites [58].

o Point Defects

Point defects typically involve one atom or ions or a pair of atoms or ions, and thus is different from extended defect, such as dislocation, grain boundaries etc. An important "point" about point defect is that although the defect occurs at one or two sites, their presence is "felt' over much larger distance in the crystalline material. A point defect can be an atom missing from a site in the crystal (a vacancy) or an impurity atom that occupies either a normal lattice site (a substitution impurity) or a hole in the lattice between atoms (an interstitial impurity).

There are 5 types of point defects.

- Vacancy
- Interstitial defect
- Substitutional defect
- Frenkel defect
- Schottky defect

❖ Vacancy

When an atom is not present in the lattices site, then the lattices site is a vacant and it create a vacancy defect. Because of this its density decreases. When the vacancies are present the entropy of the material is increases which will increases the thermodynamic stability of the crystalline material. The vacancy defect is shown in below fig.1.9.1

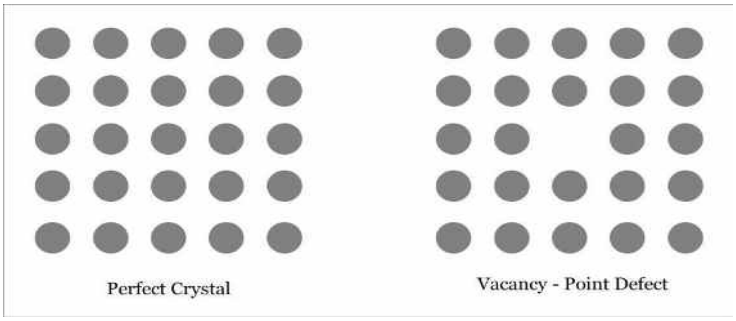

Fig 1.10.1; Vacancy defect –point defect

All the crystalline material have vacancy defect and the vacancies are introduced into metal and alloys during solidification at high temperature. In pure metals the vacancies have an important role to determine the rate at which atom r ion can move around or diffuse in solid materials. The vacancy created in ceramic material is used to certain applications which are mainly depending on the electrical properties. The ceramic is used as conductive and transparent oxides such as Indium tin oxide (ITO) and zirconia oxygen sensors.

At room temperature the concentration of vacancies will be small, but the concentration of vacancy increases as the temperature increases. The temperature increases will be based on the Arrhenius behaviour and the equation is given as

$n_v = n \exp(-Q_v/RT)$ …… (1.1)

The term n_v is the number of vacancies per cm^3. n is the number of atoms per cm^3.Q_v is the energy required to produce one mole of vacancies, in cal/mol or Joules/mol. R is the gas constant and its value is given by 1.987 cal/mol-k. T is the temperature in degree Kelvin. Near to melting point due to the large thermal energy there may be as many as one vacancy per 1000 atoms. This equation gives for equilibrium concentration of vacancies at a given temperature. It also possible to retain the concentration of vacancies produced at a high temperature by quenching the material rapidly. Thus, in most situation concentration of vacancies at room temperature will not be same as the equilibrium concentration predicted by the equation.

- **Interstitial Defects**

The interstitial defects is formed if the an extra atom or ion is presented in the crystal structure at normally unoccupied position. Interstitial atom or ion is smaller than the atoms

occupied at the lattice point and it will be much larger than the interstitial site that occupied. Consequently the surrounding crystal region is compressed and distorted.

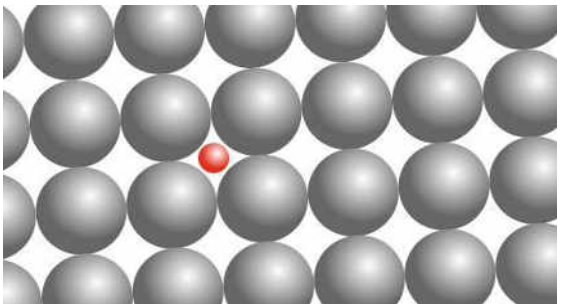

Fig 1.10.2-Interstitial defect

If the crystal contains the atom which is same as those already present in lattice is called self-interstitial. In some crystals small atoms may occupies in interstitial site such as hydrogen in palladium. Interstitial can be produced by bombarding a crystal with elementary particle with energy above the displacement threshold for that crystal. But it also exhibit in small concentration in thermodynamic equilibrium. These interstitial defects can modify the physical and chemical properties of a material. The carbon atom is intentionally added to iron to make steel. For small concentrations, carbon atoms occupy interstitial sites in the iron crystal structure, when introducing stress in the localized region of the crystal in the vicinity. When crystal dislocations move around such defects, they encounter resistance, making it difficult for permanent deformation to occur in metal or alloys. It is an important way to create a permanent deformation in materials.

- **Substitutional Defects**

Substitutional defect occurs when the original atom in the lattice site of a crystalline solid is replaced by a different atom. The Substitutional atom or ion will occupy the normal lattice site, not the interstitial site. Suppose a substitutional atom or ion is larger than the normal atom or ions in the crystal lattice. In that case, the interatomic space of the surrounding will be reduced and it will cause the surrounding atom to have large interatomic spacing. The substitutional defect can be introduced either as an impurity or as a deliberately alloying addition, and, once introduced the number of defects or relatively independent of temperature.

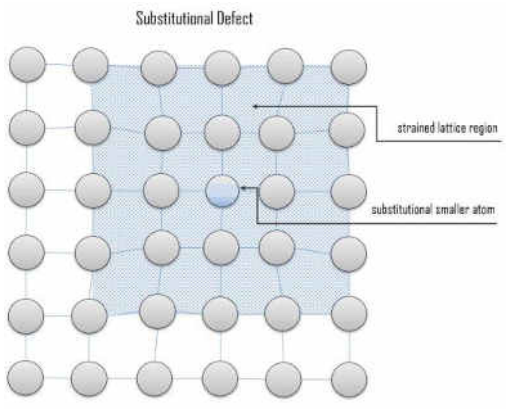

Fig 1.10.3- Substitutional defect

- **Frenkel Defect**

It is a vacancy-interstitial pair formed when an ion jumps from a normal lattice point to an interstitial site, leaving behind a vacancy. This is described as an ionic material. But it can occur in metals and covalently bonded material. In ionic crystals, which usually possess low coordination numbers or a considerable disparity in the sizes of the ions, this defect can be generated also spontaneously, where the smaller ion (usually the cation) is dislocated. Even though Frenkel defects involve only the migration of the ions within the crystal, the total volume and thus the density is not necessarily changed: in particular for close-packed systems, the lattice expansion due to the strains induced by the interstitial atom typically dominates over the lattice contraction due to the vacancy, leading to a decrease of density.

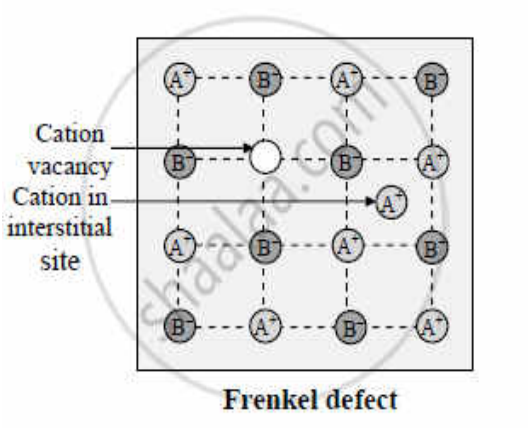

Fig 1.10.4-Frenkel defect

- **Schottky Defect**

It is unique to ionic material and is commonly found in any ceramic material. In this defect, vacancies occur in ionically bonded materials, a stoichiometric number of anions and cations

must be missing from the crystal if electrical neutrality is to be preserved in the crystal. It consists of unoccupied anion and cation sites in a stoichiometric ratio. For a simple ionic crystal of type A^-B^+, a Schottky defect consists of a single anion vacancy (A) and a single cation vacancy (B), or $v_A^{\bullet}+v_B^{'}$ following Kröger–Vink notation. For a more general crystal with formula $A_x B_y$, a Schottky cluster is formed of x vacancies of A and y vacancies of B, thus the overall stoichiometry and charge neutrality are conserved. Conceptually, a Schottky defect is generated if the crystal is expanded by one unit cell, whose a prior empty sites are filled by atoms that diffused out of the interior, thus creating vacancies in the crystal. Schottky defects are observed most frequently when there is a small difference in size between the cations and anions that make up a material. Typically, the formation volume of a vacancy is positive: the lattice contraction due to the strains around the defect does not make up for the expansion of the crystal due to the additional number of sites. Thus, the density of the solid crystal is less than the theoretical density of the material [59].

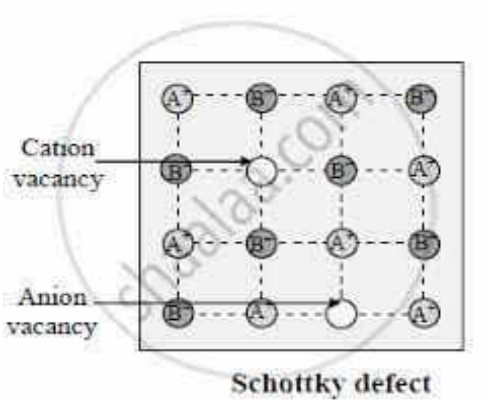

Fig-1.10.5 Schottky defect

1.11Application of ZnO

The metal oxide semiconducting nanoparticles is applicable in biological sensing, biological labelling, drug and gene delivery, and nanomedicines [60-63].Due to the easy fabrication environmentally friendly nature, and non-toxic synthesis route, ZnO nanoparticles can provide a better option for various biological applications[64], and also different nanostructure forms of ZnO particles such as rods, springs, flowers, belts, etc are used in numerous application include supercapacitors, paints, sensor material, antimicrobial materials, and others [65].

- **Agricultural Application**

Zinc oxide NPs have the potential to boost the yield and growth of food crops. The colloidal solution of zinc oxide nanoparticles is used as fertilizer. This type of nano fertilizer plays an

important role in agriculture. Nano fertilizer is a plant nutrient that is more than a fertilizer because it supplies nutrients for the plant and revives the soil to an organic state without the harmful factors of chemical fertilizer [66]. One of the advantages of nano fertilizers is that they can be used in very small amounts. An adult tree requires only 40–50 kg of fertilizer while an amount of 150 kg would be required for ordinary fertilizers. Nanopowders can be successfully used as fertilizers and pesticides as well [67-68]. The importance of zinc oxide NPs in the biotechnology area was investigated by Paul and Ban. They observed the effect of chemically prepared ZnO NPs on the biological system. Zinc oxide is also used at different concentrations (Streptococcus pneumonia, Bacillus subtitles, E.Coli, and Pseudomonas aeruginosa). A quick rise of enzymatic activity was found through high concentrations of zinc oxide [69].

- **Sensors**

ZnO nanostructures have been widely used for sensing applications due of their high sensitivity to the chemical environment. Nanostructures have the advantage of a high surface area, and electronic processes are strongly influenced by surface processes. ZnO nanowires have demonstrated high sensitivity even at room temperature, whereas thin-film gas sensors often need to be operated at elevated temperatures. The sensing process is governed by surface oxygen releases which influence ZnO's electronic properties [70]. By using ZnO nanorod H_2 sensor has been developed. The sensitivity is developed by sputter deposition of Pd clusters on the ZnO rod surface. The addition of Pd seems to be effective in catalytic dissociation of H_2 in atom hydrogen, increasing the sensitivity of the screening device [71]. The sensor detects hydrogen concentrations up to 10 ppm N_2 at ambient temperature, with no response to O_2. When the sensor is exposed to air or O_2, the conductivity recovers to 95% after 20 s. The same group also displayed H2 sensitivity for ZnO nanorods coated with Pt [72]. A different group used a thick film of ZnO nanoparticles for H_2 sensing.

- **Photocatalysis**

Photocatalysis is a phenomenon, in which an electron-hole pair is generated on exposure of a semiconducting material to light. The photocatalytic reactions can be categorized into two types on the basis of the appearance of the physical state of reactants. Extensive scientific work has taken place over the last few years on photocatalysis. In this process, an electron-hole pair is produced below the intensity of light through oxidation or reduction reactions occurring on the surface. The most commonly used catalysts are TiO_2 and ZnO. TiO_2 exhibits

photocatalytic activity below the intensity of UV light. ZnO provides similar or superior activity to that of TiO_2 but is less stable and less sensitive to photo corrosion. Better stability, however, is provided by zinc oxide of nanometric dimensions, which offers better crystallinity and smaller defects. The photocatalytic activity of ZnO can be further improved, and the range of the visible spectrum for zinc oxide can be extended, by adding other components [73]. With a 3.37 eV direct energy band gap, the ZnO semiconductor offers a wide range of catalytic uses in organic processes, particularly in its nanoform. The catalytic applications of ZnO include Friedel-craft reaction [74], methyl orange dye degradation [75], rhodamine B degradation [76], O-acylation of alcohol and phenol [77] and synthesis of methanol[78].Due to their outstanding biological and catalytic uses, metal oxide and conducting polymer nanocomposites have recently received attention and have been used in research on materials chemistry. Hybrid transition metal oxide and polymer nanocomposites also produced improved physical properties.

- **The Electronics and Electro technology Industries**

Zinc oxide is a new and important semiconductor with a range of electronic and electrotechnical applications. In optical emitters, its high exciton binding energy (60 meV) gives ZnO an edge over other semiconductors such as GaN if reproducible and reliable p-type doping in ZnO were to be achieved, which currently remains to be the main obstacle to the realization of bipolar devices [79]. Due to its high optical transmissivity and high conductivity, ZnO has some potential for transparent thin film transistors (TFTs) on the electronic side. Due to their excellent charge carrier transport characteristics and outstanding crystalline purity, ZnO nanowires have received a lot of interest.[80-82].Such 1-D structures have special qualities that make them potentially appealing for nanoscale electronics, including surface acoustic wave (SAW) devices, LEDs, lasers, photodetectors, chemical/biosensors, and so on[83-84].

ZnO nanorod/nanowire FET sensors could make it possible to detect a range of gas molecules and biomolecules in real time with extreme sensitivity and selectivity. The operation of a gas sensor is based on the changing of the conductivity of a nanowire FET channel and is dependent on the characteristics of the gas molecules. On oxide surfaces, ZnO's oxygen vacancies serve as n-type donors and are electrically and chemically active. The creation of compact gas sensors with extended low-power operation and sensitivity in the parts per million (ppm) range is of great interest. Typically, the resistivity change of either the nanocrystalline ZnO sheets or the nanowire channel of a FET is used to detect gas molecules.

Due to their extensive range and technological applications in the electronic and electrical industries, polymer composites' dielectric characteristics have received a lot of attention [85]. For polymer nanocomposites, zinc oxide nanoparticles are also very attractive as dielectric fillers [86]. From an application standpoint, the two main metrics that reveal how well a material performs in common applications are its dielectric constant and its dielectric loss values. Due to a relative mismatch in their interfacial characteristics, different materials exhibit distinct dielectric behaviour. Recently, a variety of ZnO/polymer nanocomposites have had their dielectric characteristics studied for a wide range of potential applications [87-88].

- **Nonlinear Applications**

Transition metal (TM) oxide nanomaterials received significant attention because of their great chemical and physical characteristics. Among this group of materials, zinc oxide (ZnO) is a suitable multifunctional one because of its cost-effective, abundance, good mechanical and chemical stability, nontoxicity, high excitonic binding energy (60 meV), large direct band gap (3.37 eV), and ability to tolerate the high electric fields, which makes it suitable for various application such as electroluminescent devices, nano-optoelectronic devices, nonlinear optical (NLO) devices like passive Q-switching, dual nonlinear dielectric resonance, sensors, solar cell and electro-optic modulators. As an essential optical process, the NLO response is the key to future photonic and optoelectronic applications such as the optical transistor, optical memory, optical wiring, and random lasing. The ZnO nanomaterials are suitable candidates for NLO applications because of the feasibility of doping them with a transition metal like Mn, Co, Cr, and Ni which influence the optical and electrical properties. Besides, as a dopant, Ni is used to improve the photocatalytic activity because of the same ionic radii and valence state. The third-order susceptibility ($\chi(3)$) is an essential parameter in the NLO characteristics of the NPs evaluations. Also, the NLO characteristics of nanomaterials are forcefully relevant to the electrical, optical, structural (surface, shapes, distributions, and crystallite sizes of the NPs) characteristics of the matter [89].

LITERATURE REVIEW

TanumoyDebnath et al synthesized the Cr doped semiconducting ZnO nanorods by hydrothermal method. The modulation of the dielectric response of undoped and Cr^{3+} ion

doped semiconducting ZnO nanoparticles is investigated. The XRD reveals it is a polycrystalline single phase of a hexagonal wurtzite structure of ZnO and the SEM specified it is a rod-like structure. In the photoluminescence measurement, no significant peak has been observed in the visible region. The frequency and temperature-dependent dielectric constants of all the samples were investigated. The consequences of the dielectric measurement suggest that the hydrothermal synthesis route influences the growth mechanism of the semiconducting nanoparticles mostly towards the rod-like structure and the doping element influences the charge density, nature of defects, and the defect densities inside the structure of ZnO nanomaterials [90].

Alan Meng et al prepared a series of Cr-doped ZnO nanoparticles with different Cr^{3+} 3 contents. The adsorption on Cr-doped ZnO was studied by kinetics, thermodynamics, and isotherm technologies which indicate the adsorption was fast and followed the pseudo-second-order model, the adsorption process was spontaneous and endothermic and it agreed well with Langmuir isotherm with a maximum adsorption capacity. Developed a simple and low-cost chemical method was developed to separate and recycle ZnO and MO from used absorbents [91].

Changle Wu et al fabricated Cr-doped ZnO nanowire by the solvothermal route. Inductively coupled plasma optical emission spectroscopy, XRD, TEM, and high-resolution TEM studies confirmed the doping of Cr into ZnO lattices. The UV analysis confirmed that pure ZnO and Cr-doped ZnO displayed a band gap absorption peak at about 365 nm. The photocatalytic studies indicated that the as-synthesized Cr-doped ZnO nanowires were a kind of promising photocatalyst in the remediation of water polluted by some chemically stable azo dyes under visible light [92].

Son Ngoc Nguyen et al studied the removal of nitrogen oxide pollution by the photocatalytic process. This paper is the first investigation of photocatalytic removal of NO under visible light over Cr doped ZnO nanoparticles. Here Cr−ZnO is synthesized by the sol-gel method with a narrow band gap. The results show that the Cr−ZnO has well NO photocatalytic degradation activity, low NO2 conversion yield, and high stability [93].

Chi-Jung Chang et al synthesized Cr-doped ZnO nanorods on glass substrate by hydrothermal method and studied photocatalysis with high catalytic activity under UV light.SEM, diffuse reflectance spectra, photoelectron chemical scanning electrochemical microscopy, and X-ray photoemission spectroscopy studies were conducted to find the effects of Cr dopant on the

surface texture, crystallinity, surface chemistry, and photo-induced charge separation and their relation with the photocatalytic degradation of Cr-doped ZnO. Adding the additional Cr dopant will enhance the separation of charge carriers in ZnO photocatalytic. The photocatalytic activity was improved due to the increase in surface oxygen vacancies, the separation of charge carriers, modification of the band gap, and the large surface area of the doped ZnO nanorods photocatalyst [94].

FalakNaz et al prepared ZnO and Cr-doped ZnO nanoparticles by co-precipitation method and the synthesized nanoparticle are characterized by FTIR, SEM, XRD, and TGA. The morphological study specifies that ZnO and Cr-doped ZnO have an irregular round shape. The XRD analysis confirms that the crystallite size of undoped ZnO and Cr-doped ZnO were 30.07 and 28.14 nm and the precursor decomposition to ZnO after annealing at 500° C was confirmed by TGA. The photodegradation study presented that the Cr-doped ZnO and undoped ZnO NPs degraded about 92 and 89% dye within 100 min, respectively. The effect of different parameters like dye initial concentration, contact time, pH, and temperature on the photocatalytic degradation of dye was studied [95].

Zinc sulphate and sodium hydroxide were used as starting ingredients in the simple precipitation approach used by Kumar et al. to create ZnO nanoparticles. X-ray diffraction (XRD), scanning electron microscopy (SEM), energy dispersive spectroscopy (EDS), and proton-induced X-ray emission (PIXE) studies were used to characterize the materials. A hexagonal ZnO wurtzite structure is revealed by the XRD diffraction peak. The excellent purity of the synthesized compounds is confirmed by the diffraction peak. As the calcination temperature rises, the peak's strength rises as well, suggesting more crystallinity. With an increase in calcination temperature, the average crystallite size grows. The temperature at which calcination takes place alters the morphologies of ZnO. The agglomerations of particles are significantly fewer in this way of preparation, as seen by the SEM pictures of ZnO samples. The sample generated using this approach has pure ZnO phases, as demonstrated by SEM-EDS examination. The materials' UV-visible absorption spectra reveal a robust maximum of absorption below 400 nm. With a rise in calcinations temperature, ZnO's band gap narrows. This is because ZnO's particle size grows as the temperature of calcinations rises. The produced substance has a high purity and is validated by PIXE analysis to contain trace amounts of elements like Fe and Ti. By raising the calcinations temperature, ZnO's band gap was reduced, and the absorption maximum was moved to longer wavelengths [96].

Zinc oxide and manganese doped zinc oxide nanoparticles have been examined for their structural, optical, photocatalytic and antibacterial properties by K. Rekha et al. They prepared polycrystalline ZnO by co-precipitation method and it is doped with Mn. The samples were characterized by X-ray diffraction (XRD). The optical spectra showed a blue shift in the absorbance spectrum with increasing dopant concentration. The photocatalytic activities of ZnO powders were evaluated by measuring the degradation of methylene blue (MB) in water under the UV region. It was found that undoped ZnO bleaches MB much faster than manganese-doped ZnO upon its exposure to UV light. EDX spectra showed the purity of the material. Mn-doped ZnO nanoparticles have better antibacterial activity than pure ones [97].

Khalafi, Tariq et al synthesized ZnO nanoparticles simply using zinc nitrate and microalgae Chlorella extract which was conducted under ambient conditions. The microalgae Chlorella extract acted as the reducing agent and a stabilizing layer on fresh ZnO NPs. The sample is characterized by UV-visible, FTIR, XRD, SEM, and TEM. XRD results demonstrated that prepared ZnO NPS has a high-crystalline hexagonal (Wurtzite) structure, with an average size of about 19.44nm in diameter. FT-IR spectral analysis indicated an active contribution of algae-derived biomolecules in zinc ions bioreduction. According to SEM and TEM observations, ZnO NPs are well dispersed and have a hexagonal shape with an average size of 20±2.2nm, respectively. Under optimum experimental conditions, gas chromatograph (GC) results revealed that as-obtained ZnO NPs demonstrate an excellent photocatalytic activity toward DBT photodegradation as a hazardous pollutant in the aquatic environment. In this study, the synthesis of ZnO NPs in a neutral aqueous solution at a gentle temperature offers a facile, non-toxic, biocompatible, and viable economic route for biological and environmental applications. The degradation rate of DBT continued almost constant after five cycle times showing higher stability and effectiveness of bio-assisted ZnO NPs [98].

Stan, Manuela et al successfully prepared ZnO particles by biological synthesis using aqueous extracts of Allium sativum (garlic), Allium cepa (onion), and Petroselinum crispum (parsley). The biomolecules involved in the biosynthetic procedure as evidenced by FTIR spectroscopy. Zn vacancy complexes and oxygen vacancies are present in all analyzed samples. A narrowing of the band gap for the ZnO prepared with plant extracts was observed as compared to that of the ZnO, prepared using solely ultrapure water. Photodegradation studies of methylene blue in an aqueous solution in the presence of UV light indicate that the

ZnO nanoparticles synthesized with plant extracts possess higher efficiency for the photodegradation of dye compared to ZnO nanoparticles [99].

Balcha et al synthesized nanosized zinc oxide (ZnO) photocatalyst powders by precipitation and sol-gel methods and were characterized by XRD and UV-Visible spectroscopic techniques. The powder synthesized by the sol-gel method has a smaller crystallite size and higher wavelength photo absorption when compared to that prepared by the precipitation method. Photocatalytic degradation of Methylene blue increases up to a limiting value as the increase in catalyst load and then decreases at higher catalyst concentrations. ZnO nanostructures of higher aspect ratio and intentional inclusion of defects can lead to even higher photocatalytic activity by appropriately modifying the synthetic routes. This study offers a low-cost eco-friendly solution to the water purification problem [100].

Bharat et al studied doping of ZnO nanoparticles using distinct dopants by various techniques, respective changes in properties, and feasible applications. Doped ZnO nanostructures are multifunctional materials that can exhibit photocatalysis in an aqueous medium for deterioration of various exotic dyes released into water bodies by industries with or without illuminating, generating hydrogen which can solve energy as well as environmental issues, sense toxic gases, assist in the development of cheap and efficient solar, fuel cells and play an important role in the field of spintronics, medicine, photoluminescence [101].

Kezhen et al studied the application of photocatalytic degradation and the antibacterial properties of zinc oxide (ZnO) nanomaterials. This paper reviews various methods to modify ZnO nanomaterials and improve the photocatalytic degradation of organic pollutants. ZnO NP applications are limited by their low toxicity to some bacterial species. The development of ZnO-based antimicrobial agents as an alternative to traditional antibiotics may be promising materials for future applications in pharmaceutics and medicine [102].

Sirelkhatim et al, discussed and analyse research works that addressed the potential use of ZnO-NPs for antibacterial activity. The factors like UV illumination, ZnO particle size, concentration, morphology, and surface modification, powerful antibacterial influence a variety of toxicity mechanisms. ZnO-NPs possess unique properties and excellent stability with long life compared with organic-based disinfectants that stimulated its use as an antibacterial agent. The large surface area-to-volume ratio allows their use as novel antimicrobial agents. ZnO-NPs can act as a smart weapon toward multidrug-resistant

microorganisms and a talented substitute approach to antibiotics. The toxicological influence of ZnO-NPs should be evaluated to determine the consequences of using these NPs in food safety [103].

Rajalakshmi et al, investigated the effect of confinement on optical phonons of different symmetries in the nanoparticles of zinc oxide with wurtzite structure using Raman spectroscopy. Raman scattering revealed the pieces of evidence for confined optic phonons. An optical phonon confinement model is used for calculating the theoretical line shapes, which exhibit different asymmetric broadening and shifts, depending on the symmetries of phonon and their dispersion curves. They found that the effect of phonon confinement is depending on the symmetry of the phonons [104].

Siddiqi et al studied the Properties of Zinc Oxide Nanoparticles and their activity against Microbes. Zinc oxide microcrystals are very efficient light absorbers in the UVA and UVB region of spectra due to the wide bandgap. The impact of zinc oxide on biological functions depends on its morphology, particle size, exposure time, concentration, pH, and biocompatibility. It has been confirmed from SEM and TEM images of the bacterial cells that zinc oxide nanoparticles disintegrate the cell membrane and accumulate in the cytoplasm where they interact with biomolecules causing cell apoptosis and leading to cell death [105].

Wang et al synthesized ZnO nanoparticles with a chemical composition method by controlled morphology. It forms a spherical or rod-like shape of zinc oxide. The sample is analyzed using IR, SEM, XRD, and TGA techniques. Using the FIS technique it is possible to prepare a uniform powder with a particle size smaller than that obtained for the synthesis of powders from solution under the same conditions. . Compared with conventional solution methods, this technique avoids large concentration gradients and gives better control of the particle growth in chemical processing systems. As precipitation is carried out at a low concentration, agglomeration is reduced, while when the reactant concentration is high, a high particle number density results, and agglomeration is observed [106].

Fakhari et al, synthesized zinc oxide nanoparticles with green synthesis using Laurus nobilis L. leaves, and the sample is characterized by Ultraviolet-Visible spectroscopy (UV–Vis), Fourier Transform Infrared Spectroscopy (FT-IR), X-Ray Diffraction analysis (XRD), Energy-Dispersive X-ray analysis (EDX) and Scanning Electron Microscopy (SEM). UV–Visible absorption spectrum gives peak due to their large excitation binding energy and the band gap increases on decreasing particle size. The XRD results confirmed the efficiency of

the synthesis process, evidencing the production of single crystalline ZNPs with a hexagonal wurtzite structure. the average size of ZNPs synthesized by zinc acetate and zinc nitrate was found to be bullets and flower-like structures which were confirmed by XRD and SEM analyses. EDX results confirmed the presence of zinc and oxygen and FT-IR studies indicated that the plant extract contains various photochemical, which work as capping and stabilizing agents for the synthesized ZNPs [107].

Alessio Becheri et al, report the synthesis and characterization of nanosized zinc oxide particles and their application on cotton and wool fabrics for UV shielding. They were prepared ZNPs through a homogeneous phase reaction starting from zinc chloride and sodium hydroxide at high temperature, in water, or 1,2-ethanediol, and the sample is studied through electron microscopy, X-ray diffraction, FTIR, and specific surface area experiments. The UV tests indicate a significant increment of the UV absorbing activity in the ZnO-treated fabrics. Such results can be exploited for the protection of the body against solar radiation and other technological applications [108].

Agarwal et al, give a review on green synthesis of zinc oxide nanoparticles – An eco-friendly approach. Green sources act as both stabilizing and reducing agents for the synthesis of shape and size-controlled nanoparticles. The plant-based nanoparticle can have huge applications in the field of food, pharmaceutical, and cosmetic industries and thus become a major area of research [109].

Ramimoghadam et al, synthesized Zinc oxide nanoparticles by hydrothermal method using rice as a soft bio-template. This bio-template is used to modify the shape and size of zinc oxide particles. Different types of morphologies were obtained like a flower, flake, rose, star, and rod-like. Pore size and texture of the resulting zinc oxide particles were found to be template-dependent and the resulting specific surface area was enhanced compared to the zinc oxide synthesized without rice under the same condition [110].

Sonima Mohan et al, synthesized ZNPs by the hydrothermal method in different reaction conditions. The sample is characterized by FTIR, XRD, SEM, and TEM, Thermo gravimetric analysis (TGA), PL, and UV. The FTIR confirms the effect of reaction parameters on vibrations of various functional groups. The sample has the structure of nanoflowers and nanorods which shows photoluminescence, UV absorption, and a suitable band gap. It is understood that based on their optical properties and thermal stability we can

propose hydrothermally synthesized nanorods and nanoflowers for different layers of solar-cell [111].

Mahendiran et al, synthesized zinc oxide nanoparticles by simple hydrothermal method and characterized by X-ray Diffraction (XRD), High resolution scanning electron microscope (HR-SEM), UV-Visible spectroscopy (UV-Vis) Fourier Transform Infrared Spectroscopy (FT-IR) and Dielectric studies. The dielectric constant, dielectric loss and ac conductivity obtained from the dielectric studies showed the electric properties of the zinc oxide nanoparticles [112].

Objectives

- To synthesize ZnO and Cr doped ZnO (2,4%) nanorods using Hydrothermal method
- To study the structural optical and morphological features of samples using XRD, UV visible spectroscopy and FESEM
- To analyze vibrational bands and functional groups by Raman and FTIR.
- To understand the Oxidation state of samples through XPS
- Investigate the Nonlinear and photocatalytic properties

References

[1]- Nano_Materials-A.K.Bandyopadhyay New Age Publishers (1)

[2]- http://crnano.org/benefits.htm

[3]- Bayda, S., Adeel, M., Tuccinardi, T., Cordani, M., & Rizzolio, F. (2019). *The History of Nanoscience and Nanotechnology: From Chemical–Physical Applications to Nanomedicine. Molecules, 25(1), 112.* doi:10.3390/molecules25010112 10.3390/molecules25010112

[4]-https://en.wikipedia.org/wiki/History_of_nanotechnology

[5]-https://en.wikipedia.org/wiki/Sumio_Iijima

[6]-https://www.azonano.com/article.aspx?ArticleID=4843

[7]- Han, Jie; Globus, Al; Jaffe, Richard; Deardorff, Glenn (1997). Molecular dynamics simulations of carbon nanotube-based gears. Nanotechnology, 8(3), 95–102. doi:10.1088/0957-4484/8/3/001

[8]- Rita John, Solid State Physics, McGraw Hill Publications, (2014), Edition 13

[9]- Daniel L. Schodek, Paulo Ferreira, Michael F. Ashby - Nanomaterials, Nanotechnologies and Design_ An Introduction for Engineers and Architects-Butterworth-Heinemann (2009)

[10]- S. Szunerits, R. Boukherroub, in Encyclopedia of Interfacial Chemistry, 2018

[11]- https://en.wikipedia.org/wiki/Lustreware

[12]- Singh, V., Yadav, P., & Mishra, V. (2020). *Recent Advances on Classification, Properties, Synthesis, and Characterization of Nanomaterials. Green Synthesis of Nanomaterials for Bioenergy Applications, 83–97.* doi:10.1002/9781119576785.ch3 10.1002/9781119576785.ch3

[13]-.Dan Guo[1], Guoxin Xie[1] and Jianbin Luo[1]

[14]-Published 3 December 2013 • © 2014 IOP Publishing LtdJournal of Physics D: Applied Physics, Volume 47, Number 1Citation Dan Guo *et al* 2014 *J. Phys. D: Appl. Phys.* 47 013001

[15]-https://doi.org/10.1016/j.arabjc.2017.05.011Khan, Ibrahim; Saeed, Khalid; Khan, Idrees (2017). Nanoparticles: Properties, Applications and Toxicities. Arabian Journal of Chemistry, (), S1878535217300990–. doi:10.1016/j.arabjc.2017.05.011

[16]- Vincenzo Amendola[1,2], Roberto Pilot[1,2], Marco Frasconi[1], Onofrio M Maragò[3] and Maria Antonia Iatì[3] Published 20 April 2017 • © 2017 IOP Publishing Ltd Journal of Physics: Condensed Matter, Volume 29, Number 20 Citation Vincenzo Amendola et al 2017 J. Phys.: Condens. Matter 29 203002

[17]-Vatta, L. L., Sanderson, R. D., & Koch, K. R. (2006). *Magnetic nanoparticles: Properties and potential applications. Pure and Applied Chemistry, 78(9), 1793–1801.* doi:10.1351/pac200678091793 10.1351/pac200678091793

[18]-https://doi.org/10.1016/j.tibtech.2012.06.004 Mohammad J. Hajipour; Katharina M. Fromm; Ali Akbar Ashkarran; Dorleta Jimenez de Aberasturi; Idoia Ruiz de Larramendi; Teofilo Rojo; Vahid Serpooshan; Wolfgang J. Parak; Morteza Mahmoudi

(2012). Antibacterial properties of nanoparticles. , 30(10), – . doi:10.1016/j.tibtech.2012.06.004

[19]-N. A. Smirnov, S. I. Kudryashov, A. A. Nastulyavichus, A. A. Rudenko, I. N. Saraeva, E. R. Tolordava, S. A. Gonchukov, Yu M. Romanova, A. A. Ionin and D. A. Zayarny, "Antibacterial properties of silicon nanoparticles", IOP Publishing, Laser Phy. Lett. 15, (2018), 105602.

[20]-Marwath M. Mohamed, Shereen A. Fouad, Hisham A. Elshoky, Gina M. Mohamed and Taher A. Salaheldin, "Antibacterial effect of gold nanoparticles against Corynebacterium pseudotuberculosis", International Journal of Veterinary Science and Medicine, Vol. 5, (2017), Issue – 1, 23-29. https://doi.org/10.1016/j.ijvsm.2017.02.003

[21]- Lee, S., Choi, S. U.-S., Li, S., & Eastman, J. A. (1999). *Measuring Thermal Conductivity of Fluids Containing Oxide Nanoparticles. Journal of Heat Transfer, 121(2), 280.* doi:10.1115/1.2825978

[22]- Volume 2014 |ArticleID 431787 | https://doi.org/10.1155/2014/431787
Rizwan, M., Singh, M., Mitra, C. K., & Morve, R. K. (2014). Ecofriendly Application of Nanomaterials: Nanobioremediation. Journal of Nanoparticles, 2014, 1-7. doi:10.1155/2014/431787

[23]-https://doi.org/10.2217/nnm-2020-0117Nikaeen, G., Abbaszadeh, S., & Yousefinejad, S. (2020). Application of nanomaterials in treatment, anti-infection and detection of coronaviruses. Nanomedicine, 15(15), 1501–1512. doi:10.2217/nnm-2020-0117

[24]-https://doi.org/10.3390/nano10091764Saleem, H., & Zaidi, S. J. (2020). Developments in the Application of Nanomaterials for Water Treatment and Their Impact on the Environment. Nanomaterials, 10(9), 1764. doi:10.3390/nano10091764.

[25]-FABRICATION OF NANOMATERIALS BY TOP-DOWNAND BOTTOM-UP APPROACHES – AN OVERVIEW Dr. V.M.Arole1, Prof.S.V.Munde2 JAAST:Material Science (Special Issue) December – 2014 Vol. 1|Issue 2|Page 89-93

[26] Sciencedirect.com/topics/chemistry/ball milling

[27]-en.wikipedia.org/wiki/Electron-beam-lithography

[28]-tandfonline.com/doi/full/10.1080/23746149.2016.1142828

[29]-hindawi.com/journals/amse/2021/5102014

[30] Sciencedirect.com/topic/materials-science/electrodeposition

[31]- Yan, M. F. (1991). Zinc Oxide. Concise Encyclopedia of Advanced Ceramic Materials, 523–525. doi:10.1016/b978-0-08-034720-2.50144-1

[32]- AzoNano 2013 Zinc Oxide (ZnO) Nanoparticles—Properties, Application

[33]-Rajeshkumar, S., Lakshmi, T., & Naik, P. (2019). Recent advances and biomedical applications of zinc oxide nanoparticles. Green Synthesis, Characterization and Applications of Nanoparticles, 445–457. doi:10.1016/b978-0-08-102579-6.00019-8

[34]- ZnO-(a,) G. C. Yi, C. Wang, and W. II. Park. Semicond. Sci. Technol, 20:S22, (2005).

[35]- Hingorani S, et al. Microemulsion mediated synthesis of zinc-oxide nanoparticles for varistor studies. Mater Res Bull 1993;28(12):1303–10.

[36]-Singhai M, et al. Synthesis of ZnO nanoparticles for varistor application using Znsubstituted aerosol OT microemulsion. Mater Res Bull 1997;32(2):239–47.

[37]- Z. Qiuxiang, Y. Ke, B. Wei, W. Qingyan, X. Feng, Z. Ziqiang, D. Ning, and S. Yan. Mater. Lett., 61:3890, (2007).

[38]- Mohd AMA, Julkapli NM, Abd HSB. Review on ZnO hybrid photocatalyst: impact on photocatalytic activities of water pollutant degradation. Rev Inorg Chem 2016;36:77–104. https://doi.org/10.1515/revic-2015-0015.

[39]- S. Dutta, M. Chakrabarti, S. Chattopadhyay, D. Jana, D. Sanyal, and A. Sarkar. J.Appl.Phys., 98:053513, (2005).

[40]- S. Chattopadhyay, S. Dutta, A. Banerjee, D. Jana, S. Bandyopadhyay, S.Chattopadhyay, and A. Sarkar. Physica B, 404:59, (2009).

[41]- S. Dutta, S. Chattopadhyay, D. Jana, A. Banerjee, S. Manik, S. K. Pradhan, M.Sutradhar, and A. Sarkar. J. Appl. Phys., 100:114328, (2006).

[42]- Z. Hui, Y. Deren, M. Xiangyang, J. Yujie, X. Jin, and Q. Duanlin. Nanotechnology,15:622, (2004).

[43]- J. Zhang, L. D. Sun, J. L. Yin, H. L. Su, C. S. Liao, and C. H. Yan. Chem. Mater.,14:4172, (2002).

[44] -Q. P. Zhong and E. Matijevic. J. Mater. Chem, 3:443, (1996).

[45]- W. Lingna and M. Mamoun. J. Mater. Chem, 9:2871, (1999). [16] D. W. Bahnemann, C. Kormann, and M. R. Hoffmann. J.Phys. Chem., 91:3789,(1987).

[46]- C. Y. Lee, T. Y. Tseng, S. Y. Li, and P. Lin. J. Appl. Phys., 99:024303, (2006).

[47]-Galsin, J. S. (2019). Crystal Structure of Solids. Solid State Physics, 1–36. doi:10.1016/b978-0-12-817103-5.00001-3

[48]-Grosso, G., & Parravicini, G. P. (2014). Geometrical Description of Crystals: Direct and Reciprocal Lattices. Solid State Physics, 67–105. doi:10.1016/b978-0-12-385030-0.00002-5

[49]-T. Olorunyolemi, A. Birnboim, Y. Carmel, O. C. Wilson, Jr and I. K. Lloyd, J. Am.Ceram. Soc. 85, 1249 (2002).

[50]- B. K. Meyer, H. Alves, D. M. Hofmann, W. Kriegseis, D. Forster, F. Bertram, J. Christen, A. Hoffmann, M. Straßburg, M. Dworzak, U. Haboeck, A. V. Rodina, Phys. Stat. Sol. (b) 241 (2004) 231.

[51]- Coleman, V.A. (2006). Zinc Oxide Bulk, Thin Films and Nanostructures ‖ Basic Properties and Applications of ZnO. , (), 1–20. doi:10.1016/b978-008044722-3/50001-4

[52]- S. Adachi, Properties of Group-IV, III-V and II-VI Semiconductors, John Wiley and Sons, Ltd, West Sussex, England, 2005.

[53]-Endoh, R., Awaka, J., & Nagata, S. (2003). *Ferromagnetism and the metal-insulator transition in the thiospinelCu(Ir1−xCrx)2S4. Physical Review B, 68(11).* doi:10.1103/physrevb.68.115106 10.1103/PhysRevB.68.115106

[54]- Chennupati Jagadish and Stephen J.Pearton "Zinc Oxide Bulk, Thin films and edition (2006).

[55]-Shishir, R. S., & Ferry, D. K. (2009). *Velocity saturation in intrinsic graphene. Journal of Physics: Condensed Matter, 21(34), 344201.* doi:10.1088/0953-8984/21/34/344201 10.1088/0953-8984/21/34/344201

[56]-https://core.ac.uk/download/pdf/53186969.pdf

[57] -Xiong HM, Liu DP, Xia YY, Chen JS (2005) Chem Mater 17:3062

[58]-]-H.-M. Xiong; Z.-D. Wang; Y.-Y. Xia (2006). Polymerization Initiated by Inherent Free Radicals on Nanoparticle Surfaces: A Simple Method of Obtaining Ultrastable (ZnO)Polymer Core–Shell Nanoparticles with Strong Blue Fluorescence. , 18(6), 748–751. doi:10.1002/adma.200501899

[59]-Share Donald R.Askeland, Pradeep P. Phule Essential of material for science and Engineering (2004,CL-Engineering)-libgen.ln.pdf

[60]-S. E. McNeil, J. Leukoc Biol. 78, 585 (2005).

[61]-J. K. Jaiswal and S. M. Simon, Trends Cell Biol. 14, 497 (2004).

[62]-T. K. Jain, M. A. Morales, S. K. Sahoo, D. L. Leslie-Pelecky, and V. Labhasetwar, Molecular Pharmaceutics 2, 194 (2005).

[63]-R. K. Visaria, R. J. Griffin, B. W. Williams, E. S. Ebbini, G. F. Paciotti, C. W. Song, and J. C. Bischof, Mol. Cancer Ther. 5, 1014 (2006).

[64]-Mohammad Vaseem1, Ahmad Umar2, Yoon-Bong Hahn1 1School of Semiconductor and Chemical Engineering and BK21 Centre for Future Energy, Materials and Devices,

Chonbuk National University, Chonju 561-756, South Korea 2Department of Chemistry, Faculty of Science, Advanced Materials and Nano-Engineering Laboratory (AMNEL), Najran University, P. O. Box 1988, Najran 11001, Kingdom of Saudi Arabia

[65]- J.M.RajwadeaM.D.OakbK.M.Paknikara Nanobioscience Group, Agharkar Research Institute, Pune, India, Genetics and Plant Breeding Group, Agharkar Research Institute, Pune, India https://doi.org/10.1016/B978-0-12-822836-4.00016-1

[66]-Sabir, S., Arshad, M., & Chaudhari, S. K. (2014). Zinc Oxide Nanoparticles for Revolutionizing Agriculture: Synthesis and Applications. The Scientific World Journal, 2014, 1–8. doi:10.1155/2014/925494

[67]- V. N. Selivanov and E. V. Zorin, "Sustained Action of ultrafine metal powders on seeds of grain crops," Perspekt. Materialy, vol. 4, pp. 66–69, 2001.

[68]-O. P. Raikova, L. A. Panichkin, and N. N. Raikova, "Studies on the effect of ultrafine metal powders produced by different methods on plant growth and development. Nanotechnologies and information technologies in the 21st century," in Proceedings of the International Scientific and Practical Conference, pp. 108– 111, Moscow, Russia, 2006.

[69]-(Prasad J.el al Journal of plant nutrition 35(6) 2012

[70]- Schmidt-Mende, L., & MacManus-Driscoll, J. L. (2007). ZnO – nanostructures, defects, and devices. Materials Today, 10(5), 40–48. doi:10.1016/s1369-7021(07)70078-0

[71]-Wang, H. T., et al., Appl. Phys. Lett. (2005) 86, 243503

[72]-Tien, L. C., et al., Appl. Phys. Lett. (2005) 87, 222106

[73]-Pauli s and Ban ,DK, international journal of advances in chemical engineering and biological sciences (IJACEBS),2014

[74]-M.H. Sarvari, H. SharghiReactions on a solid surface. A simple, economical and efficient friedel−crafts acylation reaction over zinc oxide (ZnO) as a new catalyst J. Organomet. Chem., 69 (2004), pp. 6953-6956.

[75]-X. Xu, X. Duan, Z. Yi, Z. Zhou, X. Fan, Y. Wang Photocatalytic production of superoxide ion in the aqueous suspensions of two kinds of ZnO under simulated solar light Catal. Commun., 12 (2010), pp. 169-172

[76]-G. Zhang, X. Shen, Y. Yang Facile synthesis of monodisperse porous ZnO spheres by a soluble starch-assisted method and their photocatalytic activity J. Phys. Chem. C, 115 (2011), pp. 7145-7152.

[77]-F.M. Moghaddam, H. Saeidian Controlled microwave-assisted synthesis of ZnO nanopowder and its catalytic activity for O-acylation of alcohol and phenol Mater. Sci. Eng. B, 139 (2007), pp. 265-269

[78]-J. Strunk, K. Kähler, X. Xia, M. Muhler The surface chemistry of ZnO nanoparticles applied as heterogeneous catalysts in methanol synthesis Surf. Sci., 603 (2009), pp. 1776-1783

[79]-Özgür, Ü., Hofstetter, D., & Morkoç, H. (2010). ZnO Devices and Applications: A Review of Current Status and Future Prospects. Proceedings of the IEEE, 98(7), 1255–1268. doi:10.1109/jproc.2010.2044550 10.1109/JPROC.2010.2044550

[80]- P. C. Chang, Z. Fan, C. J. Chien, D. Stichtenoth, C. Ronning, and J. G. Lu, BHigh-performance ZnO nanowire field effect transistors,[Appl. Phys. Lett., vol. 89, pp. 133113-1–133113-3, Sep. 2006.

[81]-W. I. Park, J. S. Kim, G.-C. Yi, M. H. Bae, and H.-J. Le, BFabrication and electrical characteristics of high-performance ZnO nanorod field-effect transistors,[Appl. Phys. Lett., vol. 85, pp. 5052–5054, Nov. 2004

[82]- Z. Fan and J. G. Lu, BElectrical properties of ZnO nanowire field effect transistors characterized with scanning probes,[Appl. Phys. Lett., vol. 86, pp. 032111-1–032111-3, Jan. 2005

[83]- Q. Wan, Q. H. Li, Y. J. Chen, T. H. Wang, X. L. He, J. P. Li, and C. L. Lin, BFabrication and ethanol sensing characteristics of ZnO nanowire gas sensors,[Appl. Phys. Lett., vol. 84, pp. 3654–3656, Apr. 2004.

[84]-C. H. Liu, J. A. Zapien, Y. Yao, X. M. Meng, C. S. Lee, S. S. Fan, Y. Lifshitz, and S. T. Lee, BHigh-density, ordered ultraviolet light-emitting ZnO nanowire arrays,[Adv. Mater., vol. 15, pp. 838–841, May 2003.

[85]-K. Deshmukh, M.B. Ahamed, R.R. Deshmukh, S.K.K. Pasha, K.K. Sadasivuni, D. Ponnamma, K. Chidambaram Synergistic effect of vanadium pentoxide and graphene oxide in polyvinyl alcohol for energy storage application Eur. Polym. J., 76 (2016), pp. 14-27

[86]-E. Helal, C. Pottier, E. David, M. Frechette, N.R. Demarquette Polyethylene/thermoplastic elastomer/zinc oxide nanocomposites for high voltage insulation applications: Dielectric, mechanical and rheological behavior Euro Polym. J., 100 (2018), pp. 258-269

[87]-G. Wang, Y. Deng, Y. Xiang, L. Guo Fabrication of radial ZnO nanowire clusters and radial ZnO/PVDF composites with enhanced dielectric properties Adv. Funct. Mater., 18 (2008), pp. 2584-2592

[88]-G.S. Wang, Y.Y. Wu, X.J. Zhang, Y. Li, L. Guo, M.S. Cao Controllable synthesis of uniform ZnO nanorods and their enhanced dielectric and absorption properties J. Mater. Chem. A, 2 (2014), pp. 8644

[89] Mabhouti, K., & Norouzzadeh, P. (2021). Notes on linear and non-linear optical characteristics of the nickel and manganese doped zinc oxide nanoparticles. *Optik*, *231*, 166465.

[90]-.https://doi.org/10.1063/1.5017792Tanumoy Debnath,1,2 Papiya Saha,1,2 Nesla Patra,1 Sukhen Das,2 and Soumyaditya Sutradhar1,a)

[91]- http://pubs.acs.org on December 3, Alan Meng, Jing Xing, Z. J. Li, and Qingdang Li

[92]-https://doi.org/10.1016/j.matlet.2011.03.070Wu, C., Shen, L., Zhang, Y.-C., & Huang, Q. (2011). Solvothermal synthesis of Cr-doped ZnO nanowires with visible-light-driven photocatalytic activity. Materials Letters, 65(12), 1794–1796. doi:10.1016/j.matlet.2011.03.070

[93]-https://doi.org/10.1021/acsomega.9b01628 Nguyen, S. N., Truong, T. K., You, S.-J., Wang, Y.-F., Cao, T. M., & Pham, V. V. (2019). Investigation on Photocatalytic Removal of NO under Visible Light over Cr-Doped ZnO Nanoparticles. ACS Omega, 4(7), 12853–12859. doi:10.1021/acsomega.9b01628

[94]-https://doi.org/10.1016/j.jssc.2013.09.039 Chang, C.-J., Yang, T.-L., &Weng, Y.-C. (2014). Synthesis and characterization of Cr-doped ZnOnanorod-array photocatalysts with improved activity. Journal of Solid State Chemistry, 214, 101–107. doi:10.1016/j.jssc.2013.09.039

[95]- https://doi.org/10.1080/24701556.2020.1749657Naz, F., & Saeed, K. (2020). Investigation of photocatalytic behavior of undoped ZnO and Cr-doped ZnO nanoparticles for the degradation of dye. Inorganic and Nano-Metal Chemistry, 1–11. doi:10.1080/24701556.2020.1749657

[96]-Kumar, S.S., Venkateswarlu, P., Rao, V.R. et al. Synthesis, characterization and optical properties of zinc oxide nanoparticles. Int Nano Lett 3, 30 (2013). https://doi.org/10.1186/2228-5326-3-30

[97]- K. Rekha; M. Nirmala; Manjula G. Nair; A. Anukaliani (2010). Structural, optical, photocatalytic, and antibacterial activity of zinc oxide and manganese doped zinc oxide nanoparticles. , 405(15), 3180–3185. doi:10.1016/j.physb.2010.04.042

[98]- Khalafi, Tariq; Buazar, Foad; Ghanemi, Kamal (2019). Phycosynthesis and Enhanced Photocatalytic Activity of Zinc Oxide Nanoparticles Toward Organosulfur Pollutants. Scientific Reports, 9(1), 6866–. doi:10.1038/s41598-019-43368-3

[99]- Stan, Manuela; Popa, Adriana; Toloman, Dana; Dehelean, Adriana; Lung, Ildiko; Katona, Gabriel (2015). Enhanced photocatalytic degradation properties of zinc oxide nanoparticles synthesized by using plant extracts. Materials Science in Semiconductor Processing, 39(), 23–29. doi:10.1016/j.mssp.2015.04.038

[100]- Balcha, Abebe; Yadav, Om Prakash; Dey, Tania (2016). Photocatalytic degradation of methylene blue dye by zinc oxide nanoparticles obtained from precipitation and sol-gel methods. Environmental Science and Pollution Research, (), –. doi:10.1007/s11356-016-7750-6

[101]- Bharat, T.C.; Shubham; Mondal, S.; S.Gupta, H.; Singh, P.K.; Das, A.K. (2019). Synthesis of Doped Zinc Oxide Nanoparticles: A Review. Materials Today: Proceedings, 11(), 767–775. doi:10.1016/j.matpr.2019.03.041

[102]- Qi, Kezhen; Cheng, Bei; Yu, Jiaguo; Ho, Wingkei (2017). Review on the improvement of the photocatalytic and antibacterial activities of ZnO. Journal of Alloys and Compounds, (), S0925838817328712–. doi:10.1016/j.jallcom.2017.08.142

[103]- Sirelkhatim, Amna; Mahmud, Shahrom; Seeni, Azman; Kaus, Noor Haida Mohamad; Ann, Ling Chuo; Bakhori, Siti Khadijah Mohd; Hasan, Habsah; Mohamad, Dasmawati (2015). Review on Zinc Oxide Nanoparticles: Antibacterial Activity and Toxicity Mechanism. Nano-Micro Letters, 7(3), 219–242. doi:10.1007/s40820-015-0040-x

[104]- Rajalakshmi, M.; Arora, Akhilesh K.; Bendre, B. S.; Mahamuni, Shailaja (2000). Optical phonon confinement in zinc oxide nanoparticles. , 87(5), 2445–0. doi:10.1063/1.372199

[105]- Siddiqi, Khwaja Salahuddin; ur Rahman, Aziz; Tajuddin, ; Husen, Azamal (2018). Properties of Zinc Oxide Nanoparticles and Their Activity Against Microbes. Nanoscale Research Letters, 13(1), 141–. doi:10.1186/s11671-018-2532-3

[106]- Wang, Lingna; Muhammed, Mamoun (1999). Synthesis of zinc oxide nanoparticles with controlled morphology. Journal of Materials Chemistry, 9(11), 2871–2878. doi:10.1039/A907098B

[107]- Fakhari, Shabnam; Jamzad, Mina; Kabiri Fard, Hassan (2019). Green synthesis of zinc oxide nanoparticles: a comparison. Green Chemistry Letters and Reviews, 12(1), 19–24. doi:10.1080/17518253.2018.1547925

[108]-Alessio Becheri; Maximilian Dürr; Pierandrea Lo Nostro; Piero Baglioni (2008). Synthesis and characterization of zinc oxide nanoparticles: application to textiles as UV-absorbers. , 10 (4), 679–689. DOI: 10.1007 / s11051-007-9318-3

[109]- Agarwal, Happy; Venkat Kumar, S.; Rajeshkumar, S. (2017). A review on green synthesis of zinc oxide nanoparticles – An eco-friendly approach. Resource-Efficient Technologies, (), S2405653717300283–. doi:10.1016/j.reffit.2017.03.002

[110]- Ramimoghadam, Donya; Bin Hussein, Mohd; Taufiq-Yap, Yun (2013). Hydrothermal synthesis of zinc oxide nanoparticles using rice as soft biotemplate. Chemistry Central Journal, 7(1), 136–. doi:10.1186/1752-153X-7-136

[111]- Sonima Mohan[1,2], Mini Vellakkat[4,1], Arun Aravind[3] and Reka U[1.] Published 30 November 2020 • © 2020 The Author(s). Published by IOP Publishing Ltd Hydrothermal synthesis and characterization of Zinc Oxide nanoparticles of various shapes under different reaction conditions, Nano Express, Volume 1, Number 3Citation Sonima Mohan et al 2020 Nano Ex. 1 030028

[112]- Mahendiran, M.; Asha, A.; Madhavan, J.; Victor Antony Raj, M. (2019). Structural and Optical Analysis of 1D Zinc Oxide Nanoparticles Synthesized Via Hydrothermal Method. Materials Today: Proceedings, 8(), 412–418. doi:10.1016/j.matpr.2019.02.130

CHAPTER-2

SYNTHESIS AND CHARACTERIZATION TECHNIQUES

2.1 SYNTHESIS METHOD

With a wide range of uses as a semiconductor, magnetic material, nanostructure varistor, thermoelectric material, gas sensor, cosmetic ingredient, etc., zinc oxide is regarded as a substance of technological prodigiousness. Ultraline oxide nanoparticles can be made using a variety of synthesis techniques, including sol-gel, spray pyrolysis, chemical vapour deposition, precipitation method, hydrothermal approach, etc. Here, we prepare the ZnO material using a hydrothermal technique. The initial pH of the medium, the length, temperature, and pressure of the synthesis process all define the kinetics of the process and the characteristics of the products that are produced.

- **Synthesis Procedure**

The precursors zinc acetate hexahydrate (Zn $(CH_3CO_2)_2.2H_2O$, Sigma Aldrich 99%), and chromium nitrate ($Cr(NO_3)_3$ Sigma Aldrich, 99.9%)are used to prepare both pure and doped ZnO nanoparticles. 1M Zinc acetate is dissolved in 40 ml of Di water and it is stirring for some time. The pH of the solution is standardised to 10 by adding ammonia. The final solution is then transferred to 100 ml Teflon beaker, keep it in an autoclave, and then place it in a hydrothermal oven at 180°C for 5 hrs. After the autoclave has naturally cooled down, centrifugation is done to separate the precipitate and dry it for 10 hours at 70°C in an oven. Obtained powder is grinded well to get fine. The same procedure is repeated for doped samples by adding required amount of ($Cr(NO_3)_3$in Zinc acetate solution.

Photocatalytic dye degradation is analysed using methyleneblue (MB) as a model dye under sunlight. 150ml of dye solution is prepared and 10mg of the photocatalyst is added to this solution and dissolved. The dye solution is kept under sunlight after reaching adsorption-desorption equilibrium. Degradation efficiency is analysed in regular intervals. The dye degradation efficiency is given as,

$$\eta = \frac{C_o - C_e}{C_0} X100 \ldots\ldots\ldots\ldots (2.10)$$

where Co and Ce represent initial and final concentrations of dye after irradiation

2.2 X-Ray Diffraction

A non-destructive method for examining the structure of materials, primarily at the atomic or molecular level, is X-ray diffraction (XRD). It can also be used to examine non-crystalline materials, but it performs best for materials that are crystalline or partially crystalline, that is, those have periodic structural order [1].The method is frequently referred to as "x-ray powder diffraction" because the substance being examined is frequently uniformly processed to a fine powder. When light strikes an obstruction, an aperture, or the edge of an object, it gently bends, which is known as diffraction. The extent to which it happens is determined by how big a wavelength is in relation to how big an obstruction or aperture is [2].William Henry Bragg argued in 1907 that X-rays were not electromagnetic radiation because of their particle-like characteristics, such as the ionisation of gases. Since Max von Laue's finding of X-ray diffraction in 1912 disproved Bragg's theory, most scientists now agree that X-rays constitute an electromagnetic radiation [3].

❖ Principle of X-Ray Diffraction

Constructive interference between monochromatic X-rays and a crystalline sample is the foundation of X-ray diffraction. A cathode ray tube produces the X-rays, which are then filtered to produce monochromatic radiation, focused by collimation, and pointed at the sample. Atomic electrons in a crystal are thrown into vibration when a monochromatic x-ray event occurs on it. Acceleration occurs with the same frequency as the incident ray's frequency. Then, these accelerated electrons radiate in all directions at the same frequency as the incident x-rays. If the incident radiation's wavelength is greater than the crystal's dimensions, the radiated X-rays will be in phase with each. However, the atomic size is almost equivalent to the X-ray wavelength [4].

When the circumstances are in accordance with Bragg's Law (n=2d sin), the interaction of the incident rays with the sample results in constructive interference (and a diffracted ray). This law establishes a connection between the lattice spacing and diffraction angle in a crystalline sample and the wavelength of electromagnetic radiation. When the conditions are as described by Bragg's Law (n=2d sin), constructive interference is produced by the interaction of the incident rays with the sample (and a diffracted ray). This law establishes a relationship between the wavelength of electromagnetic radiation and the lattice spacing and diffraction angle in a crystalline sample. This is often accomplished by comparing the d-

spacing with accepted reference patterns. The production of X-rays in an X-ray tube is the foundation of all diffraction techniques. The sample is hit with these X-rays, and the diffracted rays are captured. The angle between the incident and diffracted rays is a crucial factor in all types of diffraction. Beyond this, the apparatus for powder and single crystal diffraction differs [5].

❖ Instrumentation

In a cathode ray tube, X-rays are produced by burning a filament to produce electrons, accelerating the electrons with a voltage toward a target, and then hitting the target material with the accelerated electrons. Characteristic X-ray spectra are created when electrons have enough energy to knock off the target material's inner shell electrons. The most prevalent K_α and K_β components in these spectra are among a number of others. Kα is made up in part of $K_{\alpha 1}$ and $K_{\beta 2}$. $K_{\alpha 1}$ is twice as intense and has a slightly shorter wavelength than $K_{\beta 2}$.The particular wavelengths are indicative of the target substance (Cu, Fe, Mo, Cr). For the purpose of diffraction, monochromatic X-rays must be produced through filtering using foils or crystal monochrometers. Because $K_{\alpha 1}$ and $K_{\beta 2}$ have similar wavelengths, a weighted average of the two is employed. With a CuK radiation of 1.5418, copper is the most frequent target material for single-crystal diffraction. The sample will be exposed to collimated X-rays. The intensity of the reflected X-rays is measured while the sample and detector spin. A peak in intensity happens when the Bragg Equation is satisfied by the geometry of the incident X-rays impinging on the sample. This X-ray radiation is captured by a detector, which also processes it. The signal is then converted to a count rate and output to a printer or computer monitor, among other devices [5].

Fig 2.1.1- Bruker's X-ray Diffraction D8-Discover instrument.

An X-ray diffractometer's geometry is such that the sample spins at an angle in the direction of the collimated X-ray beam, and the X-ray detector rotates at an angle of 2 to capture the diffracted X-rays. A goniometer is the device used to hold the angle and rotate the sample. For common powder patterns, data is gathered at fixed angles in the X-ray scan, ranging from 2° to 5° to 70° [5].

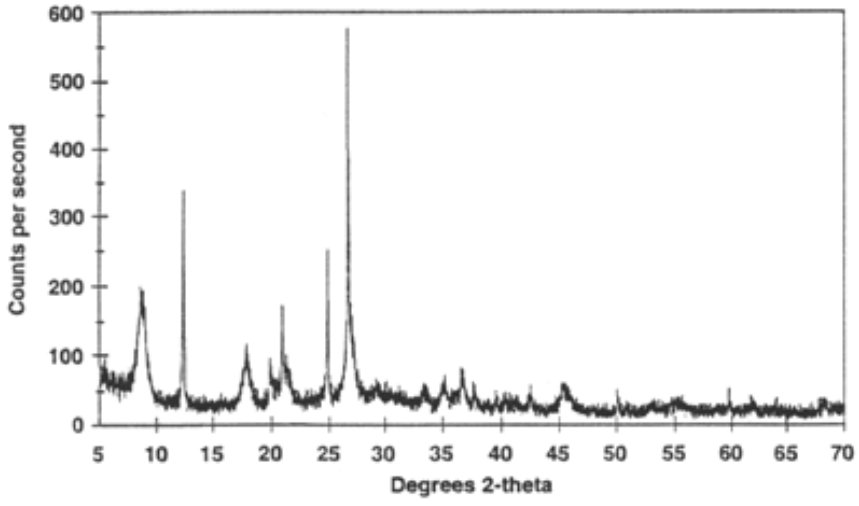

Fig 2.1.2 - X-ray powder diffractogram. Peak positions occur where the X-ray beam has been diffracted by the crystal lattice. The unique set of d-spacing derived from this patter can be used to 'fingerprint' the mineral

❖ **Braggs Law**

The angles for coherent scattering of waves from a crystal lattice are determined by Bragg's law, Wulff-condition, Bragg's or Laue-Bragg interference, a special instance of Laue diffraction, in physics and chemistry. It also includes the transfer of the wavevector with respect to the crystal lattice or the superposition of wave fronts scattered by lattice planes, resulting in a strong relationship between wavelength and scattering angle. Such a law was first developed for X-rays on crystals. However, it holds true for all quantum beams, including visible light at created periodic microscale lattices and atomically distant neutron and electron waves.

When radiation with a wavelength λ similar to atomic spacing is dispersed specularly (reflected like a mirror) by the atoms of a crystalline system and experiences constructive interference, and Bragg diffraction occurs. In a crystalline material, the waves are dispersed from lattice planes that are spaced apart by the number d between subsequent atomic layers. The scattered waves maintain phase when they constructively interfere. The glancing angle (optics) θ (see figure on the right; note that this is different from Snell's law where θ is measured from the surface normal), the wavelength λ, and the "grating constant" d of the crystal are connected by the relation. They are only reflected when they strike the surface at a specific angle.

$$n\lambda = 2d \sin(\theta) \quad \text{.....(2.1)}$$

Where n is the diffraction order. Because of the cumulative effect of reflection in subsequent crystallographic planes (h, k, l) of the crystalline lattice, the effect of the constructive or destructive interference becomes more pronounced (as described by Miller notation). As a result, Bragg's law is established, which outlines the prerequisites for the constructive interference to be at its strongest [6].

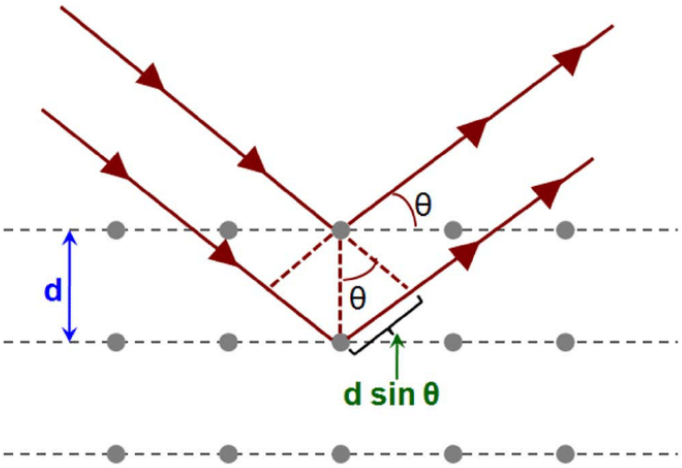

Fig 2.1.3-Bragg's law

❖ Applications

- X-ray powder diffraction is most widely used for the identification of unknown crystalline materials (e.g. minerals, inorganic compounds).
- Determination of unknown solids is critical to studies in geology, environmental science, material science, engineering and biology.
- Characterization of crystalline materials
- Identification of fine-grained minerals such as clays and mixed layer clays that are difficult to determine optically
- Determination of unit cell dimensions
- Measurement of sample purity

❖ Strength

- Powerful and rapid (< 20 min) technique for identification of an unknown mineral
- In most cases, it provides an unambiguous mineral determination
- Minimal sample preparation is required
- XRD units are widely available

❖ Limitations

- Homogeneous and single phase material is best for identification of an unknown
- Must have access to a standard reference file of inorganic compounds (d-spacing, hkls)
- Requires tenths of a gram of material which must be ground into a powder
- For mixed materials, detection limit is ~ 2% of sample [7].

2.3 Scanning Electron Microscope (SEM)

A concentrated stream of high-energy electrons is utilised by the scanning electron microscope (SEM) to produce a range of signals at the surface of solid specimens. In addition to the sample's exterior morphology (texture), chemical composition, and crystalline structure and orientation of its constituent materials, the signals resulting from electron-sample interactions also provide information about the sample. Most often, a portion of the sample's surface is chosen for data collection, and a 2-dimensional picture is created to show the spatial variations in these attributes. Using typical SEM methods (magnification ranging from 20X to about 30,000X, spatial resolution of 50 to 100 nm), areas with widths of around 1 cm to 5 microns can be scanned in a scanning mode. The SEM is also able to analyse specific point locations on the sample; this method is particularly helpful in detecting chemical compositions (using EDS), crystalline structure, and crystal orientations in a qualitative or semi-quantitative manner (using EBSD).The SEM and EPMA have a lot in common in terms of function and design, and both instruments have a wide range of possibilities [8].

Fig 2.2.1 A typical SEM instrument

❖ Principle

Significant amounts of kinetic energy are carried by accelerated electrons in a SEM, and this energy is released as a variety of signals through electron-sample interactions when the incident electrons are decelerated in the solid sample. These signals include heat, photons (characteristic X-rays used for elemental analysis and continuum X-rays), visible light (cathodoluminescence-CL), secondary electrons (which produce SEM images), backscattered

electrons (BSE), diffracted back scattered electrons (EBSD), and backscattered electrons (BSE).Both secondary electrons and backscattered electrons can be used to image samples, with secondary electrons being most useful for displaying the morphology and topography of samples and backscattered electrons being most useful for highlighting compositional contrasts in multiphase samples (i.e., for rapid phase discrimination).The Inelastic collisions between incident electrons and electrons in certain atomic orbitals (shells) in the sample result in the emission of X-rays. The difference in energy levels of the excited electrons in the various shells of a given element results in X-rays that have a constant wavelength as they return to lower energy states. As a result, each element in a mineral that the electron beam "excites" emits distinctive X-rays. As x-rays produced by electron interactions do not cause volume loss of the sample, SEM examination is regarded as "non-destructive," making it possible to repeatedly examine the same materials [8].

❖ Instrumentation

The following are vital elements of all SEMs:

- ❖ Electron Source ("Gun") Electron Lenses
- ❖ Sample Stage
- ❖ Detectors for all signals of interest
- ❖ Display / Data output devices

Infrastructure Requirements:

- ❖ Power Supply
- ❖ Vacuum System
- ❖ Cooling system
- ❖ Vibration-free floor
- ❖ Room free of ambient magnetic and electric fields

SEMs are equipped with many detectors, usually including at least one secondary electron detector. Which detectors an instrument can accommodate has a significant impact on its specific capabilities.

❖ Working

The SEM is a device that forms a picture using electrons rather than light, resulting in a significantly magnified image. An electron gun at the top of the microscope produces an

electron beam. The microscope is maintained in a vacuum and the electron beam travels through it in a vertical path. The beam is focused downward toward the sample as it passes via electromagnetic fields and lenses. Electrons and X-rays are ejected from the sample after the beam strikes it.

These secondary electrons, backscattered electrons, and X-rays are collected by detectors, which then turn them into a signal that is transmitted to a screen akin to a television. The result is the finished picture [9].

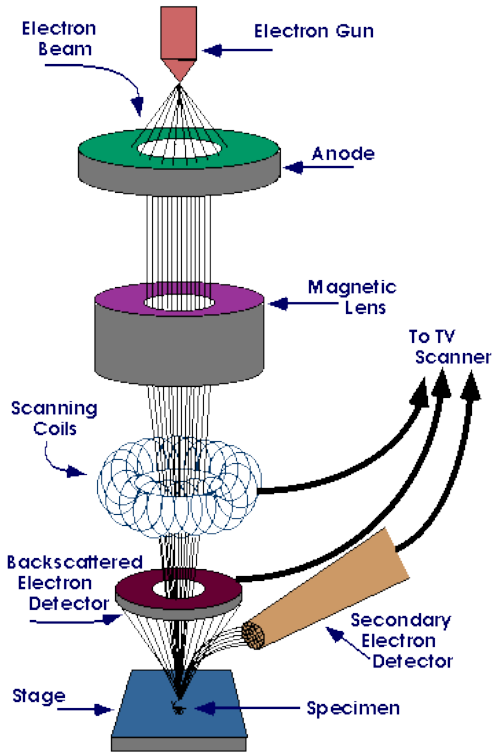

Fig 2.2.2- Diagram of SEM

❖ Applications

Regular applications of the SEM include producing high-resolution pictures of object forms (SEI) and illuminating spatial changes in chemical compositions:

- ❖ Acquiring elemental maps or spot chemical analyses using EDS.
- ❖ Discrimination of phases based on mean atomic number (commonly related to relative density) using BSE.
- ❖ Compositional maps based on differences in trace element "activators" (typically transition metal and Rare Earth elements) using CL.
- ❖ The SEM is also widely used to identify phases based on qualitative chemical analysis and/or crystalline structure.

❖ Strength

- Most SEM's are comparatively easy to operate, with user-friendly "intuitive" interfaces.
- Many applications require minimal sample preparation.
- For many applications, data acquisition is rapid (less than 5 minutes/image for SEI, BSE, spot EDS analyses.)
- Modern SEMs generate data in digital formats, which are highly portable.

❖ Limitations

- Samples must be solid and they must fit into the microscope chamber.
- Maximum size in horizontal dimensions is usually on the order of 10 cm, vertical dimensions are generally much more limited and rarely exceed 40 mm.
- For most instruments samples must be stable in a vacuum on the order of 10-5 - 10-6 torr [9].

2.4 UV-Visible spectroscopy

The liquids, gases and solids samples are analyzing through spectrophotometer by the use of radiant energy in the far and near ultraviolet, visible and near infrared regions of the electromagnetic spectrum. For that reason, the predetermined electromagnetic radiation wavelengths for ultra−violet (UV) radiation range is 300 to 400 nm, visible (Vis) and near infra−red (NIR) radiation are 400 to 765 nm and 765 to 3200 nm[10].

❖ Principle of UV-Visible spectroscopy

The UV instrument operates by passing a beam of light through a sample and measuring wavelength of light reaching a detector. The wavelength gives valuable information about the chemical structure and the intensity is related to the number of molecules, means quantity or concentration. Analytical information can be revealed in terms of transmittance, absorbance or reflectance of energy in the wavelength range between 160 and 3500 mill microns. Light is quantized into tiny packets called photons, the energy of which can be transferred to an electron upon collision. However, transfer occurs only when the energy level of the photon equals the energy required for the electron to get promoted onto the next energy state, for example from the ground state to the first excitation state. This process is the basis for absorption spectroscopy. Generally, light of a certain wavelength and energy is illuminated on the sample, which absorbs a certain amount of energy from the incident light. The energy of the light transmitted from the sample afterwards is measured using a photo detector, which registers the absorbance of the sample. A spectrum is a graphical representation of the amount of light absorbed or transmitted by matter as a function of wavelength. UV−Vis−NIR

spectrophotometer measures absorbance or transmittance from the UV range to which the human eye is not sensitive to the visible wavelength range to which the human eye is sensitive. Bouguer–Beer law is a basic principle of quantitative analysis, is also called the Lambert–Beer rule [11].

❖ Band gap calculation

The synthesized material was primarily confirmed by using UV visible (JASCO V650) spectroscopy technique. From the UV- Visible spectroscopy, the optical energy band gap was calculated by the following Tauc's relation:

$(\alpha h\upsilon)\ n=A*(h\upsilon-Eg)$..... (2.2)

Where, hυ - denotes the photon energy, Eg - represents the energy band gap of the semiconductor. The energy band gap of the synthesized materials were calculated by using given formula

$Eg = h\upsilon$…… (2.3)

where, h = (6.626 x 10-34 Js) is planks constant, $\upsilon=c/\lambda$; c = (3 x 108 m/s) is the velocity of light and λ is the wave length of the synthesized material and n -representing the nature of optical transition may have direct, indirect, forbidden direct or forbidden indirect transitions which corresponds to the values of 1/2, 2, 3/2 or 3 respectively and α is the optical (or) absorbance coefficient defined by the Beer–Lambert law as follows:

$\alpha= -lnA/l$…….(2.4)

Where, A - denotes the absorbance and l - denotes the optical path length respectively. The direct band gap was estimated by the relation between $(\alpha h\upsilon)$ 1/2 and (hυ) [12].

❖Tauc Plot Method

The tauc method of optical absorption edge determination as applied specifically to direct bandgap material. A misuse of the tauc plot to determine the bandgap energy of semi-conductors may lead to erroneous estimates, particularly large errors can be associated with characterization of modified semi-conductors showing a significant absorption of sub bandgap energy photon. The bandgap energy of a semi-conductor describes the energy needed to excite an electron from the valence band to the conduction band. We determine the bandgap by plotting $[(F(r)\ h\nu)^2$ vs. hν] , where hν is the photon energy and F(r) is the (kubelka-munk) K-M function , thus extrapolating these regions we get the energy of the

optical bandgap of the material. So, with the help of DRS we calculate the bandgap with the help of K-M function.

$(\boldsymbol{r}) = \boldsymbol{k/s}$…… (2.5)

Where k is the molar absorption co-efficient, k= (1-R) ^2, R is the Reflectance.

S is the scattering factor, S=2R

The photon energy hν can be calculated using the equation,

$\boldsymbol{h\nu} = \mathbf{1240}/\boldsymbol{wavelength}$…….. (2.6)

The tauc method uses simple multi-wavelength absorption spectroscopy and is relied upon for material evaluation of functional photovoltaic layers, transparent conductors, sensor coatings and films used for many other applications [13].

❖ Transmittance and Absorbance

The transmittance of a sample (T) is defined as the fraction of photons that pass through the sample over the incident number of photons, i.e.,

T=I/I0…….. (2.7)

In a typical UV/Vis spectroscopy measurement, we are measuring those photons that are not absorbed or scattered by the sample. It is common to report the absorbance (A) of the sample, which is related to the transmittance by

A=-log10(T)…….(2.8)

The relative percentage of scatter or absorption from the measured extinction spectrum depends on the size, shape, composition, and aggregation states of the sample. The sample may absorb light, scatter light, or both. As a general rule, smear particle will have a higher percentage of their extinction due to absorption [14].

❖ Experimental set up of the UV Visible Spectroscopy

The spectrometer automatically scans all the component wavelengths in the manner described. The ultraviolet (UV) region scanned is normally from 200 to 400 nm, and the visible portion is from 400 to 800 nm. Therefore, this method is excellent to both determine the concentration and identify the molecular structure or the structural changes. Spectrophotometer is also useful to study the changes in the vibration and conformation

energy levels after and before an interaction with a substrate, or another molecule. Figure. 2.6 shows experimental set−up of UV−Vis−NIR Spectrophotometer. The UV visible absorption spectroscopy instrument consist of following components: (i) Light source, (ii) Diffraction grating and the slit, (iii) Rotating disk, (iv) Sample and reference cells, (v) Detector and computer and (vi) Chart recorder.

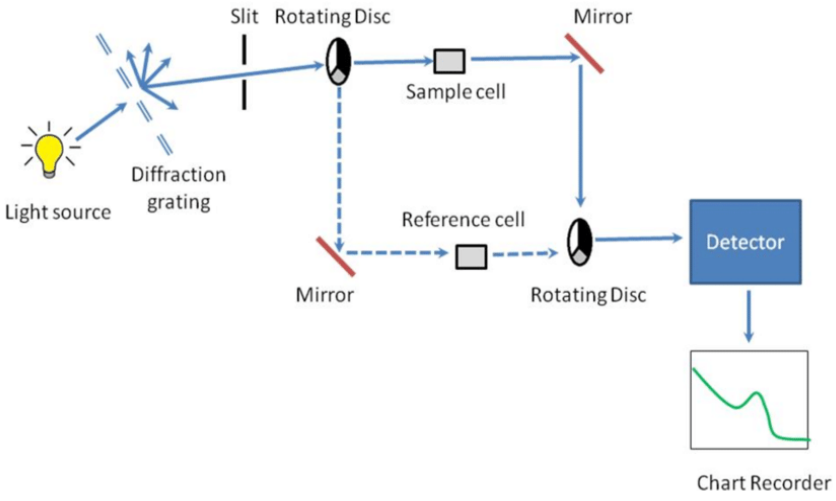

Fig; 2.3.1-UV Visible Spectroscopy Instrument setup

Light Source

Tungsten filament lamps and Hydrogen-Deuterium lamps are most widely used and suitable light source as they cover the whole UV region. Tungsten filament lamps are rich in red radiations; more specifically they emit the radiations of 375 nm, while the intensity of Hydrogen-Deuterium lamps falls below 375 nm.

Monochromator

Monochromators generally is composed of prisms and slits. Most of the spectrophotometers are double beam spectrophotometers. The radiation emitted from the primary source is dispersed with the help of rotating prisms. The various wavelengths of the light source which are separated by the prism are then selected by the slits such the rotation of the prism results in a series of continuously increasing wavelength to pass through the slits for recording purpose. The beam selected by the slit is monochromatic and further divided into two beams with the help of another prism.

Sample and reference cells

One of the two divided beams is passed through the sample solution and second beam is passé through the reference solution. Both sample and reference solution are contained in the

cells. These cells are made of either silica or quartz. Glass can't be used for the cells as it also absorbs light in the UV region.

Detector

Generally, two photocells serve the purpose of detector in UV spectroscopy. One of the photocell receives the beam from sample cell and second detector receives the beam from the reference. The intensity of the radiation from the reference cell is stronger than the beam of sample cell. This results in the generation of pulsating or alternating currents in the photocells.

Amplifier

The alternating current generated in the photocells is transferred to the amplifier. The amplifier is coupled to a small servo-meter. Generally current generated in the photocells is of very low intensity, the main purpose of amplifier is to amplify the signals many times so we can get clear and recordable signals.

Recording devices

Most of the time amplifier is coupled to a pen recorder which is connected to the computer. Computer stores all the data generated and produces the spectrum of the desired compound [15].

2.5 Energy Dispersive Analysis of X−rays (EDAX)

Energy Dispersive X-Ray Analysis (EDX), referred to as EDS or EDAX, is an x-ray technique used to identify the elemental composition of materials. Applications include materials and product research, troubleshooting, reformulation, and more. EDX systems are attachments to Electron Microscopy instruments (Scanning Electron Microscopy (SEM) or Transmission Electron Microscopy (TEM)) instruments where the imaging capability of the microscope identifies the specimen of interest. The data generated by EDX analysis consist of spectra showing peaks corresponding to the elements making up the true composition of the sample being analyzed. Elemental mapping of a sample and image analysis are also possible. In a multi-technique approach EDX becomes very powerful, particularly in contamination analysis and industrial forensic science investigations. The technique can be qualitative, semi quantitative, quantitative and also provide spatial distribution of elements through mapping. The EDX technique is non-destructive and specimens of interest can be examined in situ with little or no sample preparation. In situations where combined Microscopy and EDX data

acquired are insufficient to identify a specimen, complementary techniques are available, typically Infra-red (FTIR) Microscopy, RAMAN Microscopy, Nuclear Magnetic Resonance Spectroscopy (NMR) and Surface Analysis (X-ray photoelectron spectroscopy (XPS) or Time-of-Flight Secondary Ion Mass Spectrometry (SIMS)) [16]

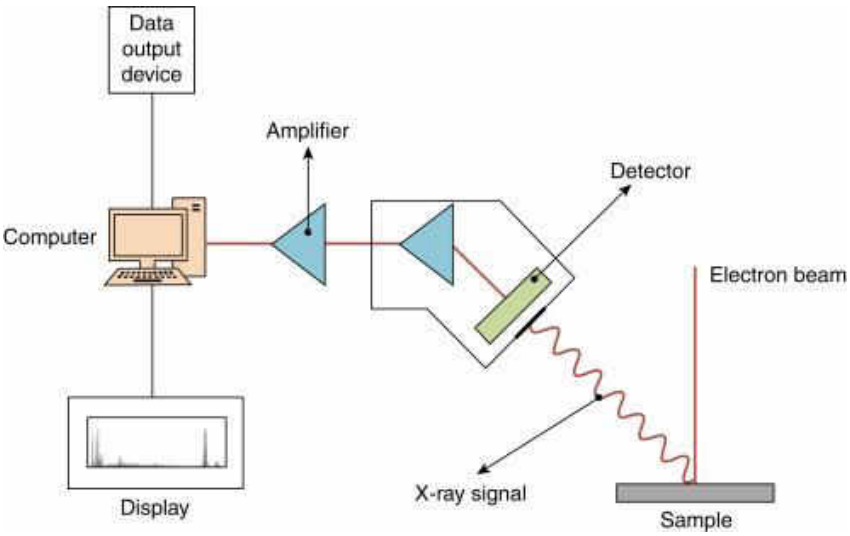

Fig 2.4.1-Schematic describing the EDX Spectroscopy method

❖ Principle

A typical set up of the EDAX is similar with that of SEM set up. More specifically, EDAX is actually inbuilt within the SEM set up. The working of EDX is based on electron focusing same as in SEM. Electron beam excitation is employed in SEM and scanning transmission electron microscopes (STEM) whereas the X-ray beam excitation is present in X-ray fluorescence (XRF) spectrometers. A detector converts X-rays into voltage signals; which feed a pulse processor, to measure the signals and pass them to data analyzer for display and investigation. Si(Li) detector cooled at cryogenic temperatures by liquid nitrogen is often employed; additionally, some modern systems come with silicon drift detectors (SDD) employing Peltier cooling systems. To produce characteristic X-rays from an object, it is bombarded by either a highly energetic beam of charge carriers (electrons or protons) or X-rays. The atoms of the sample contain ground state (unexcited) electrons in discrete energy levels or electron shells bound to the nucleus. An electron from an inner shell may be excited by an incident beam, thereby removing it from its shell and generating a hole where electron was present before excitation. This hole can be occupied by an electron of a higher-energy shell. The difference in energies of the higher- and lower- energy shells is emitted as an X-

ray. Quantitative measurement of the energy and number of these X-rays can be done with energy-dispersive analysis of X-rays. Since the energy of these X-rays is characteristic feature of energy difference between two shells and atomic structure of discharging element, EDAX can be employed to identify the elemental composition of an object [17].

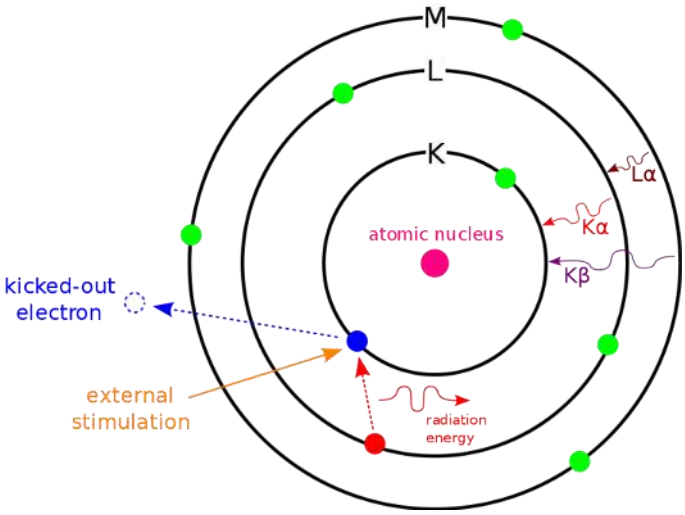

Fig; 2.4.2-Principle of EDAX

❖ Instrumentation

Figure 2.4.3 shows the working arrangement of EDS with SEM. This instrument is mainly composed of four components:

- Electron beam source
- X−ray Detector
- Pulse Processor
- Analyzer

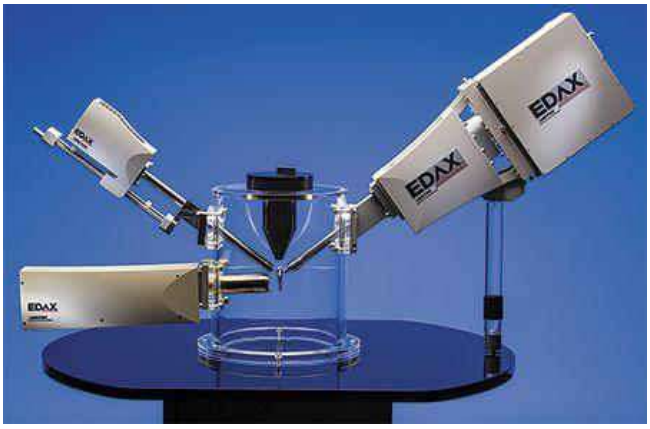

Fig 2.4.3-Experimental set up of EDAX spectrum

Brief Description of Components-

I. Electron beam source: As EDS is employed with the scanning electron microscope therefore the same electron gun (Field Emission) is used as the incident electron source and to focus the beam lenses are used along with aperture. The energy of the electron beam has to be carefully selected to overcome the compromise between the resolution requirements and the production efficiency of X-rays. The produced X-rays are detected by two crystal spectrometers.

II. X−ray Detector: The X-rays counts (which is the abundance of emitted X-rays) versus X-rays energies are measured by the EDS detector. Detector, a solid state device which is based on lithium drifted silicon. As X−rays strike the surface of the detector, a charge pulse is created. This charge pulse is directly proportional to the energy of the incident X−ray.

III. Pulse Processor: A charge sensitive preamplifier is employed to convert the charge pulse to a voltage pulse.

IV. Analyzer: Multi-channel analyser is used to sort pulses by voltage in the signals which are received by the analyser. The energy of the X-ray can be obtained by measuring the voltage of the charge pulses. This energy is then sent for display and data processing. Here, data is displayed as histogram of intensity vs voltage [17].

❖ Working

With an SEM, a variety of signals offer up different information about a given sample. For example, backscattered electrons produce images with contrast that carry information about the differences in the atomic number, while secondary electrons produce topographic information about the sample. Yet when SEM is joined with an EDX detector, X-rays can also be used as a signal to produce chemical information. To understand how these X-rays are generated, it's important to consider that every atom has a unique number of electrons that reside in specific energy levels. Under normal conditions, these positions belong to certain shells, which have different, discrete energy. The way EDX analysis works is that the electron beam hits the inner shell of an atom, knocking off an electron from the shell, while leaving a positively charged electron hole. When the electron is displaced, it attracts another electron from an outer shell to fill the vacancy. As the electron moves from the outer higher-energy to the inner lower-energy shell of the atom, this energy difference can be released in the form of an X-ray. The energy of this X-ray is unique to the specific element and transition [18].

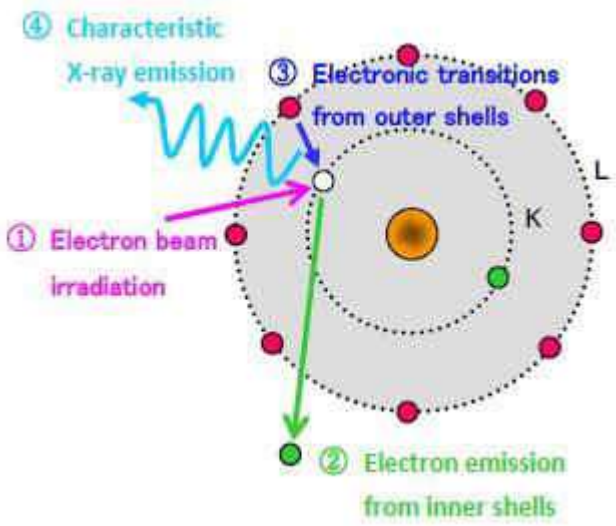

Fig; 2.4.4-X-rays are generated using EDX following a two-step process.

The X-rays emitted during the process are collected by a silicon drift detector, which measures the signal and interprets it using software. In essence, the chemical information can be visualized in several ways including elemental mapping and line scans. In this way, X-rays can be used to identify each element that exists in a sample. Interestingly, EDX can be used for both qualitative and quantitative analysis, enabling users to identify both the type of elements that are present as well as the percentage of each element's concentration within the sample. And as with traditional SEM, the technique requires little to no sample preparation and is non-destructive, meaning that it doesn't damage the sample. Because of its many advantages, EDX analysis has become common practice across industries ranging from manufacturing or research to energy and resource management to consumer-packaged goods. In fact, it's so practical that it's now an essential part of owning an SEM. Using an SEM to perform EDX analyses, researchers can improve production quality while saving valuable time—all using a very simple experiment [18].

2.6 Photoluminescence Spectroscopy

Fluorescence and phosphorescence are used in PL spectroscopy. In biochemistry and molecular biology, PL is frequently used to describe complex molecules, their surroundings, or their locations. The optoelectronic characteristics of semiconductors are also described using PL. The energy difference between the participating orbitals or bands is directly measured by the photon energy of the photon that was emitted. This method can also be used to calculate the HOMO-LUMO gap in molecules or the direct band gap of semiconductors.

Metals do not exhibit PL because their electronic states are continuous around the Fermi level and no radiative transitions between states above and below the Fermi level are feasible [19]

❖ Principle

The optical and photochemical properties of the synthesized material were studied by the Photoluminescence (PL) spectrum. The PL studies were used to find out the structural defects (or) impurities such as oxygen vacancies and zinc interstitials, as well as the charge distribution and Fermi level equilibrium of the materials. Also, the electronic band gap of the semiconductor material was determined by this study. PL is a process in which a substance absorbs photons of a particular wavelength and equivalent photons are emits suddenly which can be described by quantum mechanically (excitation to a higher energy state and then a return to a lower energy state accompanied by the emission of a photon) which was shown in the Figure 2.11. In this process, there is no significant internal energy transition of the chemical substrate between absorption and emission which is extremely fast in the order of 10 nanoseconds [20].

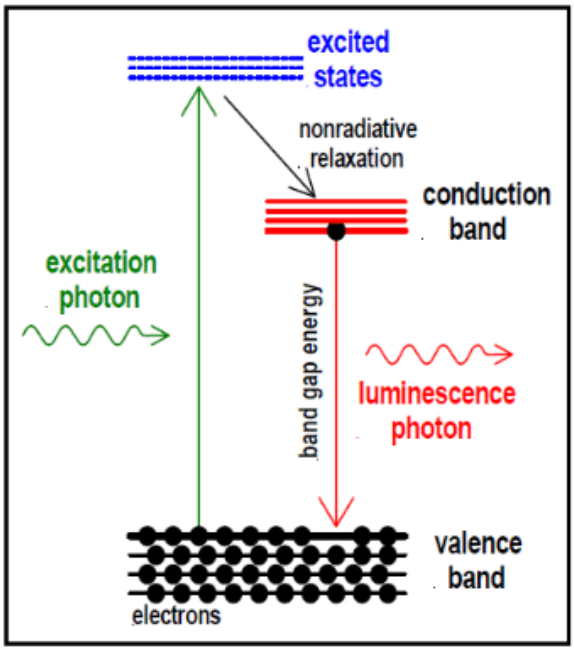

Fig; 2.5.1-Principle of PL spectrum

❖ Experimental

A spectrofluorometer is an analytical instrument for measure and record the fluorescence of a sample. While recording the fluorescence, the excitation and emission of wavelength may be scanned. With additional accessories, variation of signal with time, temperature,

concentration, polarization, or other variables may be monitored. The PL instrument set up is shown in Figure 2.12 PL spectrometers use laser sources, which contains wavelength selectors, light source, Excitation monochromator, sample illumination, detectors and corrected spectra [20].

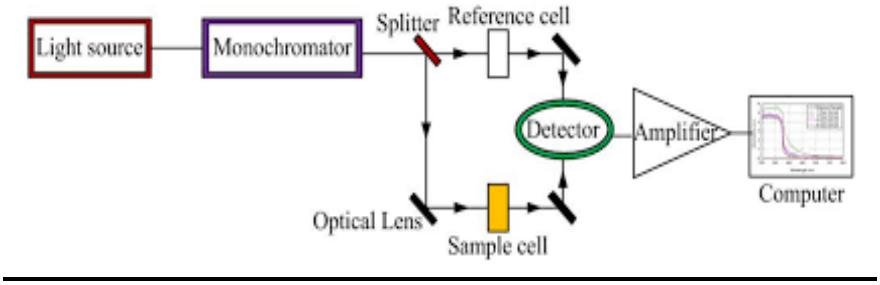

Fig 2.5.2-PL instrument set up

2.7 Raman Spectroscopy

Raman Spectroscopy is a non-destructive chemical analysis technique which provides detailed information about chemical structure, phase and polymorphy, crystallinity and molecular interactions. It is based upon the interaction of light with the chemical bonds within a material.

Raman is a light scattering technique, whereby a molecule scatters incident light from a high intensity laser light source. Most of the scattered light is at the same wavelength (or color) as the laser source and does not provide useful information – this is called Rayleigh Scatter. However a small amount of light (typically 0.0000001%) is scattered at different wavelengths (or colours), which depend on the chemical structure of the analyte – this is called Raman Scatter. A Raman spectrum features a number of peaks, showing the intensity and wavelength position of the Raman scattered light. Each peak corresponds to a specific molecular bond vibration, including individual bonds such as C-C, C=C, N-O, C-H etc., and groups of bonds such as benzene ring breathing mode, polymer chain vibrations, lattice modes, etc [20] .

When light interacts with molecules in a gas, liquid, or solid, the vast majority of the photons are dispersed or scattered at the same energy as the incident photons. This is described as elastic scattering, or Rayleigh scattering. A small number of these photons, approximately 1 photon in 10 million will scatter at a different frequency than the incident photon. This process is called inelastic scattering, or the Raman effect, named after Sir C.V. Raman who

discovered this and was awarded the 1930 Nobel Prize in Physics for his work. Since that time, Raman has been utilized for a vast array of applications from medical diagnostics to material science and reaction analysis. Raman allows the user to collect the vibrational signature of a molecule, giving insight into how it is put together, as well as how it interacts with other molecules around it [20].

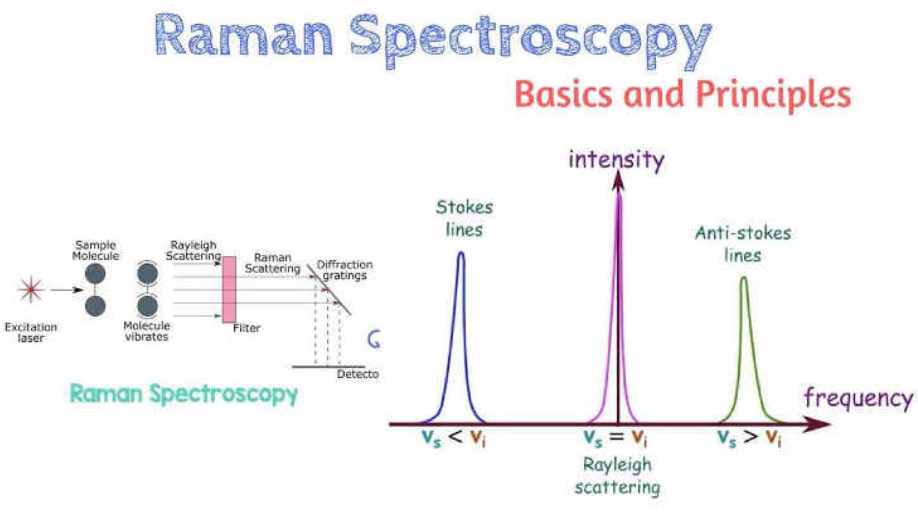

Fig 2.6.1-Raman Spectroscopy

❖ Raman Scattering Process

The Raman Scattering Process, as described by quantum mechanics, is when photons interact with a molecule, the molecule may be advanced to a higher energy, virtual state. From this higher energy state, there may be a few different outcomes. One such outcome would be that the molecule relaxes to a vibrational energy level that is different than that of its beginning state producing a photon of different energy. The difference between the energy of the incident photon and the energy of the scattered photon is the called the Raman shift. When the change in energy of the scattered photon is less than the incident photon, the scattering is called Stokes scatter. Some molecules may begin in a vibrationally excited state and when they are advanced to the higher energy virtual state, they may relax to a final energy state that is lower than that of the initial excited state. This scattering is called anti-Stokes [21]

❖ Instrumentation

A modern, compact Raman spectrometer consists of several basic components, including a laser that serves as the excitation source to induce the Raman scattering. Typically, solid state lasers are used in modern Raman instruments with popular wavelengths of 532 nm, 785 nm, 830 nm and 1064 nm. The shorter wavelength lasers have higher Raman scattering cross-

sections so the resulting signal is greater, however the incidence of fluorescence also increases at shorter wavelength. For this reason, many Raman systems feature the 785 nm laser. The laser energy is transmitted to and collected from the sample by fiber optics cables. A notch or edge filter is used to eliminate Rayleigh and anti-Stokes scattering and the remaining Stokes scattered light is passed on to a dispersion element, typically a holographic grating. A CCD detector captures the light, resulting in the Raman spectrum. Since Raman scattering yields a weak signal, it is most important that high-quality, optically well-matched components are used in the Raman spectrometer [21]

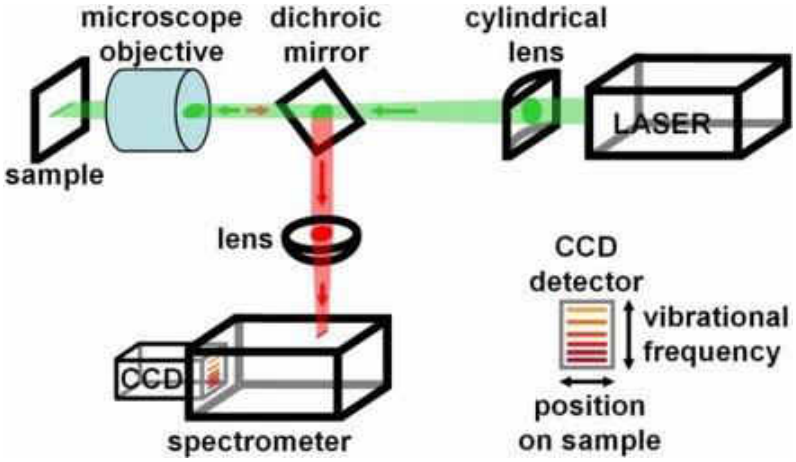

Fig 2.6.2-Raman Spectrometer

❖ Applications

Raman spectroscopy is used in industry for a variety of applications, including:

- Crystallization Processes
- Polymorphism Identification
- Polymerization Reactions
- Hydrogenation Reactions
- Chemical Synthesis
- Biocatalysts and Enzymatic Catalysis
- Flow Chemistry
- Bioprocess Monitoring
- Synthesis Reactions [21]

2.8 Fourier Transform Infrared Spectroscopy (FTIR)

The FTIR instrument is one of the most important tools to identify the chemical components that are either organic (or) inorganic compounds presence in the synthesized materials. The

mathematical procedure (Fourier transform) is used in Fourier transform infrared spectroscopy (FTIR) to convert the interferogram's raw data into the actual spectrum. The infrared spectrum of transmission or absorption of a fuel sample is obtained using the FTIR method. FTIR determines whether organic and inorganic substances are present in the sample. The specific chemical groups present in the sample will be identified using spectrum data in the automated spectroscopy programme based on the infrared absorption frequency range 600–4000 cm^1 [22].

❖ Physical Principles

At various frequencies, molecular bonds are vibrating owing to their elements and bonds presence in the synthesized material. According to the quantum mechanics, several specific frequencies were vibrating such as ground state at lowest frequency and several excited states at higher frequencies. If the frequency of a molecular vibration linearly increases, the light energy will be absorbed, which may happen by the difference between two energy states (ground state (E0) - first excited state (E1)) and the relation is given below,

$E1 - E0 = hc/\lambda$…….. (2.9)

Where, h represents the Planck's constant, c denotes the velocity of the light, λ is the wavelength of light [22].

❖ Experimental

The FTIR spectrometer's basic setup is depicted in Figure 2.15.The FTIR spectrometer comprises the following features, including an interferometer that consists of two mirrors, an infrared detector, and a beam splitter, as well as a detector, a monochromator, and a chopper. Both solid and liquid samples were analysed in the FTIR experiments. For the purposes of the FTIR study, the solid and liquid samples were collected using KBr (or) polyethylene pellets. A few milligrams of the prepared samples are combined with KBr and fine grain in a mortar to create a solid sample. The pellet was then created by pressing the fine powder under hydraulic pressure. In order to do the FTIR measurement, the pellet sample was finally fixed with a sample holder. For the liquid sample, a few drops of the sample were added to a pure KBr pellet, which was then dried at room temperature for a few minutes. The pellet was then employed for FTIR characterisation after that [23].

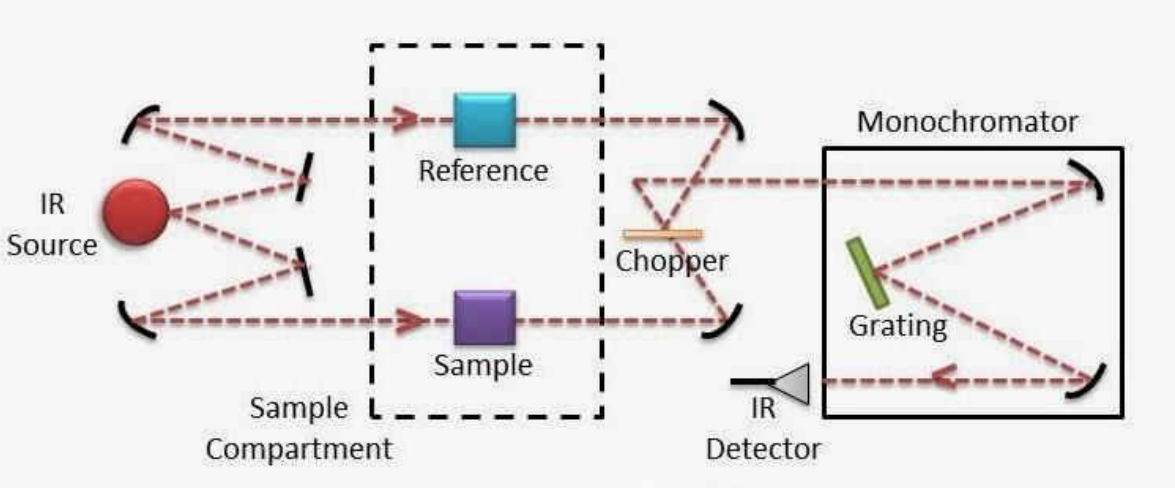

Fig 2.7.1 FTIR instrument setup

❖ Advantage

1. Dramatically improved optical throughput due to a slit-free optical design, resulting in a high signal-to-noise ratio (Jacquinot's advantage).
2. The ability to obtain data at multiple wavelengths simultaneously without the need for scanning using a moving grating/prism (Fellgett's advantage).
3. Improved wavenumber resolution by using laser source for accurate digital signal sampling and extending the mirror movement distance in the interferometer.
4. Extended wavenumber measurement range by changing the light source, beam splitter and detector for the specific purpose, either far-IR or near-IR [24].

2.9 X-ray Photoelectron Spectroscopy (XPS)

When a sample is bombarded with monochromatic soft X-rays, the basic principle of XPS is that electrons are emitted from the sample surface. The kinetic energy of a released electron provides information on the binding energies of atomic orbitals, allowing surface chemical species to be identified. XPS (figure. 2.6) can be used to determine the relative concentration of species. The following [7, 8] `relationship can be used to calculate photon interactions with the core level.

$$KE = h\nu - BE - c\varphi \ldots\ldots\ldots\ldots\ldots\ldots\ldots \quad (2.8.1)$$

Where $h\nu$ is the energy of an incident X-ray, and BE stands for the atomic orbital binding energy, $c\varphi$ stands for the spectrometer work function, and KE stands for the kinetic energy of the released electron. Each electron in an atomic orbital has its own unique binding energy. The electron kicked off from the innermost orbitals with their kinetic energy associated with

the binding energy of the atomic orbital due to the absorption of incoming X-rays. Information about the state of elements can then be obtained by analysing these energies. Peak intensity can provide quantitative information about an ingredient.

The following are the most commonly used monochromatic X-ray sources.

• $h\nu$ = 1253.6 eV for $Mg\ K\alpha$ radiation

• $Al\ K\alpha$ Radiation has a wavelength of $h\nu$ = 1486.6 eV.

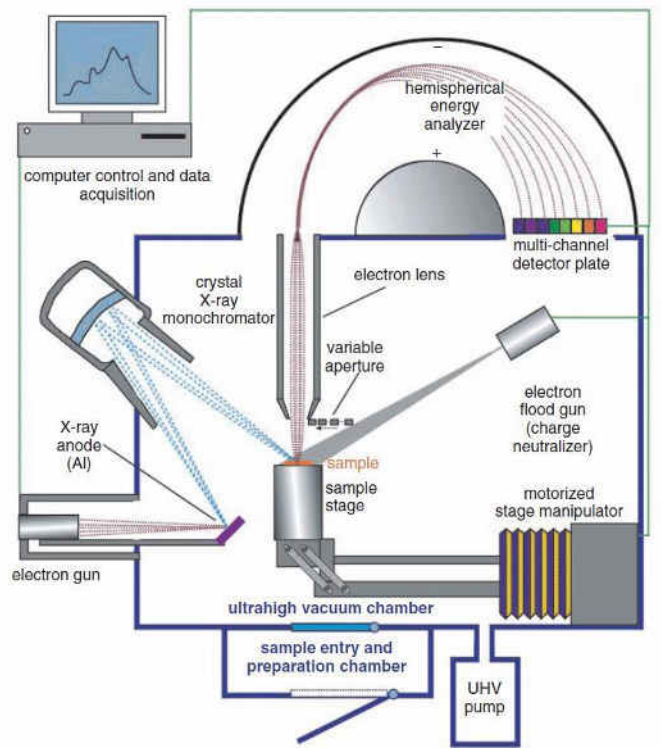

Figure. 2.8.1 Schematic of XPS

The ejected electron can have an energy range of 0–1480 eV is excited by$Al\ K\alpha$ and $Mg\ K\alpha$ excites 0–1250 eV. Generally, due to the short inelastic mean free path of electrons this technique is very strong, it is very surface sensitive. The spectra were obtained on Thermo Scientific ESCALAB 250 Xi, using monochromatic Al Kα radiation (1486.6 eV). The obtained spectra were then analysed

References

[1]-XRD Basics (upenn.edu)

[2]-What is X-Ray Diffraction (XRD) | SciMed

[3]-X-ray crystallography - Wikipedia

[4]-X-ray Diffraction Analysis Principle Instrument and Applications I Definition, Methods, XRD analysis, and 5 Advantages. (physicswave.com)

[5]-X-ray Powder Diffraction (XRD) (carleton.edu)

[6]-Bragg's law - Wikipedia

[7]-https://serc.carleton.edu/msu_nanotech/methods/XRD.html

[8]- https://serc.carleton.edu/research_education/geochemsheets/techniques/SEM.html

[9]-
https://www.purdue.edu/ehps/rem/laboratory/equipment%20safety/Research%20Equipment/sem.html

[10]- https://www2.chemistry.msu.edu/faculty/reusch/virttxtjml/spectrpy/uv-vis/uvspec.htm

[11]- https://en.wikipedia.org/wiki/Ultraviolet%E2%80%93visible_spectroscopy

[12]-. *Phys. Chem. Lett.* 2018, 9, 23, 6814–6817Publication Date:December 6, 2018https://doi.org/10.1021/acs.jpclett.8b02892

[13]- Evaluation of taue method for optical absorption edge determination:ZnO Thin films as a model system. Viezbicke, Brain D;Patel Shane ; Davis, Benjamin E:et.al

[14]-https://www.jove.com/v/10204/ultraviolet-visible-uv-vis-spectroscopy#:~:text=With%20UV%2DVis%20spectroscopy%2C%20the,a%20compound%20at%20different%20wavelengths.

[15]- https://www.technologynetworks.com/analysis/articles/uv-vis-spectroscopy-principle-strengths-and-limitations-and-applications 349865#:~:text=UV%2DVis%20spectroscopy%20is%20an,a%20reference%20or%20blank%20sample.

[16] -https://www.intertek.com/analysis/microscopy/edx/

[17] -1585214200-PHY(H) -VI-NANO-MATERIAL-1-AJAYPRADAP. pdf

[18] -Thermofisher.com/blog/microscopy/edx-analysis-wirh-sem-how-does-it-work/

[19]-A.Erbe Norwegian University of Science and Technology, Trondheim, Norway Author links open overlay panelS.Nayak University of Oxford, Oxford, United Kingdom Author links open overlay panelY.-H.ChenF.NiuM.PanderS.TecklenburgC.Toparli Max-Planck-Institut für Eisenforschung GmbH, Düsseldorf, GermanyAvailable online 23 April 2018, Version of Record 23 April 2018.

[20]- Evaluation of taue method for optical absorption edge determination:ZnO Thin films as a model system. Viezbicke, Brain D;Patel Shane ; Davis, Benjamin E:et.al

[21]- https://www.horiba.com/pol/scientific/technologies/raman- imaging-and spectroscopy /raman-spectroscopy/

[22]- Mohamed Shameer, P., & Mohamed Nishath, P. (2019). *Exploration and enhancement on fuel stability of biodiesel. Advanced Biofuels, 181–213.* doi:10.1016/b978-0-08-102791-2.00008-8

[23]- mt.com/in/en/home/applications/Raman spectroscopy. Html

[24]-https://www.jasco-global.com/principle/principles-of-infrared-spectroscopy-4 advantages-of-ftir-spectroscopy/

CHAPTER 3

LINEAR AND NON LINEAR OPTICAL PROPERTIES OF Cr DOPED ZnO NANOPARTICLES

3.0 INTRODUCTION

Nanoscience and Nanotechnology is the advanced field of materials which possess material with intriguing and fascinating features. Here in the present work we prepared and characterised the pristine and Cr doped ZnO nanoparticles. Hence this chapter briefly described about the basic characterization techniques and its non linear and photocatalytic properties of the prepared samples.

3.1 XRD

XRD spectra were used to measure the crystallinity and phase purity of samples with (x = 0.0, 0.02, 0.04). The XRD spectra of pure and Cr-doped nanoparticles are shown in Fig.1 for the two values between 10 and 90. Diffraction peaks are found at two values of 31.69, 34.20, 36.24, 47.35, 56.43, 62.76, 67.23, 68.98, 72.44, 76.75, and 89.6, which correspond to the planes (100), (002), (101), (102), (110), (103), (200), (112), (203), (004), (202), and (201) [1]. The XRD results reveal the hexagonal wurtzite structure having P63mc space group [2]. All the diffraction peaks of synthesized samples were assigned to zinc oxide and no extra impurity peaks were identified within the instrumental detection limit [3].The average crystallite size of (x= 0.0, 0.02, 0.04) was determined by the Debye-Scherrer equation,

$$\boldsymbol{D} = \frac{k\lambda}{\beta\cos\theta} \quad \text{..... (3.1)}$$

D denotes average crystallite size, k represents shape factor (0.89), λ stands for the wavelength of Cu-kα radiation($\lambda = 1.5406$ Å), and β denotes the full width at half maximum, and θ in degree is the diffraction angle. Dislocation density is determined from the average crystallite size using the relation [4].

$$\delta = \frac{1}{D^2} \quad \text{..... (3.2)}$$

Table 3.1 lists the samples' typical crystallite size and dislocation density. The average crystallite size falls from 48.015 nm to 27.792 nm as doping concentration rises. This is due to the difference in ionic radii between Cr3+ (0.63) and Zn^{2+} (0.74) [5].Rietveld analysis (shown in Fig.3.13) confirms hexagonal structure with space group P63mc.Lattice constants,

aspect ratio, unit cell volume, and refinement parameters are displayed in Table 2.Cr^{3+} ions are successfully incorporated into Zn^{2+} lattice positions without changing the crystal structure, as evidenced by the fact that the aspect ratio c/a remains constant for both pure and Cr-doped samples [6].

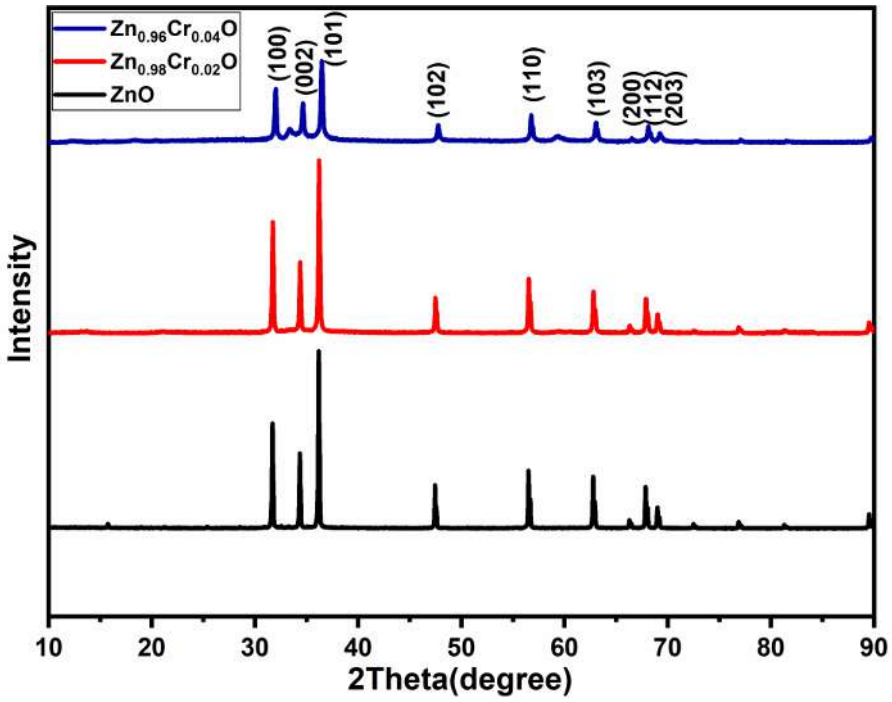

Fig 3.1.1-XRD spectra of $Zn_{(1-x)}Cr_xO$ (x = 0.0, 0.02, 0.04) nanoparticles.

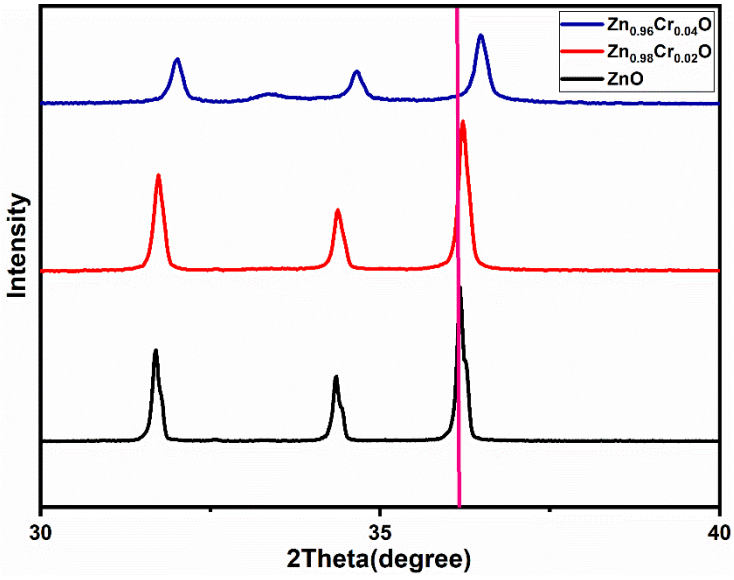

Fig 3.1.2-Peak shift in the XRD spectra

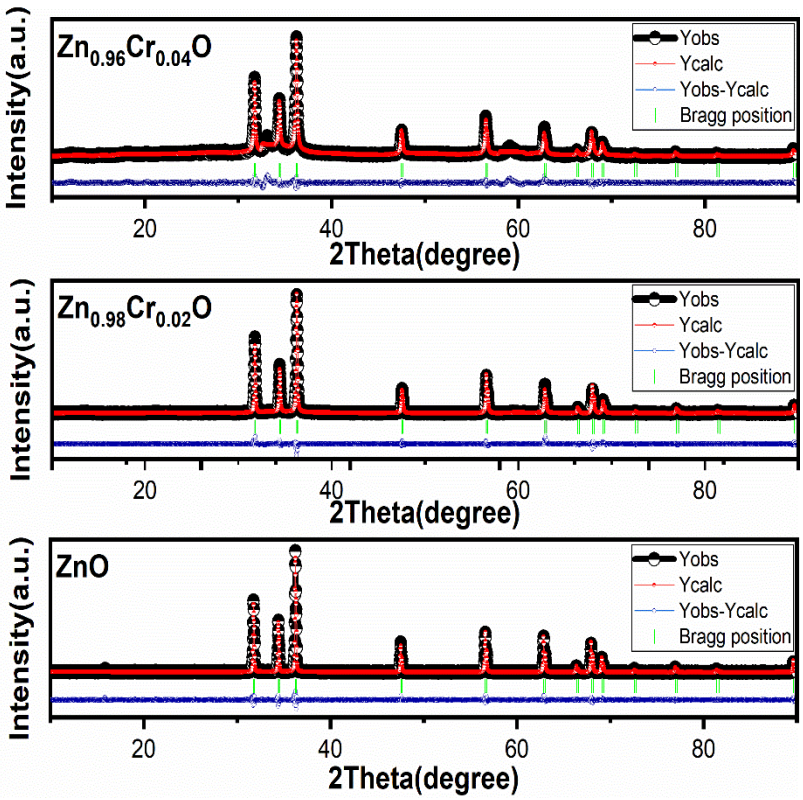

Fig 3.1.3-Rietveld refinement of $Zn_{(1-x)}Cr_xO$ (x = 0.0, 0.02, 0.04) nanoparticles.

Sample	**Crystallite Size(nm)**
ZnO	48.015
$Zn_{0.98}Cr_{0.02}O$	36.982
$Zn_{0.96}Cr_{0.04}O$	27.792

Table 3.1-Crystallite size of $Zn_{(1-x)}Cr_xO$ (x = 0.0, 0.02, 0.04)

Sample	**Lattice constants**				**R_p**	**R_{wp}**	**R_e**	**χ^2**
	a(Å)	***c***(Å)	**c/a**	**V** (Å^3)				
ZnO	3.2495	5.2059	1.6021	47.6064	20.9	20.8	8.46	6.06
$Zn_{0.98}Cr_{0.02}O$	3.2501	5.2069	1.6021	47.6321	19.1	17.9	7.75	5.31
$Zn_{0.96}Cr_{0.04}O$	3.2537	5.2121	1.6021	47.7856	34.1	26.8	11.07	5.86

Table 3.2**-:** Lattice constants and refinement parameters of $Zn_{(1-x)}Cr_xO$ (x = 0.0, 0.02, 0.04) nanoparticles.

3.2 Morphological analysis

The morphology of the unadulterated and doped samples, as evaluated by FESEM, is shown in Fig.3.2.1 (a)-(c). Samples reveal a twisted form like a rod [7]. The photos make it clear that Cr doping has an impact on the nanoparticles' shape. Particle size decreases and agglomeration rises with Cr doping. According to reports, particle agglomeration can result from synthesis at high temperatures [8].

An EDAX analysis can be used to determine the chemical makeup of the elements, as shown in Fig.3.2.1 (d)- (f). EDAX spectra are used to establish the presence of Zn, O in unpolluted samples as well as Zn, Cr, and O in doped samples. The carbon is a result of the measurement tape made of carbon. The exceptional purity of the samples is shown by the lack of any contaminants. For 2% and 4% doped samples, the weight percentage of Cr ions rises from 0.28 to 0.32, indicating that the Cr ions were perfectly doped to the Zn lattice sites.

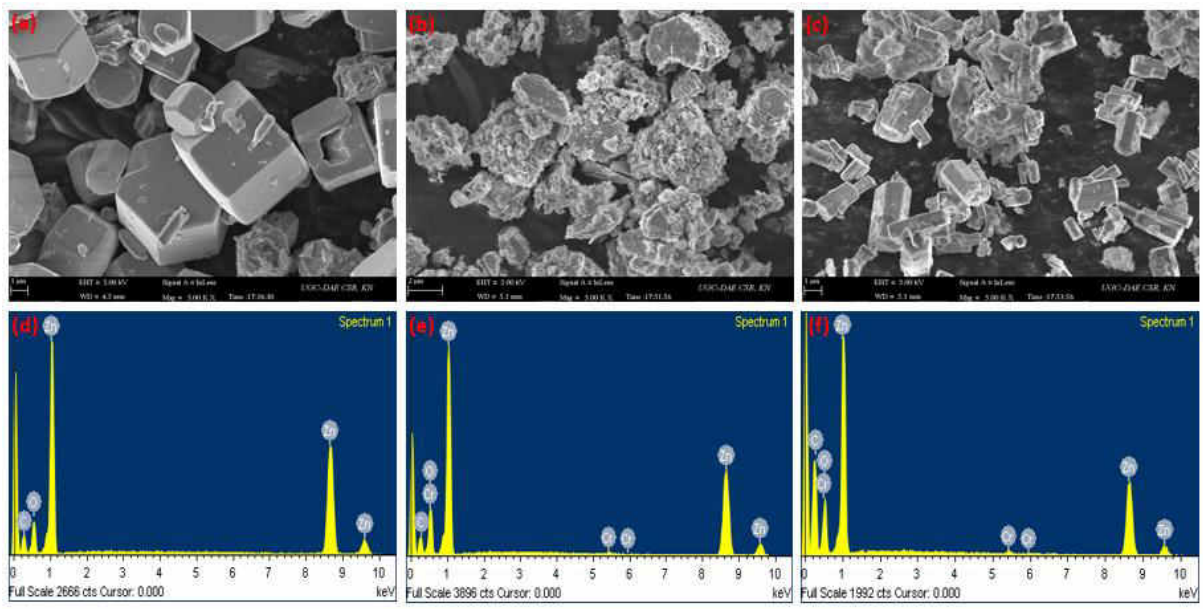

Fig. 3.2.1 (a)-(c) SEM micrographs of samples $Zn_{(1-x)}Cr_xO$ (x = 0.0, 0.02, 0.04), (d)-(f) EDAX spectra of samples $Zn_{(1-x)}Cr_xO$ (x = 0.0, 0.02, 0.04).

3.3 XPS Analysis

XPS spectra are used to determine the chemical make-up and oxidation states of pure and Cr-doped Zinc Oxide nanorods. Fig 3.3.1(a) gives survey spectra of $Zn_{(1-x)}Cr_xO$ $(x = 0,0.02)$ nanorods, which exhibit the existence of Zn, C, and O in both samples, and a characteristic peak of Cr is detected in Cr doped samples. The C1s peak at 284.72 eV indicates the presence

of carbon, which is utilised as a calibration reference in order to prevent the specimen charging effect [9].

Fig 3.3.1(b) gives the core level Zn 2p spectrum of $Zn_{(1-x)}Cr_xO$ $(x = 0,0.02)$ nanorods, which exhibit two major peaks present at 1021.68 eV and 1044.75 eV, and are assigned to $Zn2p_{3/2}$ and $Zn2p_{1/2}$ states respectively and its difference in binding energy is about 23 eV. These two symmetric peaks are attributed to Zn-O bonds in the Zinc Oxide lattice, confirming the frequent identification of Zn 2+ states in ZnO nanomaterials. The narrow Zn 2p3/2 band is caused by these Zn 2+ ions in an oxygen-poor ZnO lattice. Additionally, it supports the findings for Zn2+ in ZnO by demonstrating the Zn2+ state's dominance over the Zn ions on the surface.

The major peak seen at 577.01 eV is distinct from 574.02 eV corresponding to Cr metal, 576.0 eV for Cr2+, and 576.3 eV for Cr4+, according to Fig.3. 5(c), which provides the core level binding energy of Cr 2p. However, this signal is attributed to the Cr 3+ ions since it closely matches the reported Cr3+ states' claimed binding energy (577.2 0.2 eV).Due to the incorporation of Cr dopants into the zinc oxide lattice as Cr3+ ions rather than Cr2+ ions, the two distinct states of Cr 2p at 577.1 and 586.01 eV, respectively, correspond to Cr 2p3/2 and Cr 2p1/2 states and spin-orbit splitting energy is almost around 10 eV. It demonstrates that the parent material's Zn sites are replaced by Cr ions in their trivalent state. The O2-ions in the hexagonal wurtzite structure are surrounded by the Zn2+ ions and have a characteristic peak at 531.3 eV in the O1s spectra of the pristine and doped nanorods seen in Fig. 3.5(d). The increase in oxygen defects or chemisorbed groups (OH) in oxygen ions, which are frequently linked with Zn ions to form nanorods, may be the cause of the broadening of this peak [10].

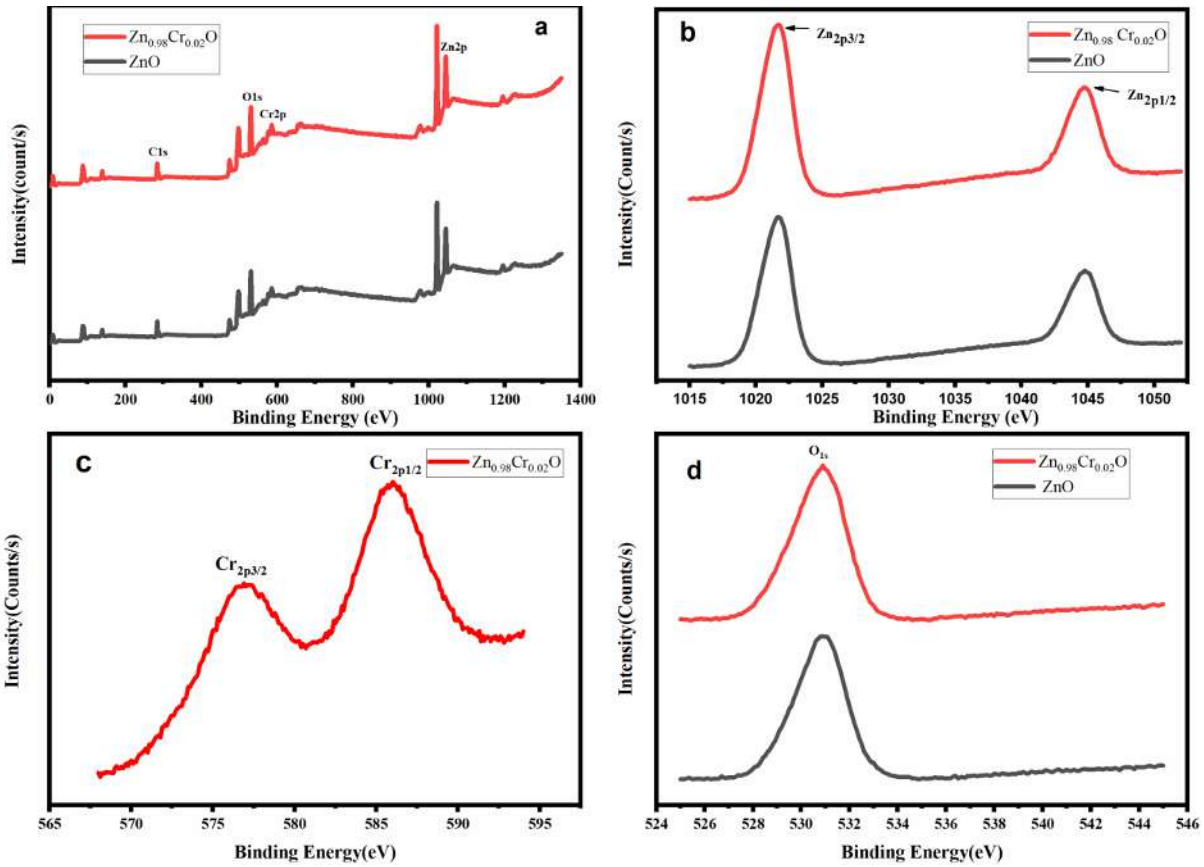

Fig 3.3.1(a) Core level spectra of $Zn_{(1-x)}Cr_xO$ (x = 0.0, 0.02) (b) $Zn2_p$ spectra (c) Cr 2_p spectra and (d) O1s spectra

3.4 Vibrational Spectral Analysis

The most adaptable and non-destructive Raman scattering method can be used to detect the presence of dopants, flaws, and structural disorders in the host lattice [11].Generally, for wurtzite type ZnO, the Brillouin zone center optical phonon modes are represented by,

$$\Gamma_{optical} = A_1 + E_1 + 2E_2 + 2B_1 \ldots\ldots\ldots\ldots\ldots\ldots\ldots (3.3)$$

Where the longitudinal optical (LO) and transverse optical (TO) phonon modes can be distinguished as the Raman active modes A_1 and E_1, which are polarised in Z and XY orientations, respectively. Raman active non-polar modes of the $2E_2$ modes are E_2 (low) and E_2 (high), while IR and silent Raman inactive modes are B_1 modes [12]. The Raman spectra of $Zn_{(1-x)}Cr_xO$ $(x = 0,0.02,0.04)$are given in Fig.6**.** For pure ZnO, prominent peak obtained at 99 cm^{-1}, 331 cm^{-1}, 378 cm^{-1}, 437 cm^{-1}, 534 cm^{-1}, and 663 cm^{-1}, corresponds to E_2 (low), $2E_2$ (M), A_1 (TO), E_2 (high),2 (LA) and 2(LO) modes of vibrations, respectively [13]. Peak obtained around 99 cm^{-1} attributed to E_2 (low) non polar mode are present in $Zn_{(1-x)}Cr_xO$ (x = 0.0, 0.02,0.04) nanorods [14].The intense Raman mode of the hexagonal wurtzite structure

is indicated by the E2 (high) vibrational mode, which can be seen at 437 cm^{-1}. The injection of Cr ions into the zinc host lattice sites causes changes in the Zn-O bond binding energy, which can be represented as variations in the intensity and peak position of the E2 (high) mode upon Cr doping. The intense Raman mode of the hexagonal wurtzite structure is indicated by the E2 (high) vibrational mode, which can be seen at 437 cm^{-1}. The injection of Cr ions into the zinc host lattice sites causes changes in the Zn-O bond binding energy, which can be represented as variations in the intensity and peak position of the E2 (high) mode upon Cr doping [15]. A few Raman active modes associated to ZnO disappear for Cr doped ZnO, while some other peaks shift from their peak locations. This change in peak position is due to optical phonon confinement, which makes the phonon wave vectors unclear [16].Due to variations in the ionic radii of Zn and Cr, the phonon absorption bands get depleted as the doping concentration rises. The atoms' surfaces become disordered and distorted as a result of the change in nanorod size, which causes local stress at the lattice points [14].

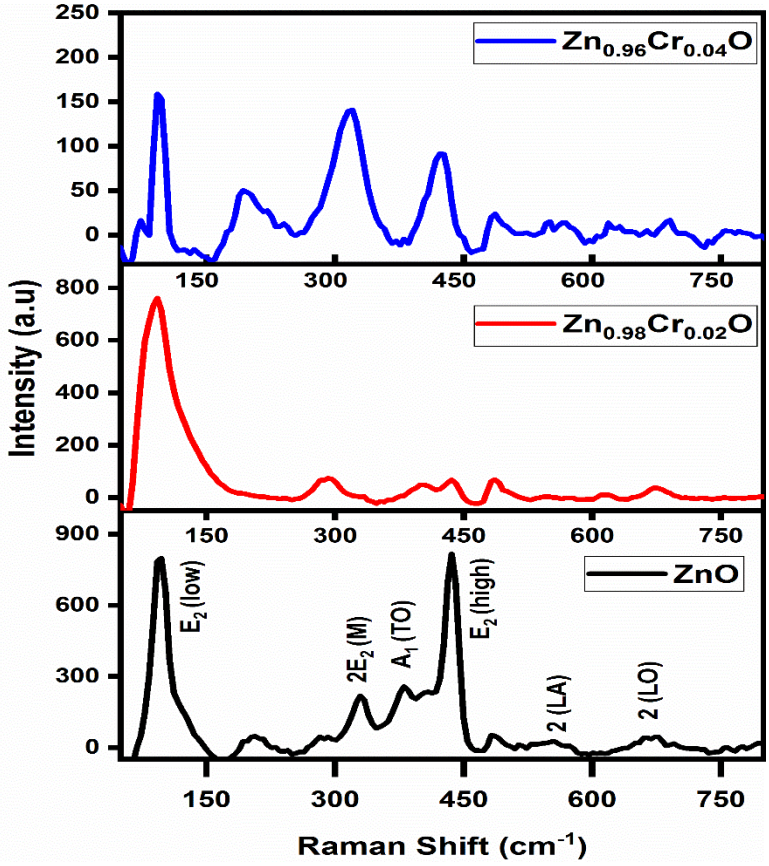

Fig.3.4.1: Raman spectra of $Zn_{(1-x)}Cr_xO$ (x = 0,0.02,0.04) nanoparticles.

The FT-IR spectra are used to describe the existence of various functional groups and chemical bonds related to their respective wavenumbers [17].The intensity and position of peaks in the spectra are affected by the crystal structure, shape, and chemical content of prepared nanoparticles. Fig.3.4.2 gives FT-IR spectra of $Zn_{(1-x)}Cr_xO$ (x = 0.0, 0.02, 0.04) nanoparticles in the spectral range of 400 – 4000 cm^{-1}.O-H stretching and bending vibrational modes with broad absorption bands at 3450–3354 $cm^{-1}$and 1549 $cm^{-1}$are caused by the presence of absorbed moisture content on the sample surface [16][18]. Generally, metal oxides exhibit peaks in the fingerprint region [19].The distinctive peaks between 550 and 680 cm^{-1} and 700 to 900 cm^{-1}, respectively, are the stretching vibrations of Cr-O and ZnO[20][21]. The peaks at 620 $cm^{-1}$and 676 cm^{-1}, respectively, correspond to the typical peaks of zinc oxide and zinc oxide nanorods. The peaks at 620 $cm^{-1}$and 676 cm^{-1}, respectively, correspond to the typical peaks of zinc oxide and zinc oxide nanorods. The produced samples' intensities change when doped, but no shift in the band of light corresponding to the hexagonal wurtzite structure is seen, indicating that the bond stretching is independent of the doping concentration. It highlights the presence of Cr ions on the zinc lattice sites [19].

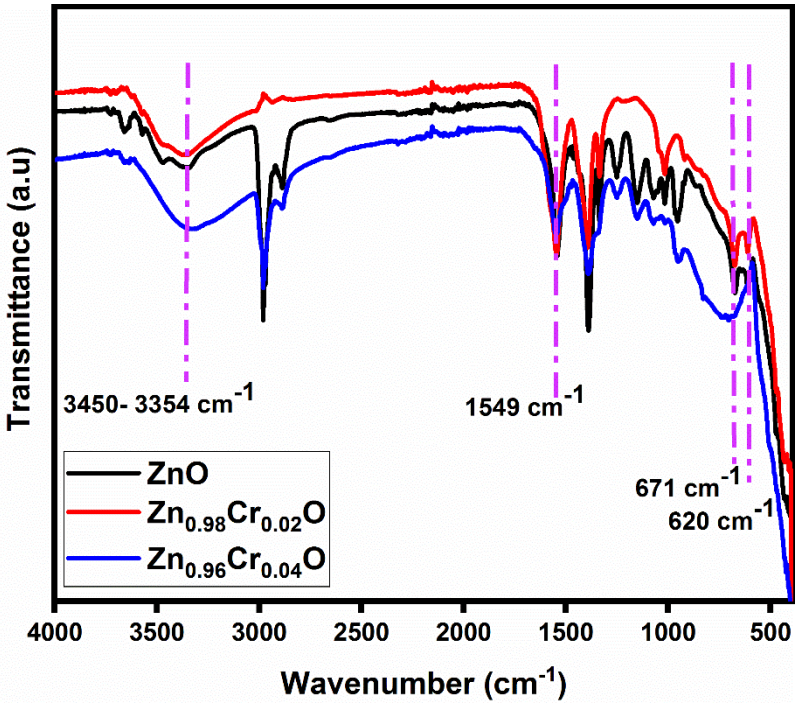

Fig.3.4.2: FTIR spectra of $Zn_{(1-x)}Cr_xO$ $(x = 0, 0.02, 0.04)$ nanoparticles.

3.5 Linear optical analysis

Using UV-Visible diffuse reflectance spectra, the optical characteristics of $Zn_{(1-x)}Cr_xO$ $(x = 0,0.02,0.04)$nanoparticles are examined to identify the bandgap and electronic transitions (DRS) [22]. Figure 3.5.1(a) and (b), respectively, show the variation in reflectance and absorbance with a wavelength in the range of 200-1000 nm. A semiconductor typically undergoes an electronic transition from the valence band (VB) to the conduction band (CB) when incident photon energy exceeds the associated energy bandgap (Eg) of the semiconductor. The material's absorbance increases as a result of this. A transition is direct if momentum is conserved during it; otherwise, it is an indirect transition [22].Strong absorption peaks in the 210–373 nm range may be seen in $Zn_{(1-x)}Cr_xO$nanoparticles. With Cr doping, the absorption edge displays a blue shift. This suggests a change in the band structure of the host material [23]. Successful doping of Zn with Cr ions induces lattice strain and a modification of the band structure [23]. To determine the bandgap energy from obtained D R S, the Kubelka-Munk-function is used.

$$F(R) = \frac{(1-R)^2}{2R} \quad \text{..... (3.4)}$$

Here, F(R) denotes the Kubelka-Munk function and R corresponds to the absolute reflectance. The bandgap (E_g) can be evaluated by plotting $[F(R).h\nu]^n$ versus photon energy ($h\nu$).Here n represents the type of transition, n = 2/3, 1/3, 2, ½ respectively corresponds to direct forbidden, indirect forbidden, direct allowed, and indirect allowed transitions [24].For a direct bandgap material like ZnO, n = 2. The curve of $[F(R).hv]^2$ with photon energy (h) is displayed in Fig. 3.8. Just above their absorption edge, nanoparticles exhibit linear behaviour, and Eg can be calculated by projecting the linear area of $[F(R).h]^2$ to the h axis, as shown in Fig. 3.5.2. Table 3.3 lists the estimated band gap values. According to research by Govindan Nadar Rajivgandhi et al., chromium doping produces optically active sub levels in specific areas of CB and VB. This leads to a decrease in bandgap energy [6].When thinking about semiconductor compounds doped with a transition metal, sp-d spin-exchange interaction occurs across the band electrons and localised d electrons of dopant ions, resulting in a reduction in the optical band gap [7]. According to Santi Septiani Sartiman et al., the exchange factor of p-like states increases the top valence band energy by a constant factor while the exchange constant of s-like states decreases the bottom conduction band

(CB)[25].The optical band gap can vary depending on a number of variables, including as grain size, lattice strain, carrier concentration, and size impact [23]. This could explain why $Zn_{(1-x)}Cr_xO$ $(x = 0.04)$ nanoparticles showed an enhanced Eg compared to $Zn_{(1-x)}Cr_xO$ $(x = 0.02)$nanoparticles.

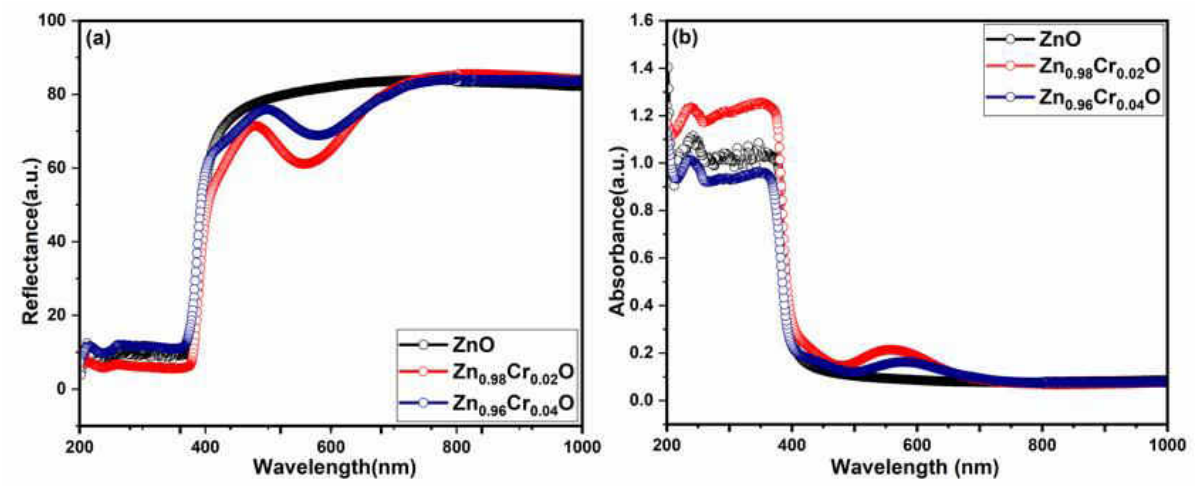

Fig.3.5.1(a) Reflectance spectra **(b)** Absorbance spectra of$Zn_{(1-x)}Cr_xO$ $(x = 0, 0.02, 0.04)$ nanoparticles

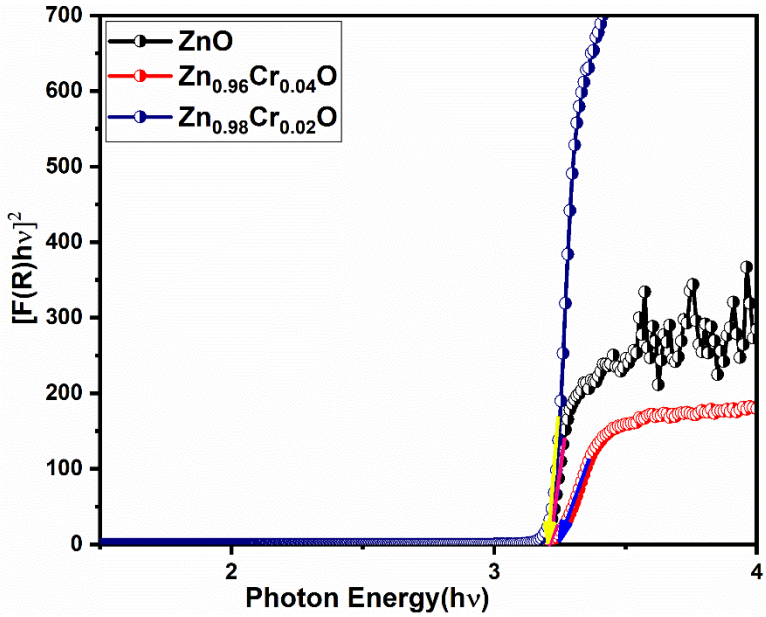

Fig. 3.5.2 $[F(R).h\nu]^2$versus (hν) for$Zn_{(1-x)}Cr_xO$ $(x = 0, 0.02, 0.04)$nanoparticles.

Table 3.3. Band gap energies of$Zn_{(1-x)}Cr_xO$ $(x = 0, 0.02, 0.04)$ nanoparticles

Sample code	Bandgap energy (eV)
ZnO	3.22
$Zn_{0.98}Cr_{0.02}O$	3.20
$Zn_{0.96}Cr_{0.04}O$	3.24

3.6 Photoluminescence Studies

Fig (3.6.1) gives Photoluminescence emission spectra of $Zn_{1-x}Cr_x$ O (x = 0, 0.02, 0.04), recorded under a λ_{ex} = 371 nm at room temperature. Similar emission peaks can be seen in all samples' spectra, indicating that doping with Cr did not create any new flaws into the materials. The intensity of the emission peak weakens with increasing dopant concentration, indicating a quenching of PL emissions as a result of the decrease in radiative recombination rate brought about by the introduction of heterojunction between the doping agent and parent material [26].The deep level emission in crystal, which is triggered by both structural flaws and impurities in ZnO nanostructures, accounts for the emission peaks seen in the visible spectrum area (400–700 nm). These deep level emissions are caused by inherent defect states in the zinc oxide lattice sites, such as zinc interstitial (Zni), oxygen interstitial (Oi), zinc vacancies (Vzn), oxygen vacancies (Vo), and O substitution at the Zn position (Ozn) [27].According to research by Liu et al [28]., Cr-doped ZnO exhibits PL spectra with peaks at 408, 434, 466, and 486 nm that are attributed to V Zn, Zni, singly negatively charged Zn vacancy (Vzn), and Vo, respectively. The increase in nonlinear and photocatalytic activity is a result of these generated flaws. The oxygen vacancies in Li-doped ZnO were studied by Puniaet al. [29] using PL peaks of approximately 538, 574, and 642 nm, which, respectively, correspond to neutral oxygen vacancies (Vo), single charge oxygen vacancies (Vo +), and doubly charged oxygen vacancies (Vo ++).In the visible and ultraviolet spectrum, zinc oxide nanostructures frequently exhibit an emission peak. Strong blue emission peaks at around 466 nm and 480 nm are related to intrinsic deformations formed within the host lattice caused by the electronic transition between the Vzn state and the bottom of the conduction level. Strong violet emission at 434 nm is related to the electronic transition from the zinc interstitial (Zni) state to the valence level. Oxygen vacancies are the largely accepted mechanism for visual emission of ZnO. (Vo).They can be found in three different charge states: neutral oxygen

vacancy (V*O), singly ionised oxygen vacancy (V +O), and doubly ionised oxygen vacancy (V++). The lattice of (V +O) tends to be singularly positively charged after capturing one electron, while (V *O) has absorbed two electrons while remaining neutral [30].Based on the (VO)in the energy band of the parent material, the formation of the blue, yellow, and green peaks is attributed to recombination of the (V ++O). The electron transition from (V + O) centres to the VB edge, the electron transfers from (V * O) centres to the VB edge, and the (V ++O) trapped centre recombination, respectively, are what lead to the yellow, green, and blue emissions [31][26][32][33].

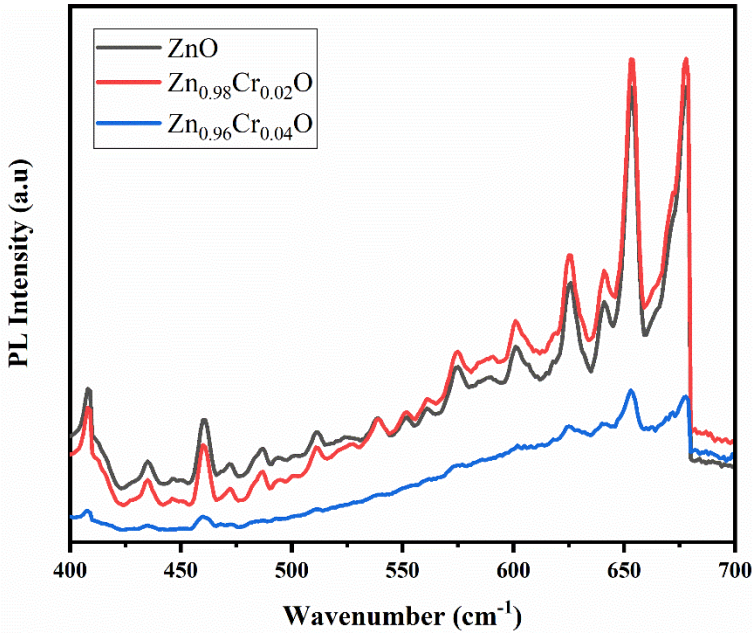

Fig 3.6.1: Pl spectra of $Zn_{(1-x)}Cr_xO$ $(x = 0,0.02,0.04)$ nanoparticles

3.7 Third-order nonlinear optical studies - Z-Scan analysis

Z-scan studies are carried out under continuous wave (cw) laser excitation by the open and closed aperture methods, formulated by Sheik-Bahae, to identify third-order nonlinear (NLO) parameters such as nonlinear absorption (NLA) coefficient, nonlinear susceptibility, and nonlinear refractive index (n $_2$) [32].The intensity-related nonlinear absorption and refraction can be expressed as, [33].

$$\alpha(I) = \alpha + \beta_{eff} \quad \text{..... (3.5)}$$

$$n(I) = n_0 + n_2 I \quad \text{..... (3.6)}$$

where α denotes the linear absorption coefficient, n_0 the linear refractive index, β_{eff} the NLA coefficient and I the intensity of the source.

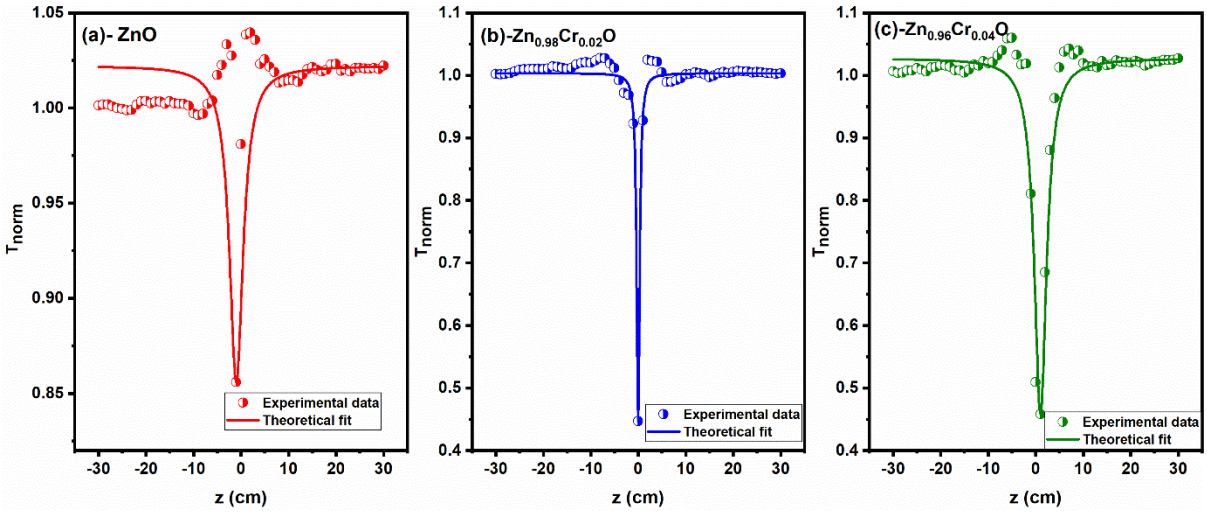

Fig.3.7.1(a)-(c) Open aperture Z-scan data of $Zn_{(1-x)}Cr_xO$(x = 0,0.02,0.04).

Z-scan measurements are carried out with a diode pumped Nd: YAG laser (532 nm), having a 13 mm focal length lens and laser beam waist ω_0 as 0.27 μm with laser power I_o - 8.76 kW/cm^2. ΔT_{p-v} Represents the difference between the $Tp-$ normalized peak and$Tv-$valley transmittance can be expressed using the function $|\Delta\varphi_0|$is,

$$\Delta T_{p-v} = 0.406\ (1-S)^{0.25}|\Delta\varphi_0| \quad \text{..... (3.7)}$$

Where $S = 1 - \exp(-r_a^2/\omega_a^2)$denotes the aperture linear transmittance$|\Delta\varphi_0|$, the on-axis phase shift

$$|\Delta\varphi_0| = kn_2L_{eff}I_0 \quad \text{..... (3.8)}$$

here $k = {}^{2\pi}/_{\lambda}$, $L_{eff} = \frac{[1-\exp(-\alpha L]}{\alpha}$gives the effective thickness of the material,I_0 the on-axis irradiance at focus (z = 0) and L the thickness of the sample,.

β_{eff} , estimated from open aperture (OA) Z-scan values are given in Fig.3.10 (a)-(c).As the value of transmittance at z = 0 decreases on increasing the intensity; the OA curve exhibits the presence of induced absorption in the nanostructures. All of the synthesised samples exhibit NLA, as seen by the valley-like curve, whereas reverse saturable absorption (RSA) behaviour accounts for the maximum transmittance value at z = 0. For pure ZnO nanostructures, a peak is also found at the focus (z = 0), indicating saturable absorption, in

addition to the valley (SA).While $Zn_{(1-x)}Cr_xO$(x = 0.02, 0.04) exhibits a little hump on both sides of focus, as the sample approaches z = 0, the transmittance value increases and illustrates SA criteria; as it reaches z = 0, the transmittance value lowers, giving a valley a curve, assigning RSA nature. Once more, the transmittance rises when the material is moved farther from z = 0, indicating a SA nature.

The normalized transmittance for the OA method is,

$$T(z, S = 1) = \sum_{m=0}^{\infty} \frac{[-q_0(z)]^m}{(m+1)^{3/2}} \quad \text{..... (3.9)}$$

For $q_0(0) < 1$, (0) < 1, where $q_0(z) = \frac{\beta_{eff} I_0 L_{eff}}{(1+ {z^2}/{z_R^2})}, z_R = \frac{k\omega_0^2}{2}$ is the diffraction length of the laser. The experimental measurements of n_2 and β_{eff}allows evaluating the real and imaginary parts of the $\chi^{(3)}$according to the equations below [34].

$$Re\chi^{(3)}(esu) = 10^{-4} \frac{\varepsilon_0 C^2 n_0^2}{\pi} n_2 \frac{cm^2}{W} \quad \text{..... (3.10)}$$

here $\varepsilon_0$is the vacuum permittivity, and c the vacuum light velocity:

$$Im\chi^{(3)}(esu) = 10^{-2} \frac{\varepsilon_0 \lambda C^2 n_0^2}{4\pi^2} \beta_{eff} \frac{cm^2}{W} \quad \text{..... (3.11)}$$

The absolute value of $\chi^{(3)}$ is estimated from

$$\left|\chi^{(3)}\right| = \left[Re\chi^{(3)^2} + Im\chi^{(3)^2}\right]^{1/2} \quad \text{.....(3.12)}$$

As shown in Fig.3.7.1 (a), closed aperture (CA) Z-scan measurements were performed to investigate the nanostructures' nonlinear refraction (c). The nonlinear absorption coefficients are provided by an aperture's absence, whereas the n_2 is provided by an aperture's presence. Additionally, nonlinear refraction occurs in conjunction with NLA rather than independently. We may assess the pure non-linear refraction using the division approach by comparing the ratio of the CA Z-scan data to the OA Z-scan data. Similar to most nanostructures, the curves in this case show a transmittance peak before z = 0 (peak) and a valley after z = 0 (valley). In closed aperture data, the peak-valley criteria indicate the self-defocusing property, which is then attributed to the negative n_2 [35]. Additionally, the sign of the n_2 acquires relevance and is readily ascertainable from the graph's shape. Nonlinear refraction can have a variety of causes, including as electronic, molecular, electrostrictive, or thermal phenomena. In our case, the nonlinearity is thermally generated because our inquiry is being conducted in a cw

environment [36]. Moreover, if the ΔT_{p-v} in the CA data is greater than 1.7 times the Rayleigh range (Z_R), then it's a perfect identification for thermally originated nonlinearity.

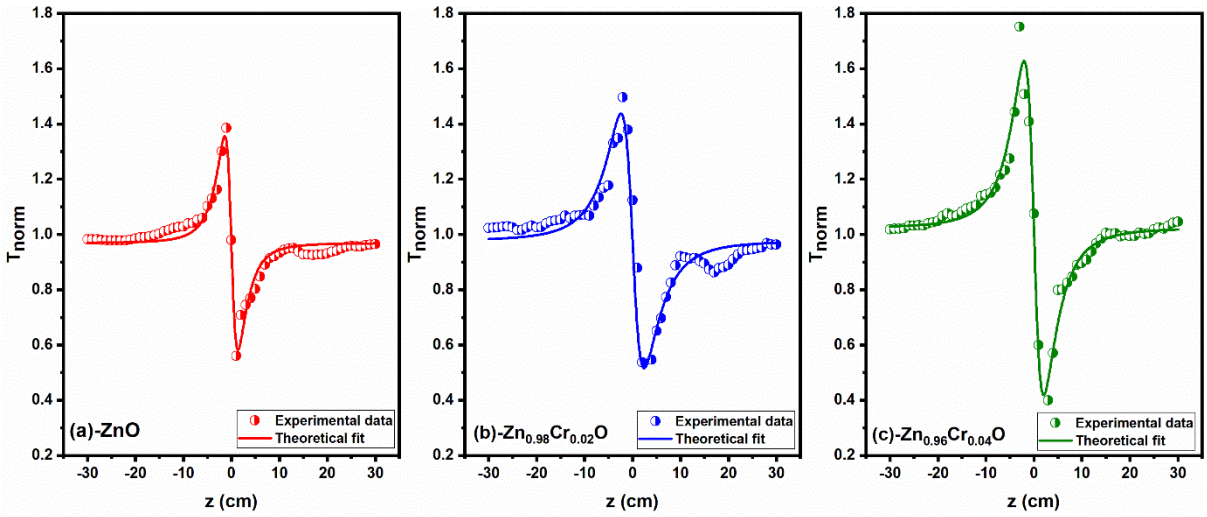

Fig.3.7.2(a)-(c) Closed aperture Z-scan data of $Zn_{(1-x)}Cr_xO$(x = 0, 0.02, 0.04) nanostructures

The nonlinear refractive index n_2 (cm^2 /w) is,

$$n_2 = \frac{\Delta\varphi_0\lambda}{2\pi L_{eff} I_0} \quad \text{..... (3.13)}$$

The normalized transmittance for non-linear refraction is,

$T(z) = 1 + \frac{4x\Delta\varphi_0}{(x^2+9)(x^2+1)}$where $x = {}^{Z}/_{Z_R}, Z_R = \frac{\pi\omega_0^2}{\lambda}, \lambda$the Rayleigh length of the laser beams. Estimated values of n_2, β_{eff} and χ^3 of $Zn_{(1-x)}Cr_xO$(x = 0, 0.02, 0.04 %) nanostructures are compared with recently available results of various materials under the cw laser because the current investigation is being conducted in the cw regime. The third-order NLO property is improved as a result of the nonlinearity, which is reliant on the laser heating process. When combined with the energy transfer from the Cr^{3+} ion to the ZnO lattice, this can be understood. The defect states serve as excited electron trapping spots and absorb a modest amount of energy whenever the nanostructures are exposed to a laser beam. By increasing the generated electron-hole pair recombination as a result, the third-order nonlinearity is also increased.

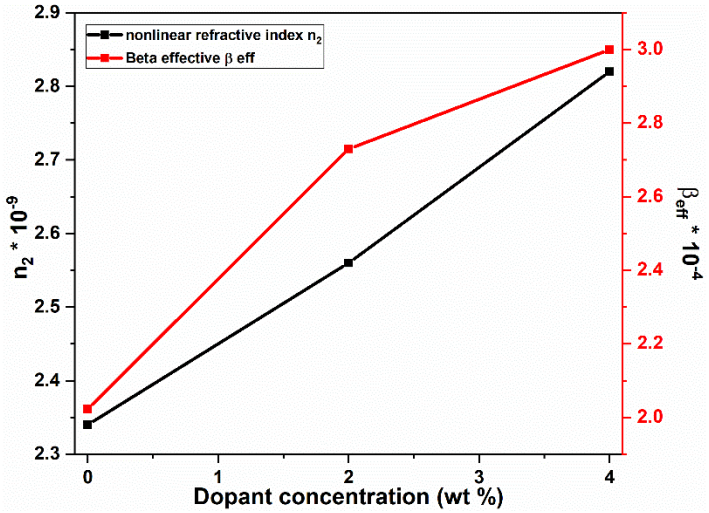

Fig. 3.7.3. Relation between dopant concentration with n_2 and β_{eff}

Sample name	$\boldsymbol{\beta_{eff}}$**(cm W^{-1})**	$\boldsymbol{n_2}$ **(cm^2 W^{-1})**	**Reference**
1 % Ni doped Cds	-1.95×10^{-5}	-0.6574×10^{-9}	[37]
ZnO films deposited on ITO/PET substrates	0.80×10^{-5}	-2.15×10^{-5}	[38]
0.03 mmol/L Azo dye	4.83×10^{-5}	-4.06×10^{-9}	[39]
5 mg/ml rGO-H	6.02×10^{-3}	4.47×10^{-8}	[40]
ZnO (Pure)	2.02×10^{-4}	2.34×10^{-9}	(Present work)
$Zn_{0.98}Cr_{0.02}O$	2.73×10^{-4}	2.56×10^{-9}	(Present work)
$Zn_{0.96}Cr_{0.04}O$	3.00×10^{-4}	3.23×10^{-9}	(Present work)

Table. 3.4 Recent reports of nonlinear materials under CW

Fig. 3.7.3 shows the prepared material's dependence on the n_2 and β_{eff}as a function of doping concentrations. Both nonlinear parameters are linearly dependent on the dopant concentrations in the examined range, according to the observed results. The concentration of the dopant has been observed to increase the absorptive and refractive nonlinearities. This

increase might be the result of the dopant being added to the process of how light interacts with matter. A limited portion of the incident laser energy is absorbed by the particles because the current work focuses on the cw regime. As the concentration rises, additional dopants thermally ignite as a result of the localised rise in temperature of the corresponding nanostructure, which causes temperature fluctuation.

3.8 Photocatalytic Studies

Since the bandgap of 2% Cr doped ZnO matches that of the dye solution, it reaches the adsorption-desorption equilibrium more quickly. The photodegradation efficiency of nanoparticles is influenced by factors like size, flaws, and bandgap. Hydroxyl radicals (*OH) are created during the photocatalysis process when holes remaining in the valence band interact with the hydroxyl molecules and the water molecules in the dye solution [41].When an oxygen molecule is reduced through the electron in the conduction band, superoxide radical anions (O2*-) are produced. The graphical representation of dye degradation is shown in Fig. 3.8.1 [42].

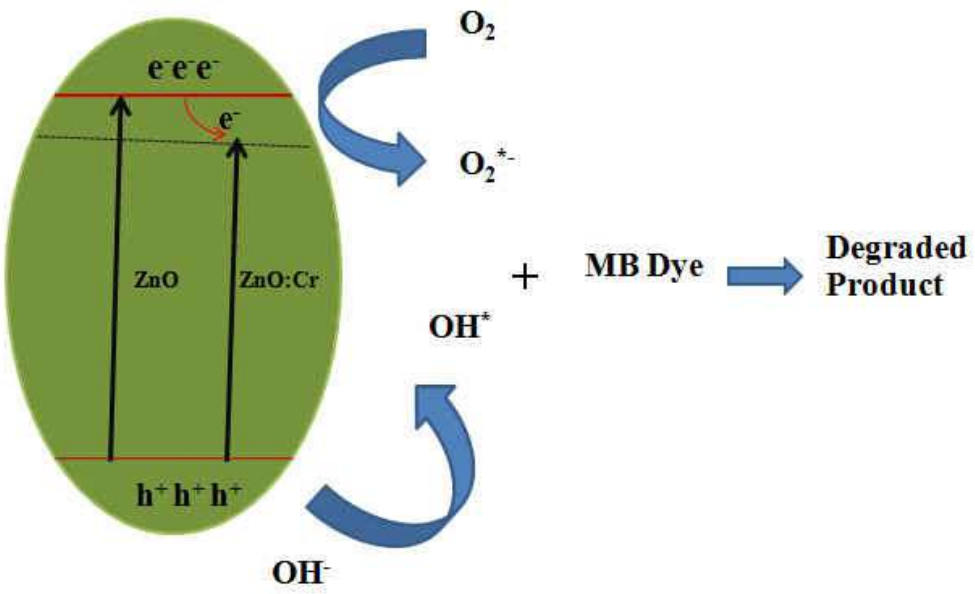

Fig 3.8.1 Pictorial representation of dye degradation mechanism

With these above formed radicals, the dye is going to degrade. The reaction steps are given as follows.

$Cr:ZnO+h\upsilon \longrightarrow e^- + h^+$

$h^+ + H_2O \longrightarrow H^+ + OH^-$

$h^+ + OH^- \longrightarrow O H^*$

$e^- + O_2 \longrightarrow O_2^{*-}$

$OH^* + O_2^{*-} + \text{MB dye} \longrightarrow \text{degraded product} + CO_2 + H_2O$

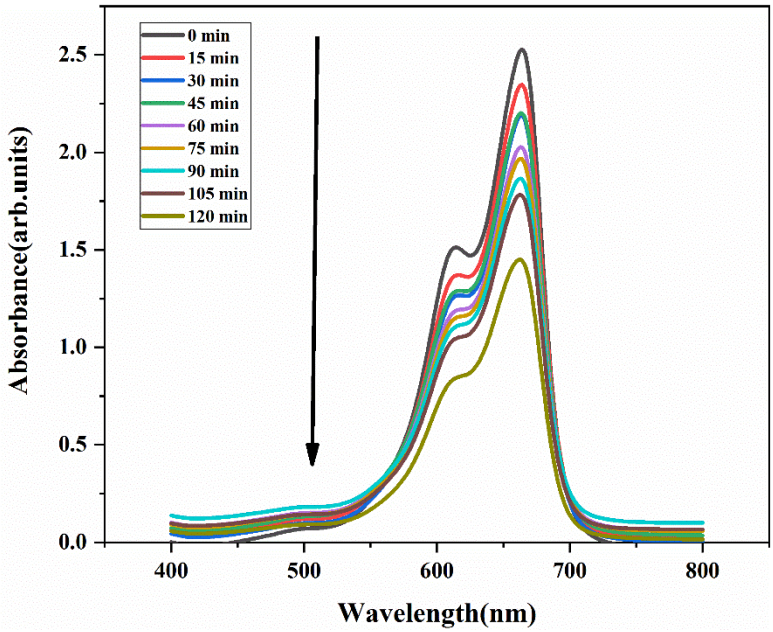

Fig.3.8.2. Dye degradation in pure ZnO

After 210 minutes, the dye degradation percentage for doped samples is around 52.23% and 42.83% for pure ZnO nanostructures. Under natural sunlight, doped samples exhibit higher photocatalytic activity than the pure sample, demonstrating that Cr is effectively boosting its photocatalytic activity.

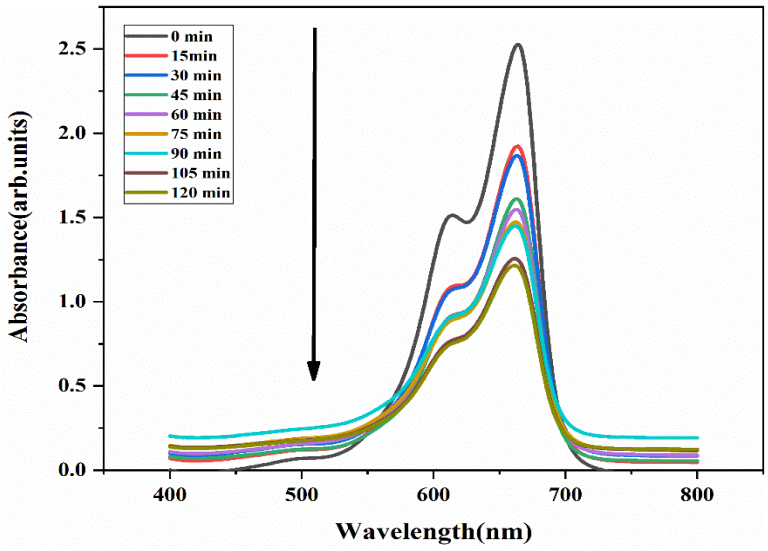

Fig. 3.8.3 Dye Degradation curve of Cr doped ZnO

The rate of degradation of ZnO and ZnO: Cr is calculated by first-order equation

$ln\ (Ce/Co) = -kt$,…….(3.14)

The rate constant is represented by k. Observe from Fig.3. 16 that the reaction rate of 2% Cr doped ZnO nanostructures is 0.00447 min-1 while that of pure ZnO is around 0.00394 min-1. Chromium ions in the ZnO lattice are causing MB dye to degrade more quickly when exposed to sunlight.

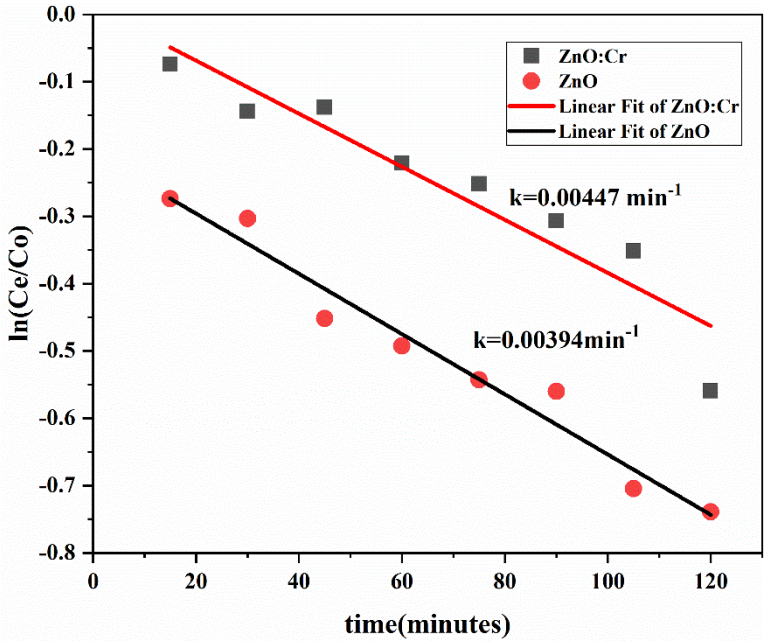

Fig.3.8.4. Rate curve of ZnO and ZnO: Cr nanostructures

The formation of an equivalent number of holes in the valence band causes the introduction of electrons in the valence band with energy greater than or equal to the parent bandgap energy into an excitation phenomenon toward the conduction band when the sample is exposed to sunlight. When transition metal is used as a dopant, it creates lattice defects, lowers the rate of electron-hole recombination, and increases photocatalytic activity.

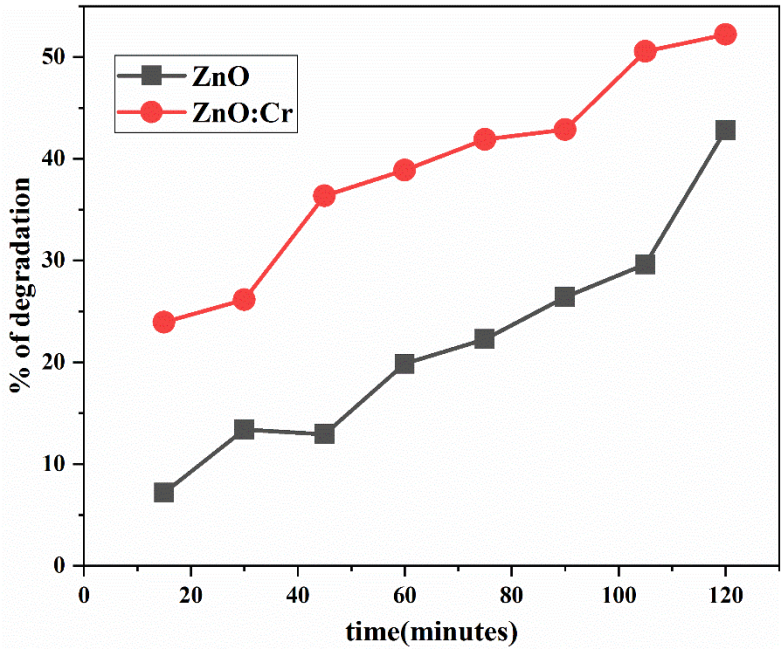

Fig.3.8.5. Percentage of degradation with time for ZnO and ZnO:Cr nanostructures

Defect states function as a transitional area between the valence and conduction bands, enabling the separation of electron-hole pairs. The flow of electrons from ZnO to Cr^{2+} is caused by a conduction band energy that is higher than the intraband level of Cr doped ZnO in ZnO nanostructures. The bandgap of 2% Cr doped ZnO nanostructures are shown by UV-visible spectroscopy to be less than that of the host lattice. The samples that include Cr show a redshift in bandgap, demonstrating that the photocatalytic effect also manifests in the visible spectrum. With an increase in adsorption capacity caused by the bandgap reduction, just a tiny amount of energy is needed to excite electrons to the CB from the VB. The photocatalytic activity is increased by the presence of Cr atoms in the surface site, which trap the electrons and stop them from recombining. Our recent research has shown that the presence of this chromium ion has a cost-effective influence on the photocatalytic activity of ZnO nanostructures without generating any negative by-products [42].

Reference

[1]-S. M. A. Naqvi, H. Soleimani, N. Yahya, and K. Irshad, "Structural and optical properties of chromium doped zinc oxide nanoparticles synthesized by sol-gel method," vol. 1621, pp. 530–537, 2014, doi: 10.1063/1.4898517.

[2]-P. S. Vindhya, T. Jeyasingh, and V. T. Kavitha, "Dielectric properties of zinc oxide nanoparticles using annonamuricata leaf," Kerala, India, 2019, p. 080005. doi: 10.1063/1.5093888.

[3]-C. J, S. N, D. A, and P. D, "Synthesis and Characterization of Ni and Cu Doped ZnO," J NanomedNanotechnol, vol. 08, no. 02, 2017, doi: 10.4172/2157-7439.1000429.

[4]-A. K. Worku *et al.*, "Structural and thermal properties of pure and chromium doped zinc oxide nanoparticles," *SN Appl. Sci.*, vol. 3, no. 7, 2021, doi: 10.1007/s42452-021-04682-6.

[5]-A. Iqbal, A. Mahmood, T. Muhammad Khan, and E. Ahmed, "Structural and optical properties of Cr doped ZnO crystalline thin films deposited by reactive electron beam evaporation technique," *Prog. Nat. Sci. Mater. Int.*, vol. 23, no. 1, pp. 64–69, 2013, doi: 10.1016/j.pnsc.2013.01.010.

[6]-S. A. Kadam, S. A. Thomas, Y. R. Ma, L. Maria Jose, D. Sajan, and A. Aravind, "Investigation of adsorption and photocatalytic behavior of manganese doped zinc oxidenanostructures," *Inorg. Chem. Commun.*, vol. 134, no. October, p. 108981, 2021, doi: 10.1016/j.inoche.2021.108981.

[7]-T. D. Malevu, B. S. Mwankemwa, M. A. M. Ahmed, T. E. Motaung, K. G. Tshabalala, and R. O. Ocaya, "Effect of Ni Doping on ZnO Nanorods Synthesized Using a Low-Temperature Chemical Bath," *J. Electron. Mater.*, vol. 48, no. 11, pp. 6954–6963, 2019, doi: 10.1007/s11664-019-07490-2.

[8]-L. V. Devi, T. Selvalakshmi, S. Sellaiyan, A. Uedono, K. Sivaji, and S. Sankar, "Effect of La doping on the lattice defects and photoluminescence properties of CuO," *J. AlloysCompd.*, vol. 709, pp. 496–504, 2017, doi: 10.1016/j.jallcom.2017.03.148.

[9]-M. M. Hassan, W. Khan, P. Mishra, S. S. Islam, and A. H. Naqvi, "Enhancement in alcohol vapor sensitivity of Cr doped ZnO gas sensor," *Mater. Res. Bull.*, vol. 93, pp. 391–400, 2017, doi: 10.1016/j.materresbull.2017.05.019.

[10]-S. S. Li and Y. K. Su, “Improvement of the performance in Cr-doped ZnO memory devices: Via control of oxygen defects,” *RSC Adv.*, vol. 9, no. 6, pp. 2941–2947, 2019, doi: 10.1039/c8ra10112d.

[11]-L. B. Duan, X. R. Zhao, J. M. Liu, T. Wang, and G. H. Rao, “Room-temperature ferromagnetism in lightly Cr-doped ZnO nanoparticles,” *Appl. Phys. A Mater. Sci. Process.*, vol. 99, no. 3, pp. 679–683, 2010, doi: 10.1007/s00339-010-5590-7.

[12]-M. M. Hassan, W. Khan, P. Mishra, S. S. Islam, and A. H. Naqvi, “Enhancement in alcohol vapor sensitivity of Cr doped ZnO gas sensor,” *Mater. Res. Bull.*, vol. 93, pp. 391–400, 2017, doi: 10.1016/j.materresbull.2017.05.019.

[13]-Y. Li *et al.*, “Structure and magnetic properties of Cr-doped ZnO nanoparticles prepared under high magnetic field,” *Solid State Commun.*, vol. 150, no. 15–16, pp. 751–754, 2010, doi: 10.1016/j.ssc.2010.01.027.

[14]-M. K. Gupta, N. Sinha, B. Kumar, M. K. Gupta, N. Sinha, and B. Kumar, “Dielectric studies and band gap tuning of ferroelectric Cr-doped ZnO nanorods Dielectric studies and band gap tuning of ferroelectric Cr-doped ZnO nanorods,” vol. 014303, no. 2012, pp. 1–5, 2013, doi: 10.1063/1.4730933

[15]-M. Salem, S. Akir, I. Massoudi, Y. Litaiem, M. Gaidi, and K. Khirouni, “Enhanced photoelectrochemical and optical performance of ZnO films tuned by Cr doping,” *Appl. Phys. A Mater. Sci. Process.*, vol. 123, no. 4, p. 0, 2017, doi: 10.1007/s00339-017-0880-y.

[16]-A. H. Shah, E. Manikandan, M. B. Ahamed, D. A. Mir, and S. A. Mir, “Anti-bacterial and blue shift investigations in sol-gel synthesized CrxZn1-xO nanostructures,” *J. Lumin.*, no. October 2019, 2014, doi: 10.1016/j.jlumin.2013.09.023.

[17]-J. Chen *et al.*, “Insight into the Synergistic E ff ect of Adsorption − Photocatalysis for the Removal of Organic Dye Pollutants by Cr-Doped ZnO,” 2020, doi: 10.1021/acs.langmuir.9b02879.

[18]-A. Ketema, W. Delele, W. Ayele, N. G. Habtu, and G. A. Melas, “Structural and thermal properties of pure and chromium doped zinc oxide nanoparticles,” *SN Appl. Sci.*, 2021, doi: 10.1007/s42452-021-04682-6.

[19]-A. M. K.Irshad, M.T.Khan, “Synthesis and characterization of transition-metals-doped ZnO nanoparticles by sol-gel auto combstion method.,” *Phys. B Condens. Matter*, vol.543, pp. 1–6, 2018.

[20]-V. D. Mote, V. R. Huse, and B. N. Dole, “Synthesis and Characterization of Cr Doped ZnO Nanocrystals,” vol. 2012, no. November, pp. 208–211, 2012.

[21]-S. Janet Priscilla, V. Andria Judi, R. Daniel, and K. Sivaji, “Effects of chromium doping on the electrical properties of ZnO nanoparticles,” *Emerg. Sci. J.*, vol. 4, no. 2, pp. 82–88, 2020, doi: 10.28991/esj-2020-01212.

[22]-A. A. Radhakrishnan and B. B. Beena, “Structural and Optical Absorption Analysis of CuO Nanoparticles,” *Indian J. Adv. Chem. Sci.*, vol. 2, no. 2, pp. 158–161, 2014.

[23]-R. N. Ali, H. Naz, J. Li, X. Zhu, P. Liu, and B. Xiang, “Band gap engineering of transition metal (Ni/Co) codoped in zinc oxide (ZnO) nanoparticles,” *J. Alloys Compd.*, vol. 744, pp. 90–95, 2018, doi: 10.1016/j.jallcom.2018.02.072.

[24]-E. I. Naik, H. S. B. Naik, R. Viswanath, I. K. S. Gowda, and M. C. Prabhakara, “Bright red luminescence emission of macroporous honeycomb-like Eu3+ ion-doped ZnO nanoparticles developed by gel-combustion technique,” *SN Appl. Sci.*, vol. 2, no. 5, pp. 1–13, 2020, doi: 10.1007/s42452-020-2639-x.

[25]-S. S. Sartiman, N. F. Djaja, and R. Saleh, “Chromium-Doped ZnO Nanoparticles Synthesized by Co-Precipitation: Chromium Effects,” *Mater. Sci. Appl.*, vol. 04, no. 09, pp. 528–537, 2013, doi: 10.4236/msa.2013.49065.

[26]-Z. M. Liao, H. Z. Zhang, Y. B. Zhou, J. Xu, J. M. Zhang, and D. P. Yu, “Surface effects on photoluminescence of single ZnO nanowires,” *Phys. Lett. Sect. A Gen. At. Solid State Phys.*, vol. 372, no. 24, pp. 4505–4509, Jun. 2008, doi: 10.1016/j.physleta.2008.04.013.

[27]-S. A. Kadam, S. A. Thomas, Y. R. Ma, L. Maria Jose, D. Sajan, and A. Aravind, “Investigation of adsorption and photocatalytic behavior of manganese doped zinc oxide nanostructures,” *Inorg. Chem. Commun.*, vol. 134, no. October, p. 108981, 2021, doi: 10.1016/j.inoche.2021.108981.

[28]-H. Liu *et al.*, “Role of point defects in room-temperature ferromagnetism of Cr-doped ZnO,” *Appl. Phys. Lett.*, vol. 91, no. 7, pp. 1–4, 2007, doi: 10.1063/1.2772176

[29]-K. Punia, G. Lal, S. N. Dolia, and S. Kumar, “Defects and oxygen vacancies tailored structural, optical, photoluminescence and magnetic properties of Li doped ZnO nanohexagons,” *Ceram. Int.*, vol. 46, no. 8, pp. 12296–12317, 2020, doi: 10.1016/j.ceramint.2020.01.280.

[30]-K. Karthika and K. Ravichandran, “Tuning the Microstructural and Magnetic Properties of ZnO Nanopowders through the Simultaneous Doping of Mn and Ni for Biomedical Applications,” *J. Mater. Sci. Technol.*, vol. 31, no. 11, pp. 1111–1117, 2015, doi: 10.1016/j.jmst.2015.09.001.

[31]-H. S. Kang, J. S. Kang, J. W. Kim, and S. Y. Lee, “Annealing effect on the property of ultraviolet and green emissions of ZnO thin films,” *J. Appl. Phys.*, vol. 95, no. 3, pp. 1246–1250, 2004, doi: 10.1063/1.1633343.

[32]-G. H. Du, F. Xu, Z. Y. Yuan, and G. Van Tendeloo, “Flowerlike ZnO nanocones and nanowires: Preparation, structure, and luminescence,” *Appl. Phys. Lett.*, vol. 88, no. 24, pp. 1–4, 2006, doi: 10.1063/1.2211007.

[33]-S. B. Zhang, S. H. Wei, and A. Zunger, “Intrinsic n-type versus p-type doping asymmetry and the defect physics of ZnO,” *Phys. Rev. B - Condens. Matter Mater. Phys.*, vol. 63, no. 7, pp. 1–7, 2001, doi: 10.1103/PhysRevB.63.075205.

[34]-S. V. S. Dhanuskodi, T. C. Sabari Girisun, ““Optical limiting behavior of certain thiourea metal complexes under CW laser excitation,” 2011.

[35]-L. K. Joy, M. George, J. Alex, A. Aravind, D. Sajan, and G. Vinitha, “Twisted intramolecular charge transfer investigation of semi organic L-Glutamic acid hydrochloride single crystal for organic light-emitting and optical limiting applications,” *J. Mol. Struct.*, vol. 1156, pp. 733–744, 2018, doi: 10.1016/j.molstruc.2017.11.126.

[36]-S. Elizabeth *et al.*, “Nonlinear optical and photocatalytic dye degradation of Co doped CeO 2 nanostructures synthesized through a modi fi ed combustion technique,” *Ceram. Int.*, vol. 46, no. 9, pp. 13932–13940, 2020, doi: 10.1016/j.ceramint.2020.02.189.

[37]-U. K. B. R. Bairy, A. Jayarama, G. K. Shivakumar, K. Radhakrishnan, “Investigation of

third-order nonlinear optical properties of nanostructured Ni-doped CdS thin films under continuous wave laser illumination”

[38]-J. Soudi, K. M. Sandeep, B. K. Sarojini, P. S. Patil, S. R. Maidur, and K. M. Balakrishna, “Thermo-optic effects mediated self focusing mechanism and optical power limiting studies of ZnO thin films deposited on ITO coated PET substrates by RF magnetron sputtering under continuous wave laser regime,” *Optik (Stuttg).*, vol. 225, no. October 2020, p. 165835, 2021, doi: 10.1016/j.ijleo.2020.165835.

[39]-H. A. Badran, A. Y. AL-Ahmad, M. F. AL-Mudhaffer, and C. A. Emshary, “Nonlinear optical responses and limiting behavior of sulfadiazine-chromotropic acid azo dye,” *Opt. Quantum Electron.*, vol. 47, no. 7, pp. 1859–1867, 2015, doi: 10.1007/s11082-014-0051-8.

[40]-T. C. S. G. G. Muruganandi, M. Saravanan, G. Vinitha, M. B. Jessie Raj, “‘Effect of reducing agents in tuning the third-order optical nonlinearity and optical limiting behavior of reduced graphene oxide,’”.

[41]-J. Chen *et al.*, “Insight into the Synergistic Effect of Adsorption-Photocatalysis for the Removal of Organic Dye Pollutants by Cr-Doped ZnO,” *Langmuir*, vol. 36, no. 2, pp. 520–533, 2020, doi: 10.1021/acs.langmuir.9b02879.

[42]-F. Naz and K. Saeed, “Investigation of photocatalytic behavior of undoped ZnO and Cr-doped ZnO nanoparticles for the degradation of dye,” *Inorg. Nano-Metal Chem.*, vol. 51, no. 1, pp. 1–11, 2021, doi: 10.1080/24701556.2020.1749657.

CHAPTER 4

CONCLUSION AND FUTURE SCOPE

In the present work, hydrothermal method is used to prepare pure and Cr doped ZnO with controlled morphology. Using XRD, SEM, EDAX, FTIR, and Raman spectroscopy, the structural, surface morphology, functional groups, and vibrational bands of ZnO and Cr doped ZnO have been examined. Using powder X-ray diffraction analysis, the phase purity and crystal structure of pure and Cr doped ZnO nanostructures were examined. The hexagonal wurtzite structure has a P63mc space group, according to the XRD data. No additional contaminant peaks were found within the experimental detection limit, and all of the diffraction peaks of the synthesised samples were ascribed to zinc oxide. This shows that the zinc oxide's lattice site has been doped with Cr without altering the crystal's symmetry. From the SEM image, the morphology of the synthesised sample has been seen analysed. It is clearly observe that after doping a significant change in morphology is happened. The presence of Zn,O and Cr is identified From Edax analysis. Through FTIR, the functional groups of the produced sample are identified and are comparable to those of ZnO. Raman technology is used to identify vibrational bands, which are the same as those described in published articles. Additionally, the bandgap discovered using UV-visible spectroscopy and comparable to the values given. Presence of oxidation state is also taken using XPS analysis. Also the photocatalytic and nonlinear properties of as prepared samples are investigated.

FUTURE SCOPE

1. As future work we can make several materials to form composites, improving the properties of ZnO
2. Different methods can be used to prepare ZnO and we can make a comparison in terms of morphology, Crystallanity etc
3. With ZnO, we can dope with various metal oxides utilising various synthesis techniques and concentrations. High quality zinc oxide has an interesting future ahead of it. Even more potential advancements exist for non-medical usage than for existing medical ones.
4. Different applications can be done like antibacterial studies, Anticancerous studies, Sensors etc